# HYDRAULICS, HYDROLOGY, AND RESULTING FISH PASSAGE AT THE HUNTLEY DIVERSION NATURE-LIKE BYPASS

by

Haley Noel Tupen

A thesis submitted in partial fulfillment
of the requirements for the degree

of

Master of Science

in

Civil Engineering

MONTANA STATE UNIVERSITY
Bozeman, Montana

July 2020

# DEDICATION

This thesis is dedicated to my family, who have always inspired me to work on behalf of beautiful and wild natural places, provided me endless amounts of support throughout my college years, and given me passion and grit for what I do;

To my soon-to-be-husband Kyle, who encouraged me and believed in me, dealt with the highs and lows of the whole process, was always willing to distract me for a day with ice climbing or skiing, and gave me all the love in the world;

And to Steve.

# ACKNOWLEDGEMENTS

I would like to thank my advising team of Dr. Kathryn Plymesser, Dr. Joel Cahoon, Dr. Matt Blank, and Dr. Al Zale for their technical expertise and support in both engineering and ecology aspects of this project. I would like to thank Montana Fish, Wildlife and Parks, especially Mike Ruggles, the Region 5 Fisheries Manager, for their technical support and aid during the fieldwork process in Billings. I would also like to thank the Montana Natural Resource Damage Program, especially Alicia Stickney, the NRDP Environmental Science Specialist, for their generous funding of this project.

Finally, I'd like to thank the student project partners who made the fieldwork process possible, and the graduate students who will continue to work on aspects of this project over the next few years. Your help was invaluable!

TABLE OF CONTENTS

TABLE OF CONTENTS CONTINUED

# LIST OF TABLES

Table Page

# LIST OF FIGURES

Figure Page

LIST OF FIGURES CONTINUED

Figure Page

LIST OF FIGURES CONTINUED

Figure Page

LIST OF FIGURES CONTINUED

Figure Page

LIST OF FIGURES CONTINUED

Figure Page

LIST OF FIGURES CONTINUED

Figure Page

# ABSTRACT

Dams and other instream structures have been constructed for hundreds of years in the United States for various purposes; these dams have the potential to "disconnect" rivers and negatively impact fish upstream and downstream movement. Nature-like bypasses were created to facilitate movement around these structures and provide passage to a wide variety of morphologically different fish species. The Huntley Diversion Dam nature-like bypass was constructed in 2015 on the Yellowstone River, but its effectiveness has not yet been evaluated. This project aimed to evaluate its efficacy through monitoring and determining water stage, flow rates, channel roughness, and a detailed channel bathymetry. These data were then used in the creation of multiple two-dimensional hydraulic models encompassing the nature-like bypass channel and surrounding Yellowstone River area. Velocity results from these models were compared to species-specific swimming capabilities from literature for four Yellowstone River species. Additionally, hydraulics at the downstream bypass entrance were evaluated for disorienting hydraulic formations that might prevent fish from locating the bypass entrance.

Velocity results indicate Sauger (*Sander canadensis*) may successfully ascend the bypass on all but five days of the modeled hydrograph and may face occasional difficulty in returning to their pre-spawning upstream habitat. Burbot (*Lota lota*), Channel Catfish (*Ictalurus punctatus*), and Smallmouth Bass (*Micropterus dolomieu*) are unlikely to successfully ascend the bypass for much of May, June, and July. This holds significant implications for Channel Catfish and Smallmouth Bass, both of which move upstream to spawn in the months of May and June. Hydraulics at the downstream end of the bypass indicate high attraction at high flows, but that lower flows are likely to create disorienting hydraulic characteristics at this bypass entrance and lead to low fish attraction.

# INTRODUCTION

Dams and other instream structures have been constructed for hundreds of years in the United States for hydropower, flood protection, potable water supply, and irrigation purposes. Dams are widespread throughout the rivers of the nation; a 2012 FEMA survey put the number of state-regulated dams at 88,000 (Federal Emergency Management Agency, 2012), while more recent studies have estimated the total number of low-head and storage dams to be close to 2,000,000 (Landsman et al., 2018). These dams vary in size but generally have the potential to "disconnect" rivers and negatively impact the upstream or downstream movement of fish in the river systems (Graf, 1999). Ease of mobility may be necessary for migration or spawning purposes and is often key to the survival and continuation of a fish species within a river system.

Various structures have been developed to facilitate fish movement around instream barriers. Commonly used fish passage structures, or *fishways*, include Denil, vertical slot, and pool-and-weir configurations, among many others. Fishways are relatively simple to construct and tend to be made of "hard" materials such as concrete, metal, and wood. Historically, these traditional designs have worked well for passing fish that have well-documented strong swimming abilities such as salmon and steelhead (Katopodis et al., 2001). However, studies have shown traditional fish passage structures tend to artificially select for fish that are longer, heavier, and have larger muscle fiber diameters. This unintentional culling is not limited to intra-species exclusion of juveniles or smaller-bodied fish. Entire species, such as chub or sturgeon, may be excluded from

upstream or downstream passage through fishways due to extremely small or large body sizing.

Nature-like bypasses originated in Austria in the 1970s and 1980s as an answer to these fish sizing-related passage problems. They utilize a variety of materials and roughness characteristics to mimic natural stream hydraulic conditions and therefore can provide passage to a wide variety of morphologically different species (Calles & Greenberg, 2005). These structures are still relatively unused in the United States, and as of this writing very few studies exist characterizing their effectiveness in large-scale dynamic river systems.

The Yellowstone River in Montana is colloquially described as the “longest undammed river in the United States”. There are dams on the Yellowstone River, but only low-head “run-of-the-river” dams with no storage capacity. The river is 1113.67 kilometers long and is home to over 50 species of native and nonnative fishes (Montana Fish, Wildlife and Parks). The Huntley Diversion Dam is the most upstream of these low-head diversions and is located east of Billings and just west of the small municipality of Huntley. A general layout of the Yellowstone River within the state and its diversion

dams, including Huntley, may be seen in Figure 1.

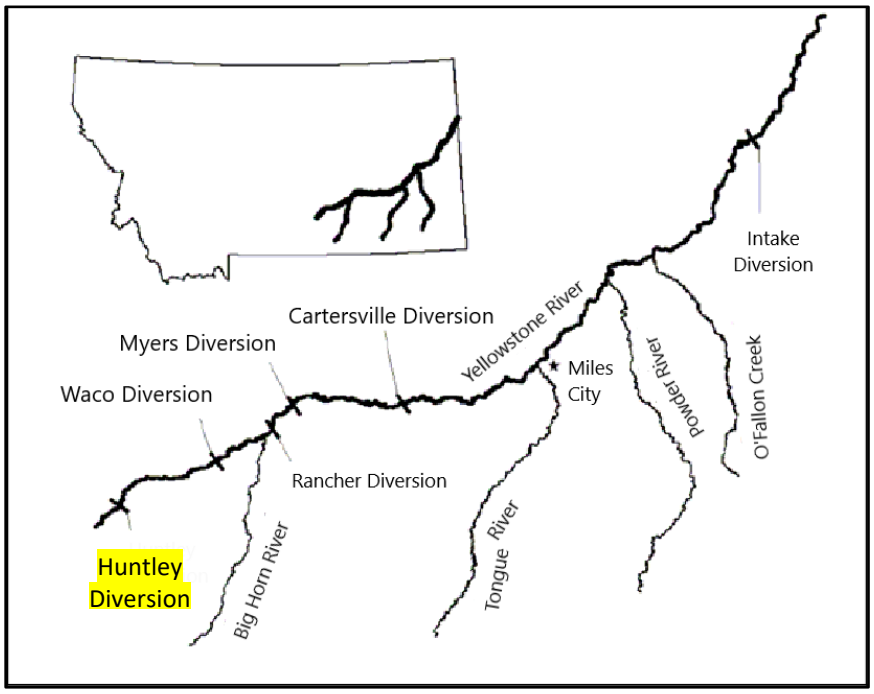


Figure 1. General layout of the Yellowstone River and its many diversions within the state. Image from Atkinson and Dood, (2006).

The 3-meter tall Huntley dam was constructed in 1934 primarily for irrigation and potable water delivery purposes; it is used to modulate the water level at the entrance to irrigation canals to ensure proper water delivery over the large range of flows in the river. The canals currently supply water to over 30,000 acres of local farmland and a few nearby municipal draws (U.S. Fish & Wildlife Service, 2008). Massive flooding occurred in the river in the spring of 1996 and 1997 and significantly damaged the dam. During the process of repairs, a riprap-lined nature-like bypass was constructed around the dam with the intent of increasing fish passage around the dam. This original bypass was suspected to be ineffective due to steep bed slope and resulting high water velocities throughout the channel (Zale et al, 2018). Following a large oil spill upstream of the dam in 2011, plans

were made to redesign this nature-like bypass, and this effort was completed in 2015. An image of the site, including the dam and old and new nature-like bypass channels, can be seen in Figure 2. This project marks the first study to determine the efficacy of this bypass.


Figure 2. Huntley Diversion and old and new nature-like bypass channels. Image from Google Earth (2020).

Of the roughly 50 morphologically different species within the Yellowstone River, four particular species are of interest for this project: Sauger (*Sander canadensis*), Burbot (*Lota lota*), Smallmouth Bass (*Micropterus dolomieu*), and Channel Catfish (*Ictalurus punctatus*). Except for Smallmouth Bass, all these species are native to the Yellowstone River. All play a part in Montana's substantial sportfishing economy; in 2018, Montana Fish, Wildlife & Parks estimated river and stream anglers spent over $760 million in the state (Lewis, 2018). Of these four species, Sauger are of special concern

due to increased hybridization with nonnative Walleye (*Sander vitreus*), which may lead to loss of genetic diversity or even complete extinction of the native species (Bingham et al., 2012). Additionally, it is estimated that the construction of the Huntley Diversion Dam prevented a genetically distinct population of Sauger from accessing their upstream habitat (Zale et al., 2018). It is vital that the nature-like bypass at this diversion creates hydraulic and hydrologic conditions suitable for passage by these four species.

This interdisciplinary project involves the work of both engineers and ecologists and is the result of a partnership between Montana State University and Montana Fish, Wildlife & Parks. The engineering portion of the project illustrates the hydraulic and hydrologic conditions throughout the nature-like bypass, characterizes the channel bathymetry and surrounding topography, and depicts channel-wide velocity and flow conditions through creation of various hydraulic models. Results of these hydraulic models are compared with species-specific swimming capabilities from literature, and estimated attraction and passage for Sauger, Burbot, Smallmouth Bass, and Channel Catfish is evaluated.

# LITERATURE REVIEW

## Nature-like Bypasses

Nature-like bypasses were first introduced in the 1970s and 1980s in Austria and are meant to provide fish with a passage environment similar to a natural stream or creek. The development of nature-like bypasses is in contrast to most conventional fishways, which have targeted salmonid species capable of leaping large vertical distances (Calles & Greenberg, 2005). Nature-like bypasses utilize natural materials and low channel slopes to increase passage success for a wide variety of morphologically different and both slower and strong-swimming species. Nature-like bypass channels are well-suited for implementation at low-head dams less than three meters in height. Additionally, nature-like bypasses are relatively cheap to construct and require little maintenance (Landsman et al., 2018).

The substrate within nature-like bypasses consists of a variety of roughness elements which results in a diverse hydraulic regime that may prove beneficial for weaker-swimming fish, especially small-bodied species. A 2018 study by Landsman et al. found roughness elements and low channel slopes within a nature-like bypass slowed velocities by greater than 50% relative to velocities through the notches in a pool-and-weir fishway. Additionally, these roughness elements created highly diverse velocities at the edges of the channel cross sections, areas the small species in this study were found to utilize the most. Landsman et al. concluded small species successfully utilized diverse edge velocities which allowed for passage at discharges that would otherwise seem too extreme for upstream movement.

Santos et al. (2005) described nature-like bypasses as structures actively "maintaining the river continuum" by use of natural channel materials and sinuosity. This 2005 study determined straightforward and optimal criteria for a nature-like bypass to pass a wide variety of lowland European species, including Brown trout (*Salmo trutta*) and the weaker-swimming small Iberian chub (*Squalius carolitertii*). Optimal bypass discharges of 0.1 to 0.2 $m^3/s$ per meter of channel width and minimum water depths of 40 centimeters were determined, though even greater depths were preferred to provide adequate resting spots for fish as they ascended the bypass. Water velocities at the downstream fish entrance to this lowland bypass were observed in the range of 1.0 to 2.4 m/s. All species within this study exhibited burst swimming speeds (see "Fish Physiology and Species of Interest", pp. 11-16) within this range; however, this may not be the most optimal metric for entrance success (Silva et al., 2018).

Nature-like bypasses are considered a viable alternative to traditional fishways. In addition to upstream passage, these bypasses provide diverse environments well-suited for fish spawning and habitat, especially salmonid species (Tamario et al., 2018). The general belief amongst river restoration practitioners is that nature-like bypasses are much "healthier" for rivers as a whole; however, questions about these bypasses providing adequate fish attraction flow remain (Silva et al., 2018).

## Attraction Flow

Fish attraction to the downstream entrance of a bypass is dependent upon several factors that are difficult to quantify. These include species-specific migratory timing, patterns and behavior, upstream movement motivation, and hydraulic phenomena near

the instream barrier. A nature-like bypass must present adequate “attraction flow” to draw fish to its downstream entrance, meaning the proportion of flow through the bypass must be large enough so that fish can find the entrance near the instream barrier (Katopodis et al., 2001). Past studies have recommended that this proportion be between 5 to 10% of total channel flow (NMFS, 2011).

Fish are physically drawn to bypass entrances through a behavioral phenomenon called rheotaxis, which causes them to be oriented head-first towards oncoming water flow. Traditionally, this was believed to be due primarily to visual cues, but more recent research has shown fish can rely on bodily sensors for this purpose. These sensors are spaced laterally along the middle of a fish’s body and have been proven to be key for upstream navigation when water velocities are low in a river (Montgomery et al., 1997). However, on large rivers, providing enough flow through a bypass to successfully activate and use these lateral sensors may prove difficult. The instream river barrier may cause backwater effects leading to fish confusion and reduced attraction. In these cases, Katopodis et al. (2001) recommended the use of multiple bypass entrances, introducing additional attraction flow, and controlling disorienting and exhausting turbulence and eddy formations near the downstream bypass entrance.

Landsman et al. (2018) recommended the downstream entrance of the nature-like bypass be placed as close as possible to the instream obstruction to ensure an adequate amount of attraction flow. This 2018 study compared fish attraction and passage at conventional and nature-like bypasses, and the results showed an inverse relationship between passage and attraction rates. Non-salmonid fish were found to pass the nature-

like bypass with a 27% success rate, but attraction rates at the conventional fishway were significantly higher.

## Hydraulic Modeling

Few studies have been performed to evaluate characteristics of nature-like bypasses using hydraulic modeling programs. Instead, researchers have primarily focused on modeling passage through culverts, guide walls, vertical slot fishways, and louver and bypass systems. However, these other modeling studies have still provided valuable insight that may be applied to a nature-like bypass model.

One-dimensional (1D), two-dimensional (2D), and three-dimensional (3D) models may be used when simulating hydraulic processes throughout a channel, a hydraulic structure, or floodplain system. Of these, 1D and 2D are most often used due to the extreme computation power and time needed for 3D simulations. Simple one-dimensional models have been commonly utilized but can only encapsulate main channel characteristics and processes at specified cross sections. For this reason, channel and floodplain models now often implement a two-dimensional or combined 1D/2D scheme.

In a 2017 study, Vozinaki et al. (2017) performed one-dimensional and combined 1D/2D modeling in HEC-RAS on the Koiliaris River basin on the island of Crete, Greece. The upstream end of the reach was gauged, permitting the authors to utilize an hourly flow hydrograph as the upstream boundary condition. Detailed satellite imagery allowed the authors to vary Manning's n coefficients with specific land uses within the river basin. The combined model necessitated use of a Weir coefficient to transfer flow from the 1D channel area to the 2D floodplain. Both models were calibrated against

observed water depth data at the downstream end of the river reach. When results of the two models were compared, the combined 1D/2D model exhibited a desirably higher NSE (Nash-Sutcliffe efficiency coefficient) and a lower RMSE (root mean squared error). The difference between observed and simulated water surface elevation values was minimized as the model grid size decreased. The authors noted the usefulness of the resulting 1D/2D hydraulic visualizations and color maps when predicting flood extents.

Tran et al. (2016) used a two-dimensional depth-averaged TELEMAC-2D program to model experimental nature-like bypass designs. The model itself relied on the shallow water (or Saint-Venant) equations to account for turbulence and flow patterns created throughout the bypass. Of main interest were maximum velocities and maximum turbulence, as turbulent kinetic energy (or TKE) is a key determinant of adequate resting zones for fish as they ascend the bypass. A shallow water model was especially useful for identifying resting zones and establishing flow behavior around the channel's large-scale roughness features. Difficulties were noted with the model easily going unstable in the wakes of the large-scale roughness elements; however, these instabilities were resolved, and model results were compared to acoustic doppler velocimeter readings of an in-lab nature-like bypass. The two-dimensional depth-averaged model was deemed useful in scenarios where the nature-like bypass in question had a bed slope of less than 7%, large-scale roughness element concentration of 6-20%, and a Froude number of less than 0.7. The authors concluded a numerical model of a nature-like bypass with the aforementioned characteristics would very often indicate velocity and turbulence profiles appropriate for generalized fish passage.

Fuentes-Pérez et al. (2017) examined best practice measures for modeling uniform and non-uniform flow through a step-pool nature-like bypass. In this bypass configuration, smaller weirs (or pools) are created throughout the channel using boulders. The small drops in water surface elevations between pools enhance hydraulic conditions suitable for passage of a wide range of species. Here, the authors noted two general approaches tend to be used when modeling bypasses of varying materials and shapes. Dimensionless relationships have often been employed but are only useful in these modeling schemes when water depth is the same in every pool throughout the bypass. This is considered a "uniform regimen" and is extremely rare due to the variability of natural conditions and flow behavior (Fuentes-Pérez et al., 2017). The second approach involves the use of classical weir equations, but if care is not taken to ensure discharge coefficients are extremely accurate, large amounts of error can occur. The authors found Villemonte's weir discharge coefficient to be particularly useful, seen here:

$$C_s = \beta_0 \left[1 - \left(\frac{h_2}{h_1}\right)^{1.5}\right]^{\beta_1} \quad (1)$$

$\beta_0$ and $\beta_1$ are dimensionless coefficients depending on the weir slot geometry and boulder arrangement, $h_2$ is the water level upstream of the boulder weir, and $h_1$ is the water level downstream of the boulder weir. The authors of this study recommended sole use of the Villemonte equation to calculate water distribution in a nature-like bypass due to its simplicity and ease of utilization with uniform and non-uniform flow in relation to upstream fish passage (Fuentes-Pérez et al., 2017).

## Fish Swimming Behavior and Species of Interest

Species-specific swimming capabilities must be considered to ensure fish do not become fatigued as they ascend a bypass. Fish swimming speeds can be classified into three distinct categories: burst, critical (or prolonged), and sustained. Burst swimming speeds are akin to a human sprinting and are generally used for extremely short durations of time. Critical speeds will cause a fish to become fatigued anywhere between 20 seconds to 30 minutes and are similar to a human jogging quickly. Finally, sustained speeds are described as "low speeds that fish can maintain indefinitely without fatigue" and are akin to a human walking or jogging slowly. These swim speeds vary between species, size, health, and sex, and may also be dependent upon factors such as water temperature and fish motivation. Swimming capabilities are typically measured in a laboratory setting (Katopodis et al., 2001).

Regardless of swimming capabilities, some general guidelines have been put forth regarding water velocities through technical and non-technical fishways. Teppel and Tymiński (2013) proposed maximum fishway water velocities of 1.0 m/s, 1.5 m/s, and 2.0 m/s for small, medium, and large fish, respectively. Additionally, a mean fishway velocity of 0.4 to 0.6 m/s was recommended to promote successful passage.

Recently, there has been a push within the fisheries community to not solely consider swimming performance and maximum velocities when designing passage structures. Instead, designers are encouraged to aim for a fish passage structure to be "transparent" in terms of the physical costs involved in finding and ascending the structure (Silva et al., 2018). In a 2018 paper, Silva et al. designated the overarching goal

of fish passage as “to achieve diverse fisheries management objectives related to upstream-downstream connectivity that encompass biological, culture, and socioeconomic components”. Furthermore, fish passage through a structure should not only be efficient, but also practical and productive. General ecosystem health and connectivity cannot adequately be analyzed by hydraulic modeling and laboratory tests alone. Additionally, recent studies have shown laboratory swimming performance tests have the potential to greatly underestimate realistic passage abilities of many species (Silva et al., 2018). Care must be taken to fully quantify greater ecological effects when designing these structures. Field studies should be conducted whenever possible to observe and understand any additional environmental factors. When effectively designing a fish passage structure, both hydraulic and species-specific biological considerations must be greatly emphasized (Silva et al., 2018).

Sauger (*Sander canadensis*), Burbot (*Lota lota*), Channel Catfish (*Ictalurus punctatus*), and Smallmouth Bass (*Micropterus dolomieu*) are the species of interest in this study due to their generally native status and high sportfishing value in Montana. Sauger is a member of the perch family (*Percidae*) and is classified as a highly migratory species whose historic range has been significantly affected by instream barriers throughout the United States. This species is native to the Yellowstone River east of Billings and is often found just below dams in large turbulent pools. They are unique in that they move downstream rather than upstream to spawn in March and April (Brown, 1971).

While no studies currently exist regarding Sauger passage in nature-like bypasses, a 2016 study examined Sauger swimming capabilities and passage success in a laboratory flume and swim chamber (Dockery et al., 2017). All fifteen adult Sauger in this study were males and showed high motivation to move upstream. Nine different test conditions with varying velocities and temperatures were implemented. Sauger passage rates were found to be lowest at low temperatures (10.1 °C) and mid-range water velocities and highest at the higher temperatures tested (14.3-18.8 °C). Sauger exhibited a mean maximum swimming velocity of 2.46 m/s, and analyses suggested a positive correlation between maximum swim velocity and water temperature (Dockery et al., 2017).

Burbot have an extensive worldwide distribution but are considered a potential species of concern in Montana (McPhail & Paragamian, 2000). Past studies have examined Burbot swimming performance and passage efficiency in both conventional and nature-like bypasses. Vokoun and Watrous (2009) tested the swimming capabilities of 42 Burbot in a smooth flume and found an inverse relationship between distance of ascent and increased water velocity, especially above 0.90 m/s. Prolonged swim speeds were found to be 0 BL/s (body lengths per second) to 5 BL/s, and Burbot were found to completely fail in ascending the fishway when water velocities were raised to 1.25 m/s (Vokoun & Watrous, 2009).

Calles and Greenberg (2007) examined passage efficiency, residency, ascension, and entrance rates of Burbot to a nature-like bypass on the Swedish River Emån. Tagged Burbot entered the bypass at a rate of 83% and tended to inhabit the bypass for months. All Burbot tagged in this study ascended the bypass; however, 40% of the tagged Burbot

moved up and down the bypass for several weeks, leading to an overall passage efficiency of 60%. The study noted motivation to move up the bypass may have been low due to many observations being performed outside the spawning season.

Channel catfish (*Ictalurus punctatus*) are an extremely popular sport fishing species native to the Yellowstone, Missouri, and Mississippi River drainages. These bottom-dwelling fish are easily identified by their highly forked tails and can commonly exceed weights of 9.07 kilograms. Due to widespread introductions throughout the 20th century, Channel Catfish now inhabit many large river systems throughout the western United States, including the Colorado River and Sacramento-San Joaquin River basins. In a 1961 study, researchers noted the tendency of Channel Catfish to migrate extremely long distances upstream, provided the entire river reach is of suitable temperature and depth (McCammon & LaFaunce, 1961). Past studies have noted sustained, prolonged, and burst swimming speeds for Channel Catfish juveniles at 0.40, 0.90, and 1.20 m/s, respectively (Beecham et al., 2007), while adults exhibited swim speeds of 0.42 m/s (Hocutt, 1973).

Studies on dammed river systems in California have drawn links between high-head dam coldwater releases and decreased Channel Catfish upstream migration (McCammon & LaFaunce, 1961). As of this writing, no studies exist regarding Channel Catfish migration around low-head dams, which are prevalent on the Yellowstone River in Montana. Past polls throughout the greater Mississippi River basin have suggested 60-65% of anglers target and harvest Channel Catfish, cementing the species' extreme importance in sportfishing in Montana (Siddons 2015).

Smallmouth bass (*Micropterus dolomieu*) are native to northern Minnesota and were introduced to Montana in the early 1900s. Members of this cold-water species can live up to 15 years and may exhibit upstream movement during spawning season in May and June (Brown, 1971). Past studies involving Smallmouth Bass have analyzed swimming performance in laboratory raceways and found water velocities of 1.20 m/s presented significant physiological barriers to upstream movement (Peake & Farrell, 2005). Additional laboratory tests have recorded critical and critical prolonged swim speeds at 1.11 and 0.75 to 0.81 m/s, respectively (Cooke & Bunt, 2001; Peake, 2004; Bunt et al., 1999).

The role these species play recreationally and economically throughout the Yellowstone and Missouri Rivers necessitates an examination of fish passage around the Yellowstone River's many low-head diversions.

# METHODS AND MATERIALS

This section describes both the field and computer-based procedures used to characterize the hydraulics and hydrologic conditions throughout the Huntley Diversion nature-like bypass. Field activities were conducted onsite at the Huntley Diversion nature-like bypass from April 2019 to November 2019. Computer-based modeling and analysis took place in the Civil Engineering Department facilities at Montana State University.

## Field Methods

In-field procedures were aimed at characterizing flow conditions and patterns in the nature-like bypass. Field procedures included measuring or monitoring water stage, flow rate, channel roughness, and detailed channel bathymetry.

### Onset HOBO Data Loggers

In April of 2019, four stilling wells were constructed and placed in the old and main fish bypass channels. The wells were labeled A, B, C, and D. Wells A, B, ad C were placed in the most upstream, downstream, and midpoint sections of the main bypass channel, respectively, while well D was placed in the old bypass channel. These wells may be seen represented by the red circles in Figure 3 below.


Figure 3. Locations of original wells (red circles), backup wells (yellow triangles), and the logger used to record barometric pressure at the Huntley Diversion nature-like bypass channel (Google Earth, 2020).

These wells were constructed for the purpose of housing Onset HOBO U20-L data loggers, which monitor water temperature, pressure, and depth at a fixed location. Each well consisted of a steel car wheelbase filled with concrete and having a length of Schedule 40 steel pipe cast into the concrete perpendicular to this base. Approximately 10 to 15 holes were drilled into each steel pipe to ensure the free movement of water throughout the stilling well. Each data logger hung in a well on a lightweight steel chain attached to a 3-inch PVC well cap. Using Onset HOBO computer software, loggers were programmed to record water temperature, pressure, and depth every half an hour throughout the field season from April to November 2019.

Additionally, each well area was outfitted with a “backup” well higher in the cross-sectional profile as represented by the yellow triangles in Figure 3. These backup wells, termed A2, B2, C2, and D2, provided access to loggers when increasing water depths caused the original wells to be unsafe or impossible to access when attempting to download data. These wells also served to provide logger data if wells A through D tipped or were lost to a high flow event.

A single logger was placed nearby in a location that was never inundated to record barometric pressure for comparison to channel logger data. Logger pressure, temperature, and depth readings were downloaded during each site visit using a HOBO U-DTW-1 Waterproof Shuttle Data Transporter. This transporter conveyed data to a computer using HOBOware Pro software.

Staff Gage Readings

Each stilling well was affixed with a staff plate, a long metal measurement plate marked in tenths of a foot. At wells A, B, C, D, and the backup D well, the bottom of the staff plate was flush with the top of the concrete well base. At the other wells, the staff plate was affixed to any point on the structure, and the distance from the bottom of the plate to a specified relation point was recorded. A staff gage observation was made at each well every day personnel were onsite. These observations provided backup water stage information in case of a HOBO failure and were used to confirm the Onset HOBO logger readings.

Survey Points

Survey points were chosen throughout the bypass channel and surrounding land area primarily to monitor fluctuations in water surface elevations throughout the field season. The locations of these six survey points may be seen in Figure 4. Observations of water surface elevation served as a source of comparison to logger depth data and as stage-boundary conditions for the hydraulic modeling portion of this project.

An auto-level, rod, and round-headed tripod were used to record the elevations of these points and characterize their relative elevation differences. These points included the following:

- a datum point at the highest immovable point onsite,
- observations at the bases of wells A, B, C, D, and all backup wells, and
- water surface elevation observations at the most upstream and downstream points of the main bypass, just downstream of the dam, and far downstream of the bypass.


Figure 4. Approximate locations of water surface elevation survey points and associated datum and setup locations (Google Earth, 2020).

These last four water surface elevation points were termed WSE-Up, WSE-Down, WSE-Weir, and WSE-Tree, respectively, and observations at these locations in relation to the datum were taken every day personnel were on site. For each observation, the bottom of the survey rod was set at the intersection of the water surface and the bed substrate. Effort was made to place the tripod in the same location every day on site to capture the datum point effectively and easily within the auto-level scope. A survey "loop" beginning and ending with this datum point was used to ensure the equipment had not moved throughout the process.

## Flow Rate Determination

The following methods were used to determine flow rates in the main and old bypass channels at specified cross sections. Each cross section was located close to a well

in the bypass channel and was meant to represent the flow rate in the channel at that well. Locations of cross sections A, B, C, and D can be seen in Figure 5 below.


Figure 5. Locations of cross sections used for flow rate determination at the Huntley Diversion nature-like bypass channel (Google Earth, 2020).

Midsection Method. When flows permitted direct in-channel measurements, the U.S. Geological Survey (USGS) Midsection method was used to determine the flow rate at a channel cross section. A Hach FH950 Portable Velocity Meter and top-setting wading rod were used to measure velocities at vertical subsections across a specified channel width. After a specific cross section was selected for flow rate determination, a measuring tape was suspended across the stream channel. The channel width and the station of the left and right edges were recorded facing downstream. Starting at the left edge of water and facing upstream, depth and velocity measurements were taken at each 0.15-meter width increment across the channel. At each increment, the station number, or

distance from the left edge of water, was recorded. The top-setting wading rod was then used to measure the total water depth at that station. If the total water depth was less than 0.762 meters, the wading rod was adjusted to measure water velocity at a single point at 0.6 times the total depth from the surface. If total water depth was greater than or equal to 0.762 meters, the rod was adjusted to take two velocity readings at 0.2 and 0.8 times the total depth from the surface, and these two measurements were then averaged. Once the wading rod was adjusted to an appropriate depth, the velocity meter was held at that point for 40 seconds to obtain time-averaged velocity. Depths and resulting water velocities at each station were then recorded.

Each measured water depth and corresponding velocity value was used to calculate a cross section flow rate using the following equation:

$$q_n = v_n * \left(\frac{\text{station}_{n+1} - \text{station}_{n-1}}{2}\right) * \text{depth}_n \quad (2)$$

where $q_n$ is the incremental flow rate, $v_n$ is the incremental velocity, and n is the station number, or distance across the channel. Each individual $q_n$ value was then summed to calculate the total flow rate at the measured cross section. This process is generally discussed among practicing engineers as having ± 10% error, although this is only an estimate as the true flow rate is difficult to ascertain accurately using any practical method.

Float-Area Method. When river flows were high, it was unsafe to enter the channel to conduct Midsection method measurements. When this was the case, but both banks of the main bypass channel were still accessible, the float-area method was used to determine a flow rate.

A straight, uniformly graded reach of channel was measured upstream from a selected cross section; at a minimum, this reach measured 6.10-7.62 meters long. The travel time of a buoyant object, such as an orange peel or a block of wood, was measured over this reach. Due to material constraints and the remote nature of the site, medium-sized and weighted pieces of wood debris were used when the float-area method was employed. Timed float experiments were repeated at least three times at each cross section and then averaged. Surface velocity was then computed using the following formula:

$$Velocity\ \left(\frac{ft}{s}\right) = \frac{distance\ (ft)}{avg.\ time\ (s)} \quad (3)$$

To determine a mean cross-sectional velocity, surface velocity was multiplied by an adjustment factor *k*, which ranged from 0.66 to 0.75 depending on the average of the measured depth values. These values can be seen in Table 1.

Table 1. Float method adjustment factors based on average cross-sectional water depth.

| Coefficients for Converting Float Velocity to Mean Channel | |
|---|---|
| Avg. Depth (m) | Coeff. |
| 0.30 | 0.66 |
| 0.61 | 0.68 |
| 0.91 | 0.7 |
| 1.22 | 0.72 |
| 1.52 | 0.74 |
| 3.66 | 0.78 |
| *Source: USBR Water Measurement Manual (1997)* | |

Cross-sectional area was computed from depth measurements on equally stationed intervals across the channel, which were then averaged and multiplied by the channel width. Flow at the cross section was then determined by multiplying mean cross-sectional velocity by area.

Even when this method is carefully performed using USGS guidelines, accuracy may be limited by “a lack of preciseness in the coefficients, too few stream segments being used, appreciable changes in stream depth along the test reach, oblique currents, wind forces, and experimental errors in measuring time and distances” (U.S. Department of the Interior - Bureau of Reclamation, 1997). Use of the Midsection method is recommended whenever possible.

Slope-Area Method. This approach is recommended when high flows and water depths make in-channel environments unsafe or impossible to access. At the Huntley Diversion bypass, three measurement points were selected along the straightest and most uniform reach of channel. These three points were labeled A, A-Up, and A-Down, and can be seen outlined in the aerial channel view of Figure 6.


Figure 6. Water surface elevation locations used for slope-area flow rate calculations (Google Earth, 2020).

The distances from the central point (A) to the upper and lower cross sections were measured to be roughly 24.38 and 15.24 meters, respectively. Each day personnel were on site, the water surface elevation was observed at the edge of water marks at these three specified locations. This approach assumes water surfaces are horizontal over the width of the channel, and measurements are only needed along one bank. Water surface elevations were later used in a one-dimensional hydraulic model to determine associated channel flow rates.

It is important to note that due to the potential for Manning's n selections to vary widely, "the discharge determined by the slope-area method is only approximate" (U.S. Department of the Interior - Bureau of Reclamation, 1997).

Roughness Characterization

A measure of channel roughness was necessary to depict flow behavior using the hydraulic models. Roughness was primarily characterized using the Wolman Pebble Count technique (Johnson & Swanson, 2014), which involves "randomly" sampling substrate particle sizes with a gravelometer. In this study, 10 measurement transects were spaced evenly throughout the main bypass channel. Per Wolman Pebble Count procedure, the sampler walked perpendicularly across the channel at each transect. At each step, the sampler utilized a step-toe procedure, reaching down and grabbing the rock or substrate piece touching their right big toe to ensure no bias in the random selection. This substrate piece was then measured across its intermediate axis and this measurement was recorded. Samples were classified into one of 18 different size categories (see Appendix B). Ten substrate measurements were recorded at each of the 10 transects for a

total of 100 particle measurements in the main bypass channel. A cumulative particle size distribution was then developed from these measurements as shown in Figure 7.

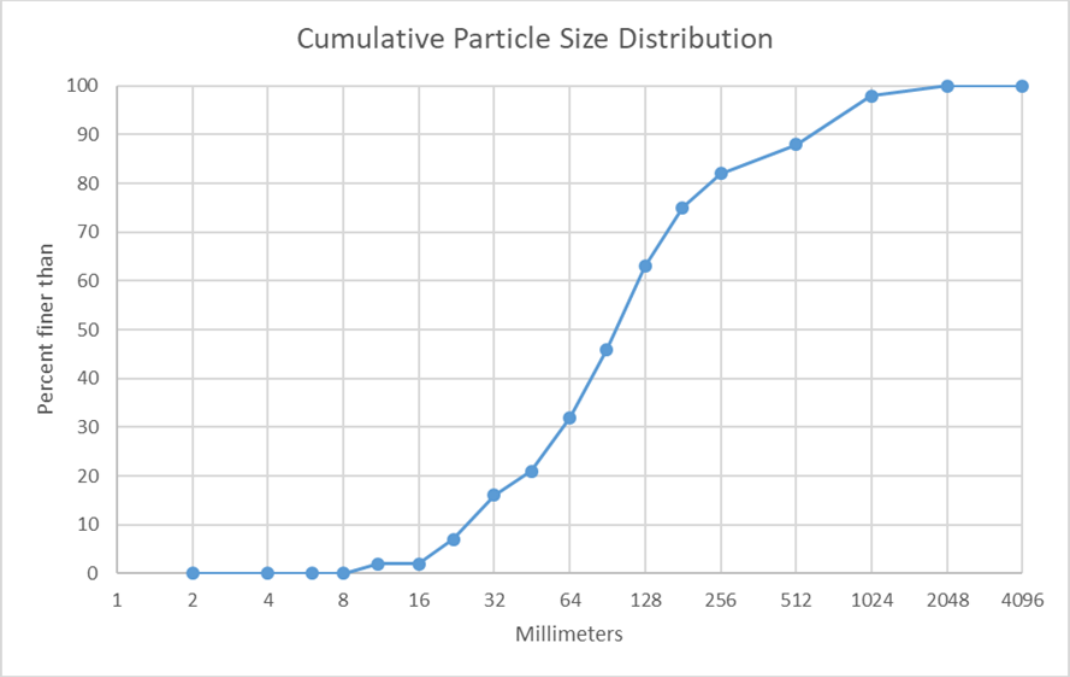


Figure 7. Cumulative particle size distribution developed from Wolman Pebble Count substrate measurements.

The particle size in millimeters that 50% of the samples were equal to or smaller than ($D_{50}$) was estimated. The Strickler equation was employed to determine a Manning's n roughness coefficient from the particle size data:

$$n = 0.0132D_{50} \quad (4)$$

Photo Points

Photographs of the channel were taken at specified points during every site visit. These routine photographs allowed visualization of how the channel topography and inundated areas varied throughout the field season. Seven photo points were designated in total, and at each point two to five pictures were taken to fully encapsulate views of the

main and old bypass channels. The location of these photo points can be seen in the aerial channel view of Figure 8. Sample pictures from several photo points can be seen in Appendix C.


Figure 8. Photo point locations at the Huntley Diversion bypass channel site (Google Earth, 2020).

Velocity Profile Sketches

Channel-wide velocity maps were hand-sketched during each site visit for corroboration of hydraulic modeling. These profiles were used to "train" the hydraulic models and ensure they correctly emulated observed flow behavior. An example velocity profile sketch can be seen in Figure 9.

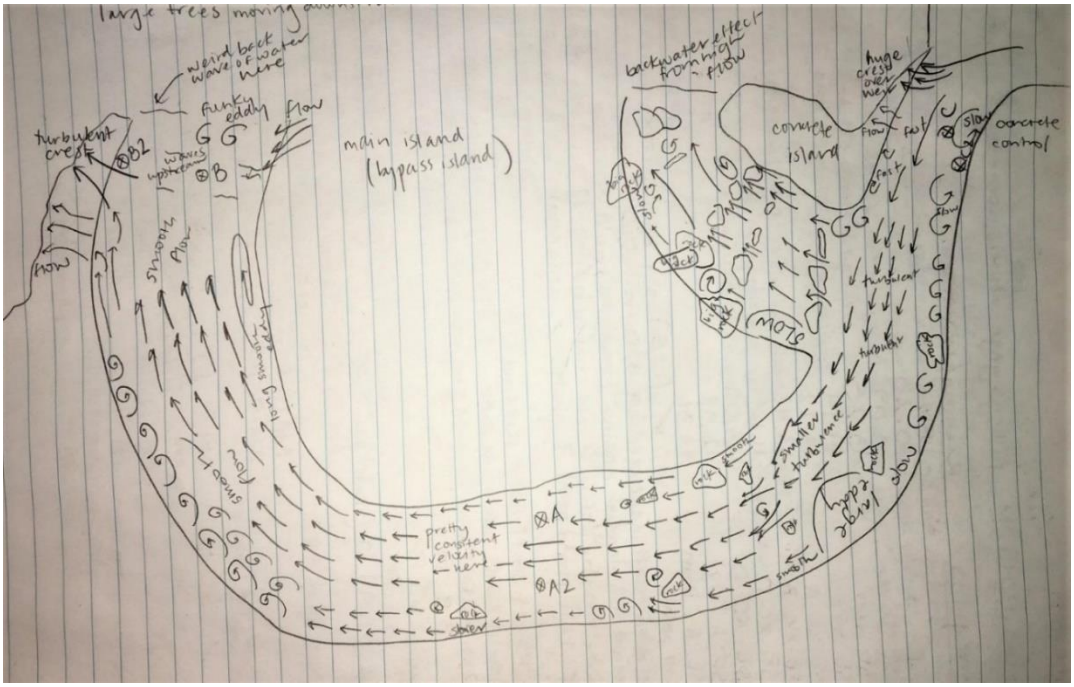


Figure 9. Velocity profile sketch of the Huntley Diversion nature-like fish bypass channel on May 15, 2019.

In the sketch of Figure 9, longer arrows represent areas where faster moving water was observed (higher velocities), while short arrows represent the opposite. Curled arrows represent areas with observed eddy behavior, and wavy lines represent areas of observed stagnation or backwater effects. The sketch above notes the general locations of all stilling wells and specific water behaviors due to high flow, like large wave crests over the rock weir at the most upstream reach of the channel.

Topographic Surveying

Topographic data of the site were needed to serve as the base terrain surface for all hydraulic models in this study. Though useful in many topographic surveys, LIDAR remote sensing was not used due to its inability to access submerged channel environments. Instead, a Trimble R8 GPS rover and base station were utilized to obtain

measurements at the site. In accordance with Trimble guidelines, the R8 base station was placed in the same central, elevated location whenever in use. GPS points were obtained with the rover on a 0.30 meter by 0.30-meter grid in the bypass channel, a 1.22 meter by 1.22-meter grid within the near-channel environment, and a 3.05 meter by 3.05-meter grid on terrain farthest from the channel. Approximately 7600 GPS points were obtained in total at the site and used to create the base terrain model, discussed at length in the following "Computer-Based Methods" section.

## Computer-Based Methods

### Modeling Theory and Hydraulic Equations

All hydraulic modeling was performed in HEC-RAS, a program developed by the Army Corps of Engineers. This program assumes the presence of gradually varied flow, or flow where the depth changes only a small amount over a comparatively large distance of longitudinal channel. Gradually varied flow may be classified as either steady, where water depth and velocity do not change at a certain location over the examined period of time, or unsteady, where the two parameters may fluctuate at the specified location (Chow, 1959). HEC-RAS can model both one-dimensional steady flow and one-dimensional or two-dimensional unsteady flow scenarios; both were utilized throughout this project and will be discussed throughout the following pages.

Past studies have noted one-dimensional models are most appropriate for non-meandering rivers where flow is mostly restricted to the channel itself. One-dimensional models also have the capacity to accurately account for instream hydraulic structures, like weirs, bridges, and culverts. Historically, 1D modeling has been the most common due to

ease of data collection, as these models only require bathymetry data to be collected at specified cross sections. Additionally, one-dimensional hydraulic modeling allows for extremely fast computation times, simulating months of flow behavior in just a few minutes of computations. However, 1D schemes may oversimplify flow behavior, as overland flow does not tend to be one-dimensional in nature. Stability issues may also arise if cross sections are coarsely spaced (Betsholtz & Nordlöf, 2017).

Steady gradually varied flow simulations in HEC-RAS rely on solving the one-dimensional energy equation, seen here:

$$z_1 + y_1 + \alpha_1 \frac{{V_1}^2}{2g} = z_2 + y_2 + \alpha_2 \frac{{V_2}^2}{2g} + h_L \quad (5)$$

Here, any terms with a subscript "1" denote characteristics of an upstream cross section, while those with a subscript "2" are associated with characteristics of a downstream cross section. The z terms represent the elevation above a specified datum, y terms represent water depth, v terms denote average cross-sectional velocity, and g is gravitational acceleration. The term α is the kinetic energy correction factor and generally ranges from 1.03 to 1.3 when turbulent flow is present; often, a value of α = 1.0 is assumed. The term $h_L$ encompasses energy losses between the two cross sections, including energy lost due to contractions, expansions, and channel bed roughness. The equation HEC-RAS uses to calculate these energy losses between cross sections may be seen below.

$$h_L = LS_f + C\left|\frac{\alpha_2 {V_2}^2}{2g} - \frac{\alpha_1 {V_1}^2}{2g}\right| \quad (6)$$

Where L is the discharge-weighted reach length, $S_f$ is the friction slope, and C is the contraction or expansion coefficient.

Steady gradually varied flow profiles may be computed using subcritical (Fr < 1), supercritical (Fr > 1), or mixed regime flow simulations. Subcritical flow is classified by its deep and slow characteristics, while supercritical flow is known to be fast and shallow. The U.S. Army Corps of Engineers recommends the utilization of a mixed flow regime when simulating flow at stream junctions or splits (Brunner, HEC-RAS River Analysis System User's Manual, 2016).

Two-dimensional hydraulic models better incorporate complex floodplain features like frictional elements, land use changes, and floodplain extents. 2D HEC-RAS models incorporate external and internal boundary conditions to add or remove flow from the model. When adding flow, a flow hydrograph or stage hydrograph at a specified location may be used. When flow is intended to leave a model, negative flow values, a stage hydrograph, rating curve, or normal depth condition may all be implemented. Precipitation may be set as an internal boundary condition over a two-dimensional flow area; however, 2D HEC-RAS models cannot currently account for evaporation or infiltration, and these should be incorporated into rainfall calculations if a precipitation value is applied. Additionally, no current process exists to accurately model instream hydraulic structures or account for energy losses caused by expansions or contractions within a 2D model. Finally, extreme computation times are required for purely 2D models, and the main assumption - that vertical velocities are negligible - is a large one potentially negating important flow characteristics (Betsholtz & Nordlöf, 2017).

Unsteady two-dimensional simulations in HEC-RAS rely on the Navier-Stokes Shallow Water equations, which assume that the flow in question is incompressible, has

uniform density, and exhibits hydrostatic pressure. In addition, the use of these equations assumes the vertical velocity length scale in question is much smaller than the horizontal scale (Brunner, HEC-RAS River Analysis System Hydraulic Reference Manual, 2016). These equations may be seen described in detail below.

$$\frac{\partial H}{\partial t} + \frac{\partial (hu)}{\partial x} + \frac{\partial (hv)}{\partial y} + q = 0 \tag{7}$$

$$\frac{\partial}{\partial t} \iiint_{\Omega} \, d\Omega + \iint_{S} \, V \cdot n dS + Q = 0 \tag{8}$$

$$\frac{\Omega(H^{n+1}) - \Omega(H^{n})}{\Delta t} + \sum_{k} V_k \cdot n_k A_k(H) + Q = 0 \tag{9}$$

$$\frac{DV}{dt} = \frac{\partial V}{\partial t} + V \cdot \nabla V = -g \nabla H + v_t \nabla^2 V - c_f V + f k \times V \tag{10}$$

$$g = g_0 \left( \frac{1 + k \sin^2 \varphi}{\sqrt{1 - e^2 \sin^2 \varphi}} \right) \tag{11}$$

$$v_t = D h u_* = D h \left( \frac{n \sqrt{g}}{R^{\frac{1}{6}}} |V| \right) \tag{12}$$

$$c_f = \frac{n^2 g |V|}{R^{\frac{4}{3}}} \tag{13}$$

$$f = 2\omega \sin \varphi \tag{14}$$

Equations (7) and (8) are the differential and integral forms of the Shallow Water mass conservation equations, respectively. Here, t is time, Ω is the three-dimensional space the water occupies, S denotes the side boundaries, and V is the velocity vector. Q is a source/sink term representing any additional inflows or outflows to the system (i.e. infiltration or evaporation), and ∇ is "the vector of the partial derivative operators given by ∇ = (∂/∂x, ∂/∂y)" (Brunner, HEC-RAS River Analysis System Hydraulic Reference Manual, 2016).

Equation (9) is another form of the mass conservation equation incorporating sub-grid bathymetry. It is recognized that appropriate mesh sizing may be much coarser than the grid on which bathymetry field data was recorded; therefore, HEC-RAS incorporates a sub-grid bathymetry approach to recognize smaller terrain features. Here, H represents water surface elevation, $V_k$ is the average velocity, $n_k$ is the normal vector, and $A_k(H)$ is the area of the cell face in terms of water surface elevation – all at cell face k.

Equation (10) is the differential vector form of the momentum conservation equation and includes acceleration ($\frac{\partial V}{\partial t}$ and $V \cdot \nabla V$), barotropic pressure ($-g\nabla H$), eddy turbulence ($v_t \nabla^2 V$), bed friction ($c_f V$), and Coriolis effect ($fk \times V$) terms. In addition to incorporating many of the variables listed above, the equation includes $v_t$, $c_f$, and fk, which represent the horizontal eddy viscosity, bottom friction, and Coriolis coefficients, respectively. Equation (11) is gravitational acceleration accounting for a non-horizontal ground surface including terms for latitude (φ), force of gravity at the equator ($g_0$), normal gravity constant (k = 0.0019318514), and e, the "square of the eccentricity of the Earth" (Brunner, HEC-RAS River Analysis System User's Manual, 2016).

Equations (12), (13), and (14) further define the variables seen in (10) and include the following: D, representing an empirical mixing constant; $u_*$, representing the shear velocity; R and S, the hydraulic radius and energy slope; V, the velocity vector magnitude; n, a roughness coefficient; φ, the latitude; and ω, the "sidereal angular velocity of the Earth" (Brunner, HEC-RAS River Analysis System Hydraulic Reference Manual, 2016).

If further physical flow constraints are assumed, a Diffusion Wave equation may be used to relate barotropic pressure gradient and bottom friction. This Diffusion Wave equation was used throughout all two-dimensional modeling procedures in this project. This equation replaces the momentum equations, and the resulting model is known as the Diffusion Wave Approximation of the Shallow Water Equations (Brunner, HEC-RAS River Analysis System Hydraulic Reference Manual, 2016). The equation for the velocity vector may be written in the following form:

$$V = \frac{-(R(H))^{\frac{2}{3}}}{n} \frac{\nabla H}{|\nabla H|^{\frac{1}{2}}} \tag{15}$$

Where R(H) is the hydraulic radius, ∇H is the water surface elevation gradient, and n is Manning's n. Here, flow and velocity are driven by pressure and bottom friction, and former terms denoting Coriolis effects, turbulence, advection, and unsteady effects may be eliminated. The resulting equation may be written as follows:

$$\frac{\partial H}{\partial t} - \nabla \cdot \beta \nabla H + q = 0 \tag{16}$$

Here, $\partial H / \partial t$ represents the change in water surface elevation over time, ∇H is the water surface gradient, and q is flow. To expand,

$$\beta = \frac{(R(H))^{\frac{5}{3}}}{n|\nabla H|^{\frac{1}{2}}} \tag{17}$$

Finally, to incorporate sub-grid bathymetry information into this model, (9) is modified to take the following form:

$$\frac{\Omega(H^{n+1}) - \Omega(H^n)}{\Delta t} - \sum_k \alpha \nabla H \cdot n + Q = 0 \tag{18}$$

Where $\Omega(H^n)$, Δt, and Q are as designated in (9), and

$$\alpha = \alpha(H) = \frac{(R(H))^{\frac{2}{3}} A_k(H)}{n|\nabla H|^{\frac{1}{2}}} \quad (19)$$

Boundary conditions are needed in unsteady flow modeling to establish time series physical conditions throughout the simulation. Boundary conditions may exist as water surface elevations ($H = H_b$), water surface slopes ($\nabla H \cdot n = S_b$), or flow rates ($V_b \cdot n_b A_b(H) = Q_b$).

When flow is deemed to be in a supercritical state, only a boundary condition at the upstream end of the system is necessary; when flow is subcritical, a boundary condition at the bottom of the system is needed. A mixed flow regime requires boundary conditions at all inflows and outflows to the system.

HEC-RAS Mesh Sizing

Terrain data must be subdivided into a grid-like structure, or mesh. Grid sizing is user-designated, and each cell is required to have no more than eight sides. Though the mesh has the capability to be structured or unstructured, a structured resolution is generally designated (i.e., cell size of 1 meter by 1 meter). At each cell, water surface elevations and pressures are computed at the center, while velocities are calculated in a perpendicular direction to cell faces.

HEC-RAS Numerical Methods

HEC-RAS two-dimensional unsteady flow models utilize numerical methods combining finite difference and finite volume schemes. In finite difference approximations, a derivative of a mathematical function is solved for by subtracting two known quantities, often involving time, water surface elevations, or velocities. HEC-RAS

approximates a directional derivative of a water surface function from adjacent cells 1 to 2 in the following manner:

$$\frac{\partial H}{\partial n\prime} \approx \frac{H_2 - H_1}{\Delta n\prime} \tag{20}$$

Where $H_1$ and $H_2$ are the water surface elevations in cells 1 and 2, respectively, and Δn' is the distance between the centers of cells 1 and 2.

This finite differencing technique would be sufficient if the directional derivative was perpendicular to the face between two cells, but this is not usually the case. This is where the finite volume technique is utilized. The general baseline equation for calculation of the water surface gradient using a finite volume approximation may be seen below.

$$\nabla H \approx \sum_j c_j H_j \tag{21}$$

Where ∇H is the gradient at a grid face for cell j, $H_j$ is the water surface elevation of the cell, and $c_j$ is a vector constant dependent on nearby grid geometry.

Equation (18) may be rewritten as

$$\Omega(H^{n+1}) + \theta \sum_j a_j H_j^{n+1} = d - (1-\theta) \sum_j a_j H_j^n \tag{22}$$

Where Δt represents the time step and θ is an implicit weight factor that is stable from 0.5 to 1. The term $a_j$ represents a multitude of coefficients dependent on α, Δt, and $c'_j$. Additionally,

$$d = \Omega(H^n) - \Delta t Q \tag{23}$$

Equation (22) is then rewritten in a more compact manner using vector notation:

$$\Omega(H) + \psi H = b \tag{24}$$

Where "Ω is the vector of all cell volumes, *H* is the vector of all cell water elevations at time n+1, ψ is the coefficient matrix of the system and *b* is the right-hand-side vector" (Brunner, HEC-RAS River Analysis System Hydraulic Reference Manual, 2016).

This setup is described as stable when $\theta < 0.5$ and

$$\frac{\Delta t}{(\Delta x)^2} < \frac{1}{2-4\theta} \tag{25}$$

And is "unconditionally stable" for $0.5 \leq \theta \leq 1$.

The solution algorithm as defined by Brunner in the HEC-RAS River Analysis System Hydraulic Reference Manual (2016) is defined as follows:

"1. The geometry, local orthogonality and sub-grid bathymetry data is obtained or pre-computed.

2. Solution starts with $H^0$ as the provided initial condition at time-step $\boldsymbol{n} = 0$.

3. Boundary conditions are provided for the next time step $\boldsymbol{n} + 1$.

4. Initial guess $\boldsymbol{H^{n+1}} = \boldsymbol{H^n}$.

5. Compute $\theta$-averaged water elevation $\boldsymbol{H} = (1-\theta)\boldsymbol{H_j^n} + \theta H_j^{n+1}$ and sub-grid bathymetry quantities that depend on it (face areas, fluid surface areas, hydraulic radii, Manning's $\boldsymbol{n}$, etc.).

6. The coefficients $\boldsymbol{a_j}$ are computed and the system of equations (23) is assembled.

7. The system of equations is solved iteratively using the Newton-like algorithm with the given boundary conditions to obtain a candidate solution $\boldsymbol{H^{n+1}}$.

8. If the residual (or alternatively, the correction) is larger than a given tolerance (and the maximum number of iterations has not been reached), go back to Step 5; otherwise, continue with the next step.

9. The computed $\boldsymbol{H^{n+1}}$ is accepted and the velocities $\boldsymbol{V^{n+1}}$ can be calculated using the discrete version of equation (15), using equations (20) and (21).

10. Increment ***n***. If there are more time steps go back to step 3, otherwise end."

Bypass Channel Model

To develop a two-dimensional model of the nature-like bypass, the following basic steps were taken. First, a terrain model was developed, and channel geometry was designated in Civil3D and imported to HEC-RAS. The terrain model was then used as a basis for the computational mesh, and the mesh was refined through a sensitivity analysis. Next, observed and best-fit interpolated data were used as the basis for model boundary conditions at inlets and outlets to the bypass. To calibrate the two-dimensional model, a one-dimensional channel model was developed; here, Manning's n was varied and calibrated to observed water surface elevations to minimize error. The two-dimensional model was finally computed, and velocity and depth results were analyzed. More details on each of these steps can be found in the following pages.

To begin, a one-dimensional hydraulic model was created to process flow data obtained by the slope-area method. The model encompassed four cross sections of the main bypass channel including A, A-Up, and A-Down, the locations of which can be seen in Figure 6. Cross sections were designated in HEC-RAS using station-elevation data and can be seen in Figure 10.

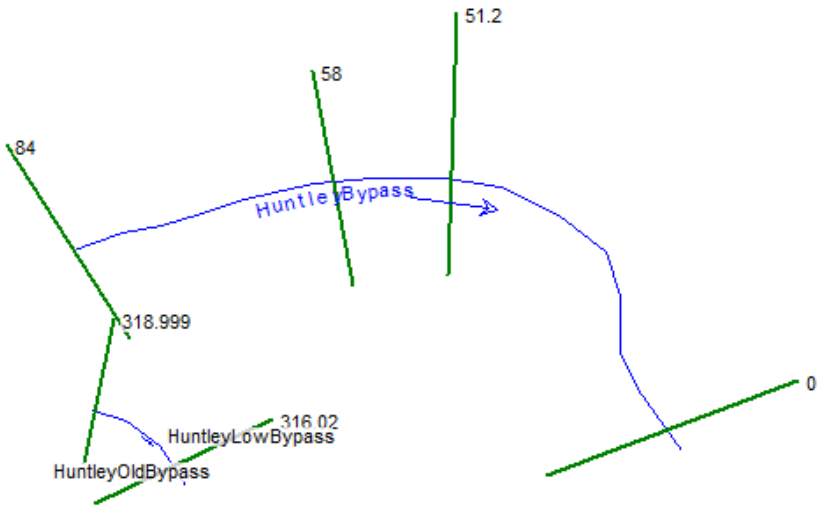


Figure 10. One-dimensional HEC-RAS model created to determine slope-area method flow rates.

Varying flow rates were tested in this model and calibrated with observed water surface elevations. Observed water surface elevations at cross section A-Up and the most downstream portion of the channel served as boundary conditions for these tests. For each pair of observed water surface elevations, test flow rates spanning the range of 3.68 to 12.74 $m^3/s$ were evaluated in the model. Total percent error, or the sum of the absolute values of water surface elevation errors at A and A-Down, was computed for each tested flow rate. The flow rate that minimized this total percent error was then determined and recorded, and this process was repeated for the next pair of observed water surface elevations. Observed and predicted water surface elevations, corresponding flow rates, and related percent error may be seen in Table 2.

Table 2. Observed and predicted water surface elevations and flow rates from the one-dimensional slope-area method model for the main bypass channel.

| Date | Observed WSE A (m) | Observed WSE A-Down (m) | Predicted WSE A (m) | Predicted WSE A-Down (ft) | Flow ($m^3/s$) | Total % Error |
|---|---|---|---|---|---|---|
| 5/15/19 | 918.83 | 918.81 | 918.83 | 918.76 | 6.82 | 0.03 |
| 5/16/19 | 919.00 | 918.97 | 919.00 | 918.95 | 7.42 | 0.01 |
| 5/21/19 | 918.87 | 918.84 | 918.87 | 918.80 | 6.68 | 0.03 |
| 5/21/19 | 918.85 | 918.83 | 918.85 | 918.80 | 5.97 | 0.02 |
| 5/22/19 | 918.82 | 918.77 | 918.82 | 918.75 | 6.68 | 0.02 |
| 5/22/19 | 918.81 | 918.79 | 918.81 | 918.74 | 6.17 | 0.03 |
| 5/28/19 | 918.89 | 918.86 | 918.80 | 919.10 | 3.68 | 0.29 |
| 5/28/19 | 918.95 | 918.94 | 918.80 | 919.10 | 3.68 | 0.19 |
| 6/13/19 | 919.11 | 919.09 | 919.11 | 919.01 | 11.27 | 0.01 |
| 6/27/19 | 918.89 | 918.88 | 918.89 | 919.83 | 6.74 | 0.03 |
| 7/17/19 | 918.78 | 918.73 | 918.78 | 918.70 | 6.34 | 0.02 |
| 7/18/19 | 918.75 | 918.71 | 918.75 | 918.65 | 6.68 | 0.04 |
| 7/24/19 | 918.47 | 918.38 | 918.47 | 918.27 | 4.76 | 0.09 |
| 7/25/19 | 918.47 | 918.46 | 918.47 | 918.28 | 4.73 | 0.16 |

This process was repeated for the slope-area method water surface elevation readings taken in the old bypass channel. Observed and predicted water surface elevation readings, corresponding flow rates, and total error may be seen in Table 3.

Table 3. Observed and predicted water surface elevations and flow rates from the one-dimensional slope-area method model for the old bypass channel.

| Date | Observed WSE D-Up (m) | Observed WSE D (m) | Predicted WSE D-Up (ft) | Predicted WSE D (ft) | Flow Rate ($m^3/s$) | Total % Error |
|---|---|---|---|---|---|---|
| 5/21/19 | 918.88 | 918.81 | 918.88 | 918.81 | 1.98 | 0.0009 |
| 5/22/19 | 918.87 | 918.74 | 918.87 | 918.74 | 2.24 | 0.0009 |
| 5/28/19 | 918.91 | 918.82 | 918.91 | 918.82 | 2.35 | 0.0009 |
| 6/13/19 | 919.05 | 919.04 | 919.05 | 919.04 | 1.42 | 0.0007 |
| 6/27/19 | 918.91 | 918.83 | 918.91 | 918.83 | 2.32 | 0.0009 |
| 7/17/19 | 918.85 | 918.75 | 918.85 | 918.75 | 1.98 | 0.0010 |
| 7/18/19 | 918.71 | 918.74 | 918.85 | 918.74 | 2.04 | 0.0010 |
| 7/24/19 | 918.71 | 918.58 | 918.71 | 918.58 | 1.22 | 0.0012 |
| 7/25/19 | 918.70 | 918.54 | 918.70 | 918.54 | 1.16 | 0.0051 |

The recorded GPS points were exported in a .csv file format from the Trimble TSC3 controller. Each individual point was exported as a PNEZD file containing the point number, northing, easting, elevation, and description (if entered). The .csv file was then imported to Civil3D, and a surface was created from the points. An aerial view of this surface can be seen in Figure 11.

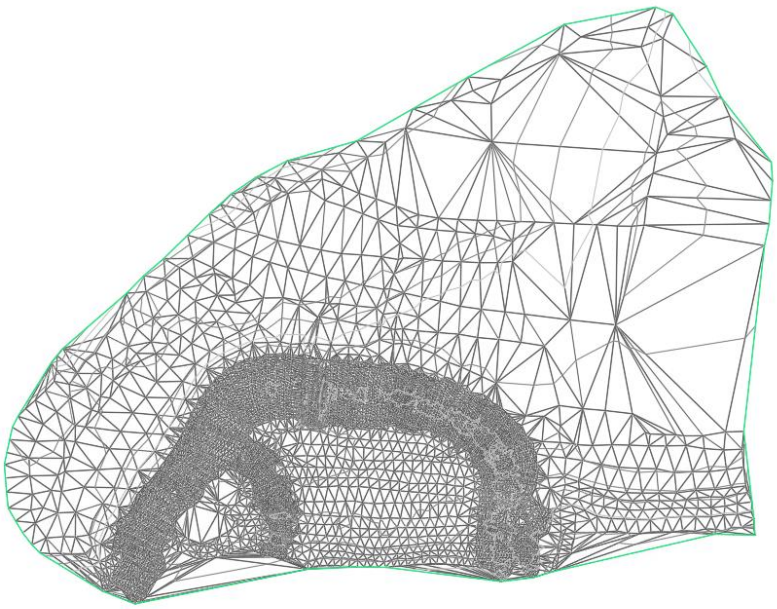

Figure 11. Civil3D surface created from GPS points taken at the Huntley Diversion fish bypass channel.

Once the surface was created, stream centerlines were drawn from downstream to upstream in the main and old bypass channels. These centerlines were converted to alignments, and multiple cross sections were drawn along both bypass channels. Care was taken to ensure cross sections were generally finely spaced and established perpendicular to the direction of flow in the channels. Cross sections were connected to the alignment, and bank lines were drawn parallel to the channel midline. The surface and

alignment were finally georeferenced with a NAD 1983 StatePlane Montana FIPS 2500 Feet projection and exported to HEC-RAS.

Stream centerline and station-elevation data were flipped using a public-domain Excel macro to ensure the exported CAD data would fit HEC-RAS stationing style. CAD geometry was imported in a GIS data format, and the spatial reference projection was once again designated as NAD 1983 StatePlane Montana FIPS 2500 Feet. A base terrain model was created using the exported GIS-format data, and the terrain model (as seen in RAS Mapper) is shown in Figure 12.

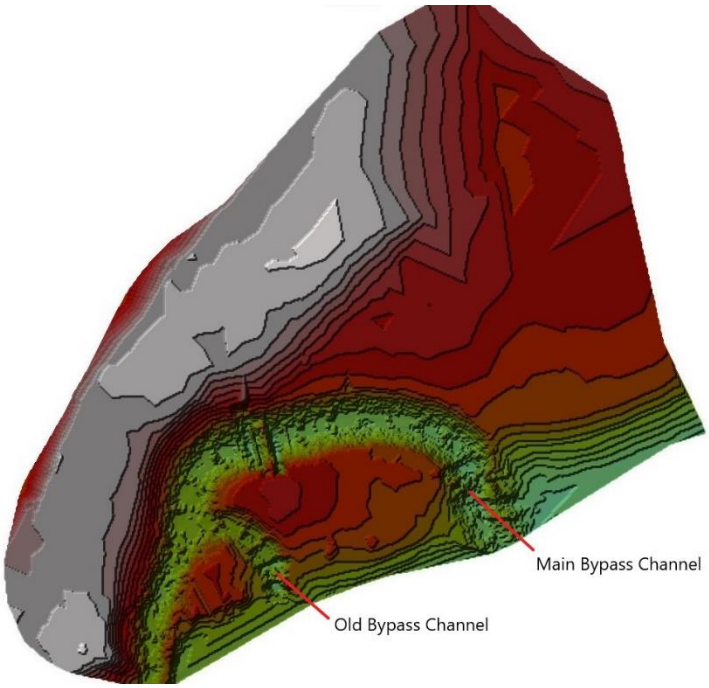


Figure 12. Base terrain and bathymetry model of bypass channel site, as seen in RAS Mapper.

The computational mesh for this two-dimensional channel model was developed using a finite volume modeling scheme. This allows for meshes to take an unstructured form and each mesh cell to have up to eight faces. These cell faces control the movement

of water throughout the entirety of the 2D modeling area using cell-specific elevation-volume relationships. At each cell, HEC-RAS pre-processes water surface elevation versus water volume, area, wetted perimeter, and Manning's n relationships in RAS Mapper using the base terrain model. An example of a water surface elevation-water volume relationship for a cell near the downstream channel exit is shown in Figure 13.

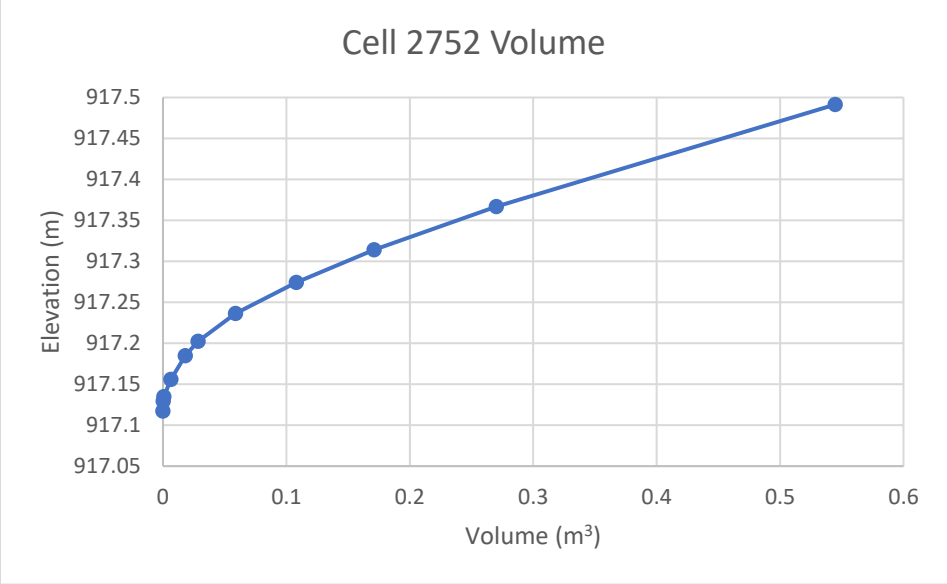


Figure 13. Elevation-volume relationship of cell located at downstream end of fish bypass channel.

Appropriate mesh cell sizing should be designated based on channel geometry - i.e., smaller sizing if the channel features sudden elevation changes, or larger sizing if the bed slope is generally very small.

To begin meshing, a 2D flow area polygon was drawn encompassing both the channel and a large part of the surrounding land mass. Break lines were next drawn to delineate the in-channel environment as well as any steep or sudden changes in elevation. The Manning's n value was set to 0.0733 in the main bypass channel and 0.0634 in the

old channel, the same roughness values previously calculated using the Wolman Pebble Count method. Finally, the 2D flow area polygon was filled with a structured computational mesh in a grid-like pattern.

A mesh sensitivity analysis was performed to determine a sizing that would both reduce computation time and provide detailed velocity outputs at each cross section. Mesh sizes of 6.096 by 6.096 meters created issues with mesh cells touching two boundary condition lines at the same time; even at this sizing, flow characteristics in the bypass did not change. A mesh cell sizing of 1.524 meters by 1.524 meters was deemed appropriate to visualize multiple velocity output values across one cross section while reducing computation time. This final computational mesh grid can be seen in Figure 14.

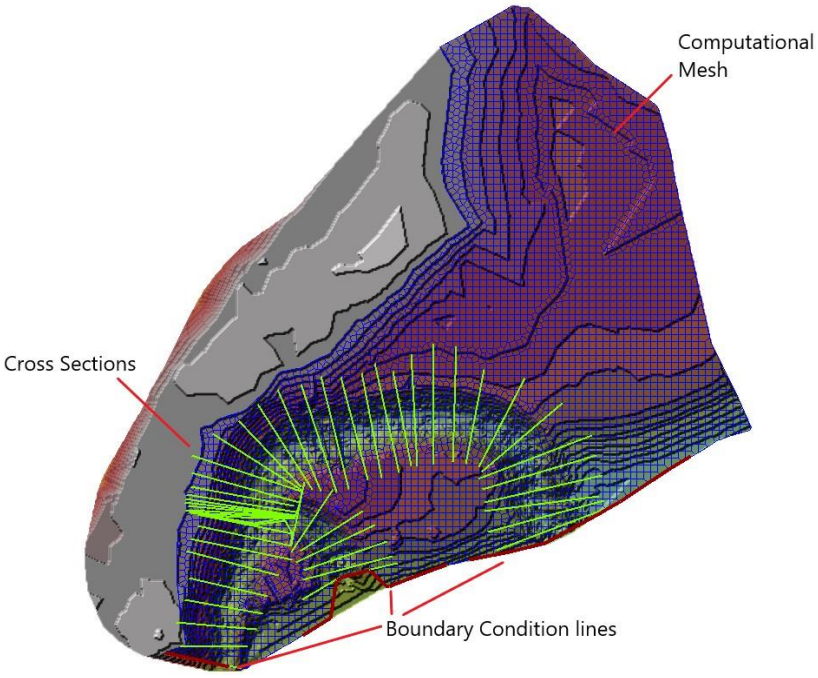


Figure 14. Computational mesh used in two-dimensional bypass channel flow model.

External 2D flow area boundary conditions were designated at the most upstream and downstream portions of the main bypass channel and the downstream flow exit of the old bypass channel. A flow hydrograph boundary condition was imposed at the most upstream portion of the main bypass channel, while stage hydrograph boundary conditions were used at the most downstream cross sections of the old and main bypass channels. These hydrograph time series data were entered on 24-hour intervals from the field season start date of April 18th through the end date of November 5th. Data at the downstream flow exits for the old and main bypass channels were designated using field survey "WSE Weir" and "WSE Down" readings, respectively.

Multiple linear regression relationships were developed to best fit model inputs to observed field data points. These relationships were developed between the following parameters:

- Cross section A flow and USGS Yellowstone River Gage 06214500 flow
- Old bypass flow and cross section A flow
- Water surface elevations at the downstream fish entrance to the main bypass and cross section A flow
- Water surface elevations at the downstream entrance to the old bypass and old bypass flow

To develop flow hydrograph time series data for the upstream end of the main bypass channel, observed flow data at cross section A and corresponding daily flow data for USGS Yellowstone River Gage 06214500 were collected. Each set of flow data was natural log-transformed, and a linear regression analysis was performed on this transformed data. Coefficients of best fit were developed and determined to be 1.47 and -7.38 with $R^2$ and p-values of 0.9274 and 4.1E-11, respectively, leading to the following relationship:

$$\ln(Lower\ Bypass\ Flow) = 1.47[\ln(Yellowstone\ River\ Flow)] - 7.38 \quad (26)$$

Remaining gaps in the measured time series flow hydrograph could then be filled using publicly available daily flow averages from USGS Gage 06214500. All observed and best fit flow values can be seen in Figure 15.

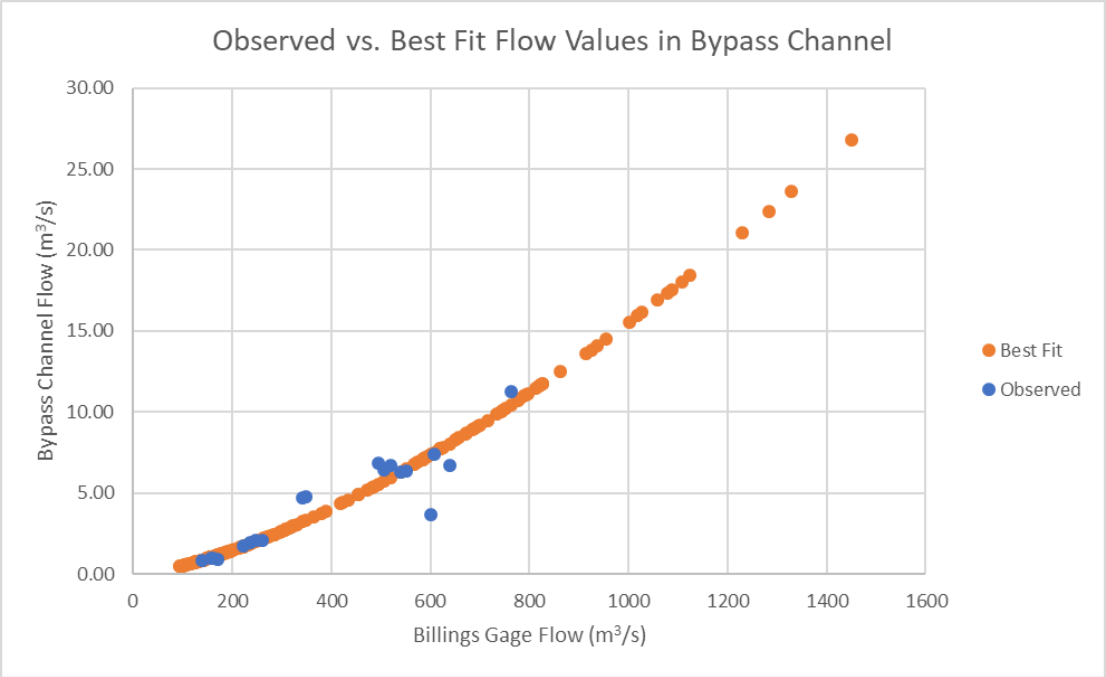


Figure 15. Observed and best fit values for flow through main nature-like bypass channel.

Next a linear regression analysis was performed on natural log-transformed lower bypass and old bypass flow data. Best fit coefficients here were found to be 1.49 and -2.17 with $R^2$ and p-values of 0.8311 and 1.4E-05, respectively, leading to the following equation relating lower bypass and old bypass flows:

$$\ln(Old\ Bypass\ Flow) = 1.49[(Lower\ Bypass\ Flow)] - 3.90 \quad (27)$$

Using this relationship, a theoretical flow rate through the lower bypass could be developed for every day throughout the field season of April 18th through November 5th.

Flow hydrographs in the lower and old bypass channels could then be summed to create the upstream inflow hydrograph boundary condition data. These theoretical flow rates may be seen in their entirety in Appendix D.

Linear regression analyses were also performed to fill in any gaps in stage hydrograph time series data. The following relationships were developed to fill in these data gaps:

$$\ln(WSE\ Down) = 0.00049[\ln(Lower\ Bypass\ Flow)] + 6.82 \quad (28)$$

$$\ln(WSE\ Weir) = 0.00034[\ln(Old\ Bypass\ Flow)] + 6.82 \quad (29)$$

Once the two-dimensional model was run, errors between observed and modeled stage readings at the most upstream and downstream portions of the bypass were determined and recorded.

To minimize error, a Monte Carlo analysis was then performed using Manning's n. This analysis relies on randomly sampling from normally distributed known data points and running many model simulations to determine the random observed value where error is at a minimum. Observed field substrate sizes obtained during the Wolman Pebble Count and corresponding individual Manning's n roughness values were put into a random number generator, and 50 unique Manning's n test values were generated. These Manning's n values spanned from 0.0507 to 0.1070 and were applied to both the main and old bypass channels. Each Manning's n value was tested in a one-dimensional HEC-RAS representation of the Huntley nature-like bypass channel, which may be seen in Figure 16.

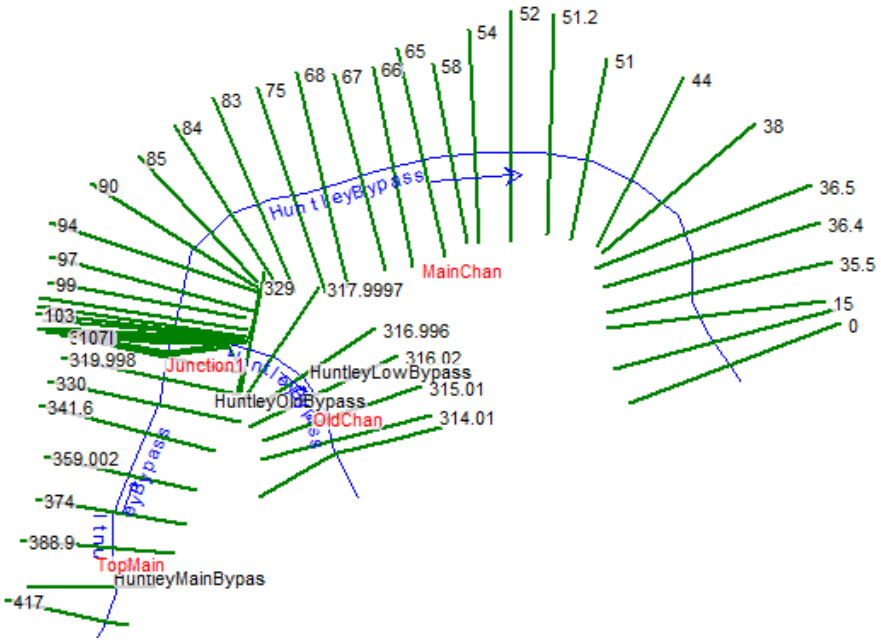


Figure 16. One-dimensional bypass channel model used to test fifty random Manning's n roughness values.

Absolute error between observed and modeled water surface elevations was then calculated for each tested Manning's n value, and these values may be seen in Figure 17. The outlying value not following the U-shape data trend in Figure 17 represents the error resulting from the original Manning's n test values. These values were 0.073 and 0.063 in the main and old bypass channels; when the Monte Carlo analysis was performed, Manning's n values were kept constant throughout both bypass channels.

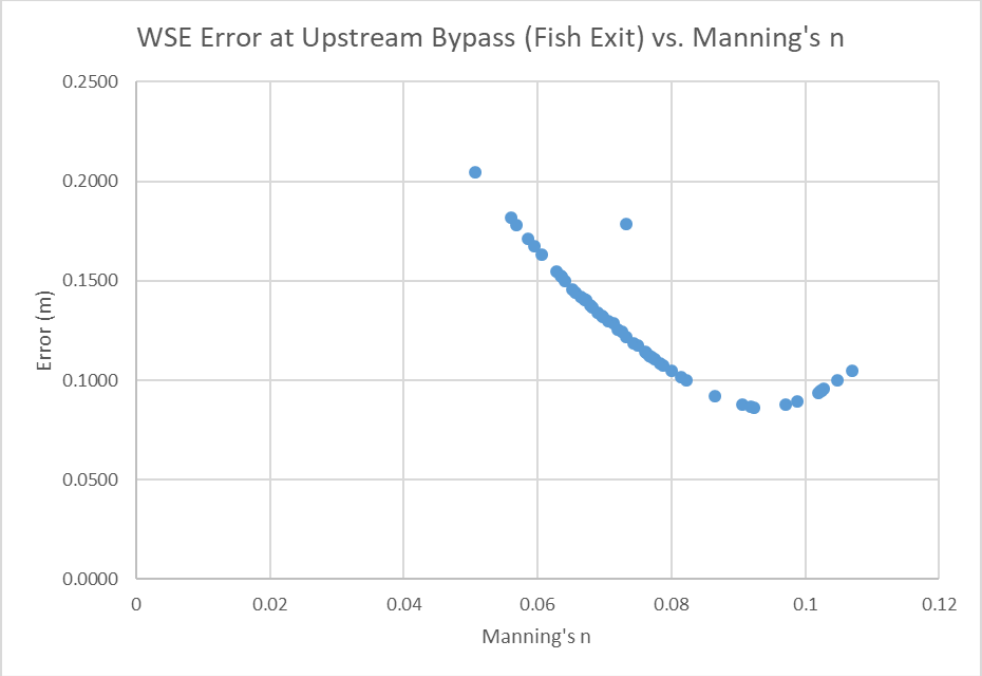


Figure 17. Absolute error between observed and modeled water surface elevations at each tested Manning's n roughness value.

The Manning's n value resulting in the minimum error was then identified, and the two-dimensional bypass channel model was rerun with this roughness value. Differences between observed, best fit, and model output flow data were then plotted, and peak and low flow values were reported.

Due to observed flow behavior in the field, it was determined that the most upstream portion of the main bypass channel would likely present the most difficulty for fish to successfully pass through and out of the bypass. An example of this flow behavior, including a large standing wave cresting over the "weir" near the bypass exit, may be seen in Figure 18.

Figure 18. Flow behavior at most upstream end of bypass channel, including wave cresting over upper "weir".

Because of this behavior, model velocity map outputs were analyzed at the two most upstream cross sections, and mesh cells with the lowest velocities at these locations were identified. These minimum cross-sectional velocity readings were recorded for each day and compared against species-specific swimming capabilities from literature. Each corresponding flow rate through the modeled hydrograph was then given a “Pass” or “No Pass” metric and plotted in green circles and red triangles for ease of visualization.

Two-Dimensional Attraction Flow Model

A two-dimensional model was created to visualize and quantify the interaction between downstream bypass channel outflow and the Yellowstone River. This model utilized the base terrain surface from the two-dimensional bypass channel model but

added additional geometry to create an “idealized” Yellowstone River base terrain surface as well. Yellowstone River terrain points were interpolated using dam height, bank slope, channel slope, and an assumed trapezoidal channel shape. Points were interpolated in a PNEZD format and imported to Civil3D, where alignments and cross sections were designated in a similar manner to the bypass channel model. The final base terrain surface, including the bypass channel and the Yellowstone River below the Huntley Dam, may be seen in Figure 19.

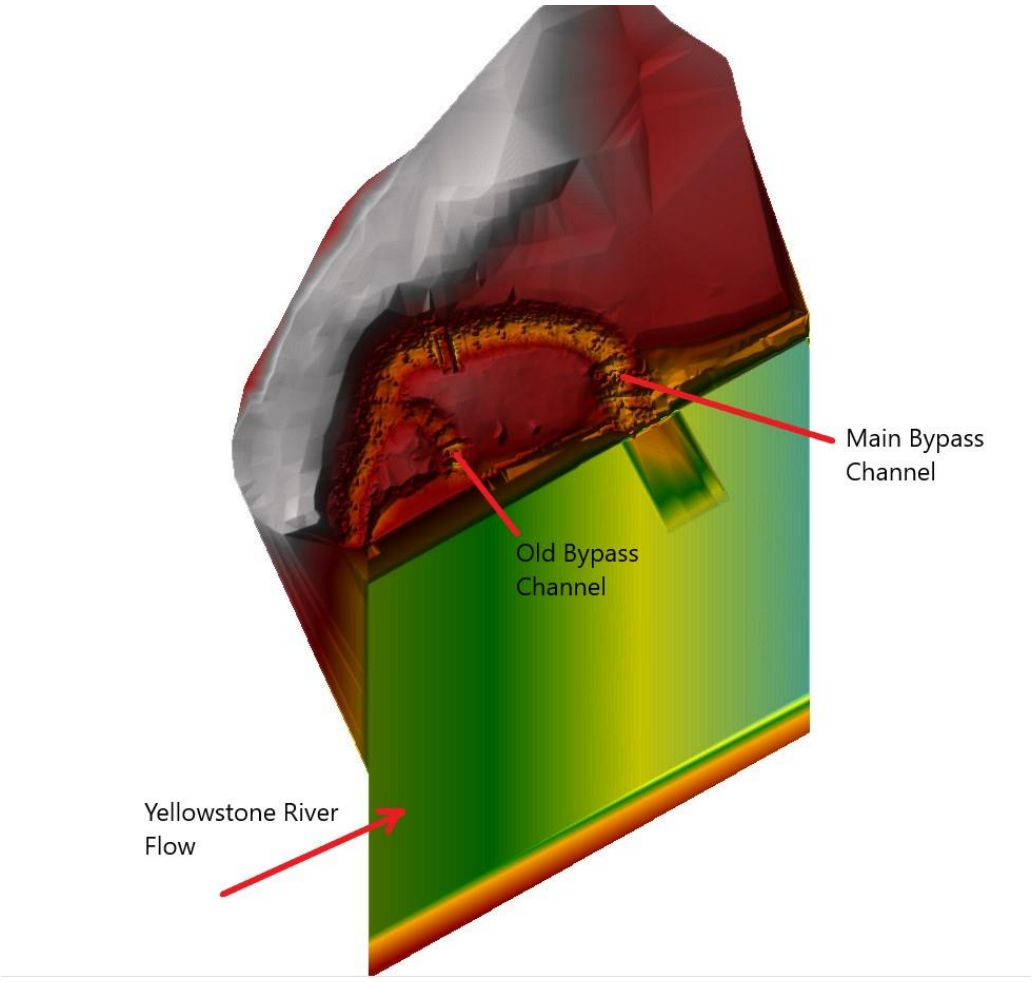


Figure 19. Attraction flow model base terrain surface, including Huntley bypass channel and Yellowstone River.

Break lines were designated at significant elevation changes, and the computational mesh consisted of nominally 1.524 meter by 1.524-meter cells. Manning's n values were set to 0.0923 and 0.03596 for the bypass channel and Yellowstone River, respectively. This latter value was developed from a range within Table 5-6 in Chow (1959) referencing large main channels with characteristics described as "clean, straight, full stage, no rifts or deep pools… stones and weeds". A sensitivity analysis was performed using 50 randomly generated Manning's n values between 0.03 and 0.04; the resulting Manning's n of 0.03596 produced only 0.00061 meters of water surface elevation error at the downstream end of the Yellowstone River reach.

Boundary conditions were specified at the midpoint of the bypass channel and the most upstream and downstream cross sections of the idealized Yellowstone River reach. The bypass channel upstream boundary utilized a flow hydrograph condition at three different time periods to ideally encompass middle, lowest, and highest observed onsite flow rates.

The period encompassing the lowest flow rates including three days (August 20, 21, and 23) when flow was observed and one interpolated data point (August 22). Observed flow readings from May 21 and 22 were used to represent the highest observed onsite flow, and data from July 24 and 25 were used as "average" flow points.

The upstream Yellowstone River boundary utilized a flow hydrograph boundary condition, and the downstream Yellowstone River cross section utilized "WSE Tree" readings as a stage hydrograph boundary condition. The final model setup, including the

base terrain surface, breaklines, mesh, cross sections, and boundary conditions, may be seen in Figure 20.

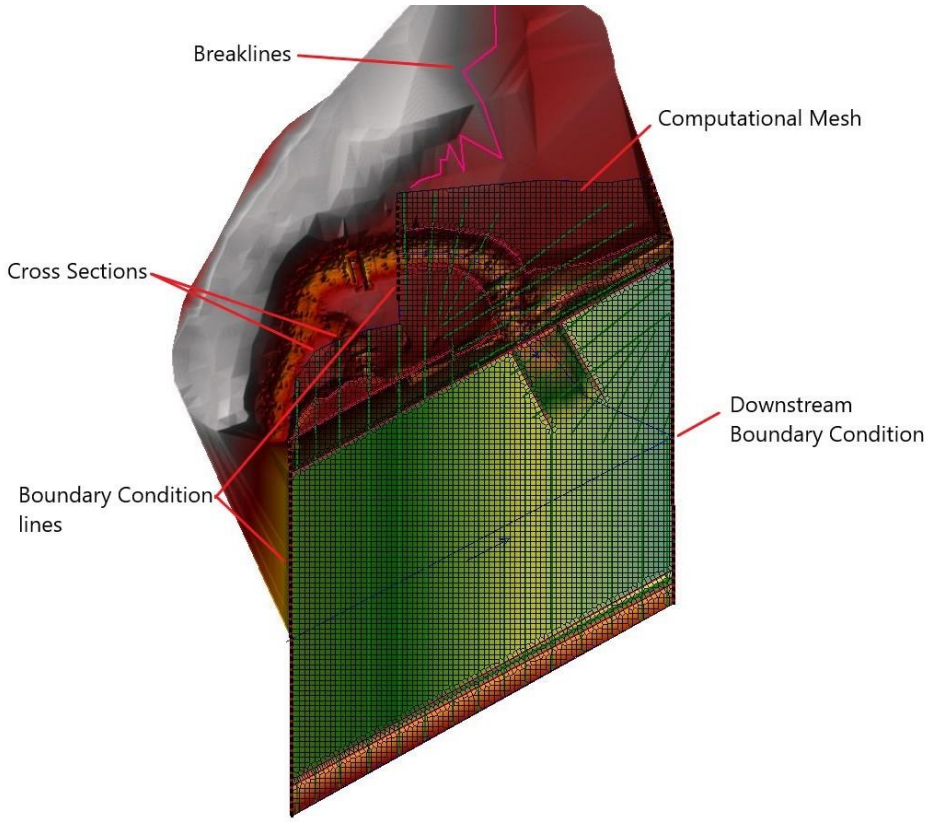


Figure 20. Final attraction flow model setup, including base terrain, cross sections, breaklines, mesh, and boundary conditions.

Initial conditions were determined using the USGS Yellowstone River Gage 06214500 flow recordings from each of the three modeled periods. This two-dimensional attraction flow model was then run on a 1-minute computational interval, and flow interaction at the bypass channel and river junction was observed at peak, low, and "average" flows throughout the bypass hydrograph. Flow interactions were monitored for disorienting hydraulic characteristics, and final fish attraction flow to the Huntley nature-like fish bypass was estimated.

# RESULTS AND DISCUSSION

To estimate attraction and passage at the Huntley Diversion nature-like bypass, field measurements, hydraulic model results, and design recommendations from literature were analyzed. Field measurements were first tabulated and if necessary, used in the creation of the two-dimensional nature-like bypass model. Velocity, depth, and flow results from the two-dimensional bypass model were then analyzed and compared to recommendations and species-specific swimming capabilities from literature. Finally, results from the attraction flow model were analyzed for disorienting hydraulic characteristics, and attraction to the bypass entrance was estimated at varying flow rates. Each of these analysis processes are discussed at length in the following sections.

## Field Measurement Results

Measured water surface elevations for WSE Up, WSE Down, WSE Weir, and WSE Tree were recorded throughout the field season from April 18$^{th}$ to November 5$^{th}$, 2019. These points correspond to the most upstream and downstream cross sections of the main bypass, the most downstream cross section of the old bypass, and far downstream of the bypass along the Yellowstone River, and these measurements may be seen in Appendix D.

Staff gage observations were recorded onsite at Wells A, B, C, D, A2, B2, C2, and D2. If the well tipped due to a high water event, a gage reading was not recorded. Figures in Appendix D illustrate these observations, which are relative to a specified base point at each well.

All measured bypass channel flow rates may be seen tabulated in Table 4. These flow rates were measured at cross section A in the main bypass channel and were obtained by one of three methods (Midsection, Float-Area, or Slope-Area). Each bypass channel flow rate may be seen with its corresponding method of obtainment and daily recorded flow at Yellowstone River Gage 06214500.

Table 4. All measured flow rates at cross section A of Huntley Bypass, methods of measurement, and corresponding daily Gage 06214500 flow readings.

| **Date** | **Measured Huntley Lower Bypass Flow Rate ($m^3/s$)** | **Method of Measurement** | **Average Yellowstone River Billings Gage Flow ($m^3/s$)** |
|---|---|---|---|
| 4/18/19 | 0.98 | Midsection | 161.69 |
| 4/29/19 | 0.97 | Midsection | 157.16 |
| 5/2/19 | 2.10 | Midsection | 247.63 |
| 5/3/19 | 1.96 | Midsection | 235.45 |
| 5/6/19 | 1.74 | Midsection | 221.58 |
| 5/8/19 | 2.10 | Midsection | 261.51 |
| 5/15/19 | 6.82 | Slope-Area | 495.54 |
| 5/16/19 | 7.42 | Slope-Area | 607.40 |
| 5/21/19 | 6.33 | Slope-Area | 539.44 |
| 5/22/19 | 6.43 | Slope-Area | 506.87 |
| 5/28/19 | 3.68 | Slope-Area | 601.73 |
| 6/13/19 | 11.27 | Slope-Area | 763.14 |
| 6/27/19 | 6.74 | Slope-Area | 638.54 |
| 7/17/19 | 6.34 | Slope-Area | 550.76 |
| 7/18/19 | 6.68 | Slope-Area | 521.03 |
| 7/24/19 | 4.76 | Slope-Area | 348.30 |
| 7/25/19 | 4.73 | Slope-Area | 342.63 |
| 8/9/19 | 0.94 | Midsection | 170.75 |
| 8/20/19 | 0.82 | Float | 138.61 |

A rating curve was developed from measured flow rate and stage readings at cross Section A. These stage readings were obtained using staff gage readings (Appendix D) or

slope-area water surface elevation measurements (see Table 2) and were all in relation to the minimum cross section elevation. This rating curve may be seen in Figure 21. Logger depth data was not used as the primary source for these rating curves as most stilling wells tipped and were submerged in May 2019. These wells were reset when the wells were safely accessible in July 2019, and the HOBO loggers resumed their pressure, temperature, and depth measurements. Additional rating curves developed from measurements at cross sections B, C, and D may be seen in Appendix E.

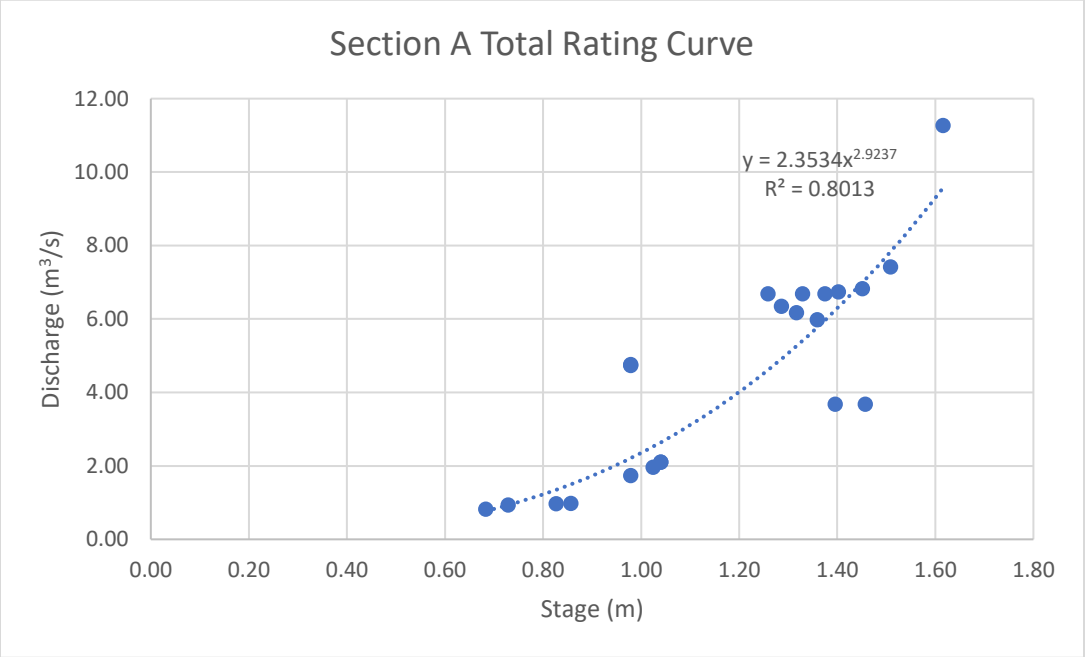


Figure 21. Rating curve composed of measured flow rates and stage readings at cross section A in main Huntley bypass channel.

## Bypass Model Results and Comparison to Metrics from Literature Review

Equations (26) and (27) were used to obtain best-fitting flow rate data for the Huntley bypass channel at cross section A and in the old bypass channel, respectively. These fitted flow rates were plotted against measured flow rates and may be seen in

Figures 22 and 23. Fitted flows for the entirety of the modeled hydrograph may also be seen in Appendix F.

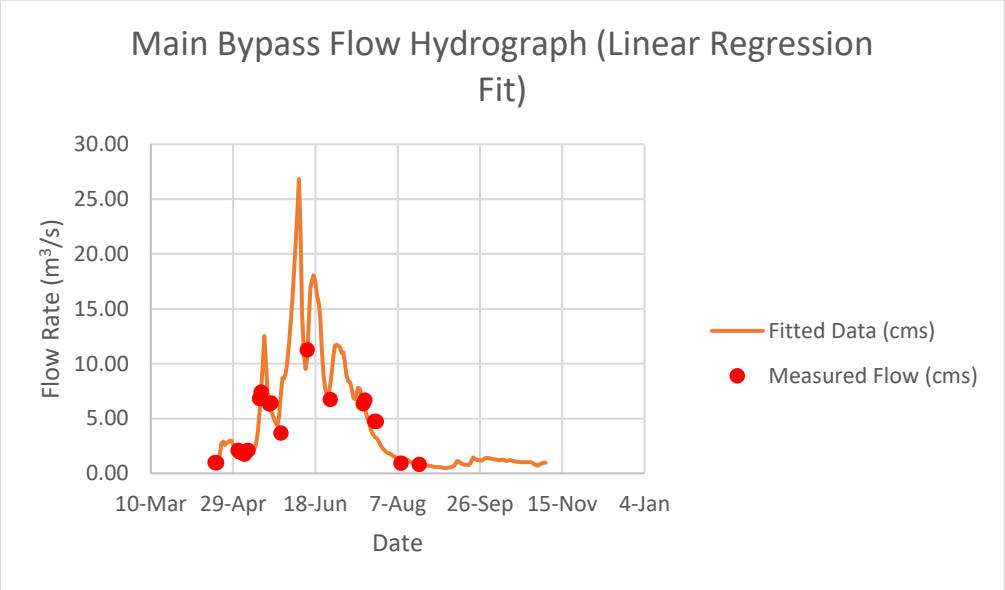


Figure 22. Huntley main bypass flow rate fitted values versus measured values.

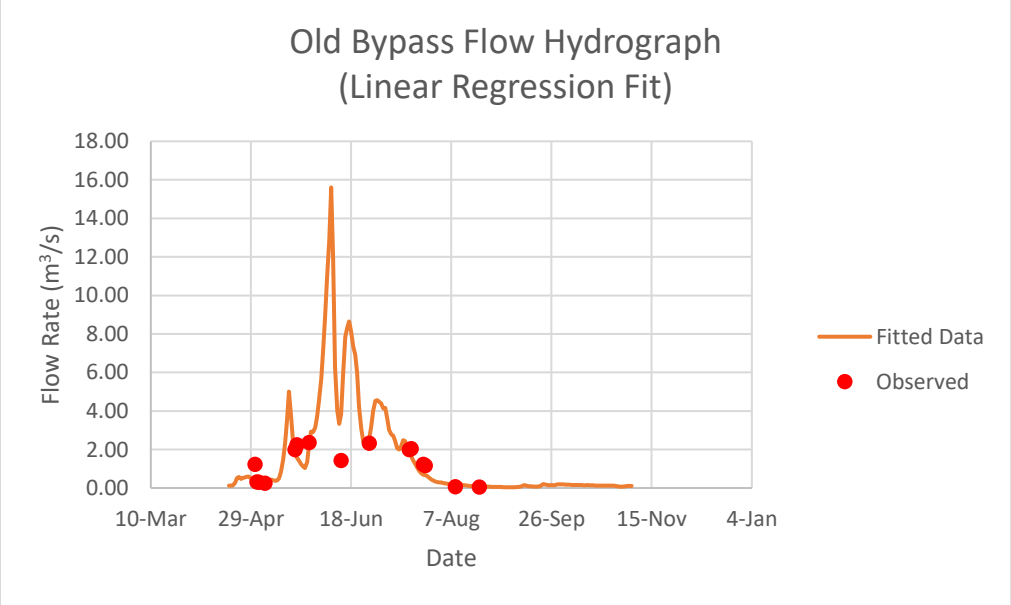


Figure 23. Huntley old bypass flow rate fitted values versus measured values.

The fitted flow rates seen in Figures 22 and 23 were added together to calculate inflow values at the most upstream cross section of the nature-like bypass. These flow rates were utilized as an upstream flow hydrograph boundary condition with data points on 24-hour intervals. Downstream stage boundary conditions were developed using fitted data from (28) and (29).

Initial iterations of the model used Manning's n roughness values of 0.0733 and 0.0634 in the main and old bypass channels, respectively. Resulting average absolute error between observed and modeled water surface elevations at the most upstream cross section of the channel was calculated to be 0.16 meters. Average error at the most downstream cross section of the main bypass channel was calculated at 0.10 meters, and average error at the downstream entrance to the old bypass channel was calculated to be 0.13 meters. A Monte Carlo analysis was then performed to determine a Manning's n value minimizing water surface elevation error; this value was found to be 0.09 in both the old and main nature-like bypass channels.

The two-dimensional bypass model was then re-run with this new Manning's n roughness value applied to both the main and old bypass channels. Resulting average water surface elevation errors at the most downstream cross sections of the old and main bypass channels remained constant at 0.13 and 0.10 meters, while error at the most upstream cross section of the main bypass was minimized to 0.09 meters. Observed versus resulting modeled water surface elevations at these three locations may be seen in Figures 24, 25, and 26.

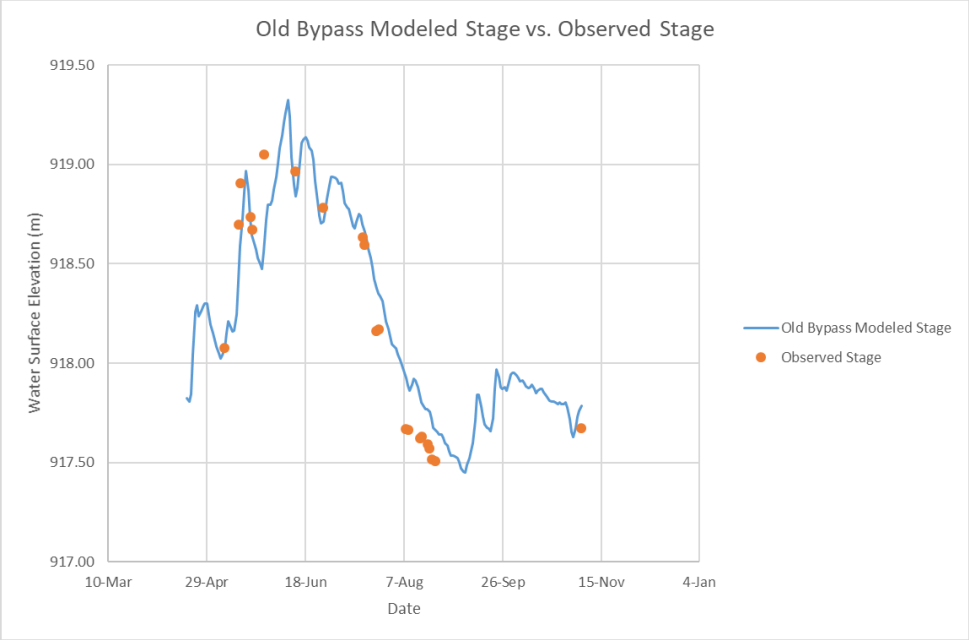


Figure 24. Observed and resulting modeled water surface elevation values at the most downstream cross section of the old bypass.

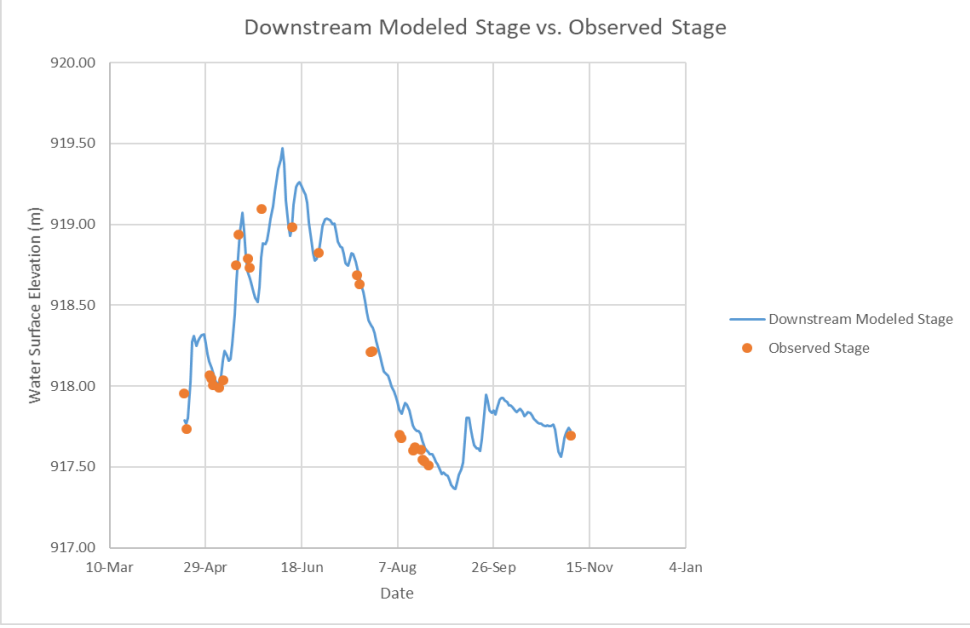


Figure 25. Observed and resulting modeled water surface elevation values at the most downstream cross section of the main bypass.

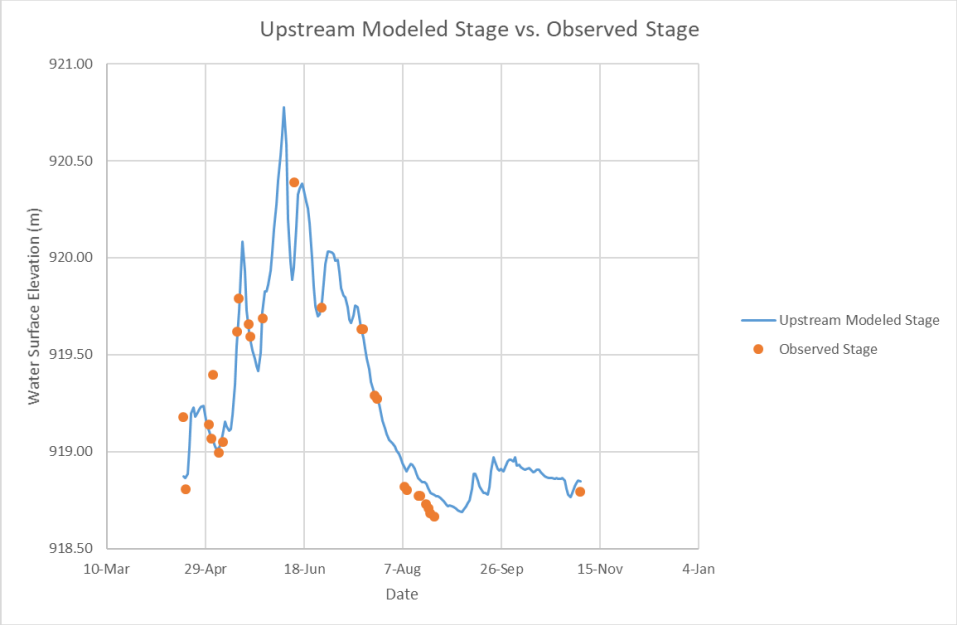


Figure 26. Observed and modeled water surface elevation values at the most upstream cross section of the bypass channel.

Resulting hydrographs of observed, fitted, and modeled flow rates through the old and main bypass channels were plotted against each other and may be seen in Figures 27, 28, and 29.

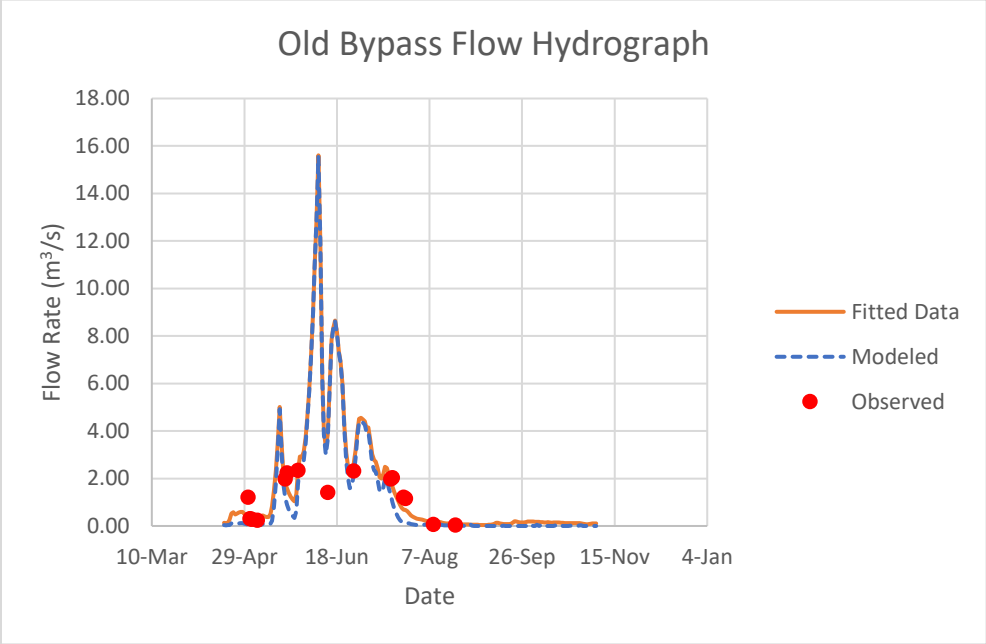


Figure 27. Observed, fitted, and resulting modeled flow rates through the old nature-like bypass channel.

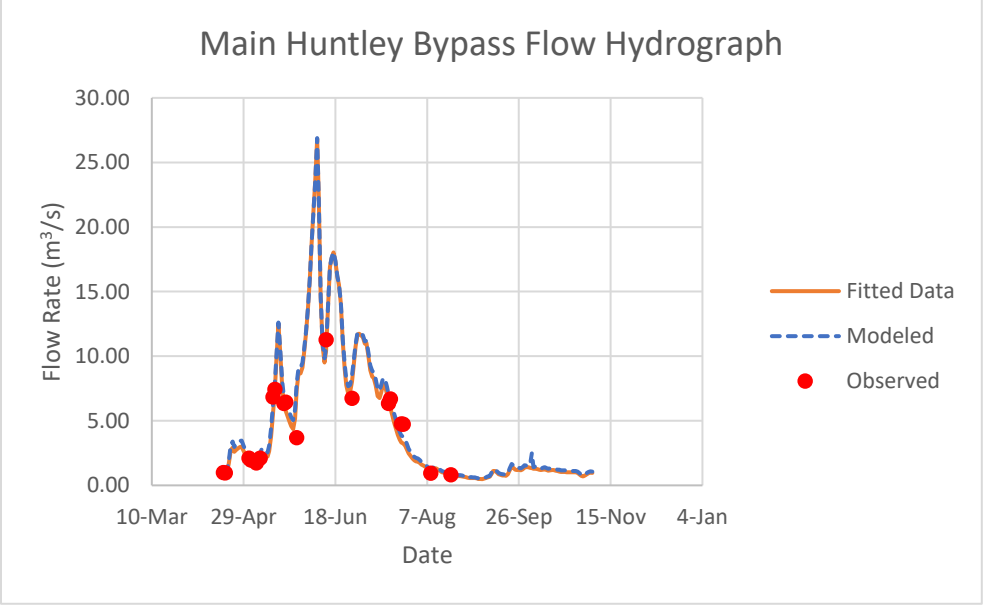


Figure 28. Observed, fitted, and resulting modeled flow rates through the lower Huntley bypass channel.

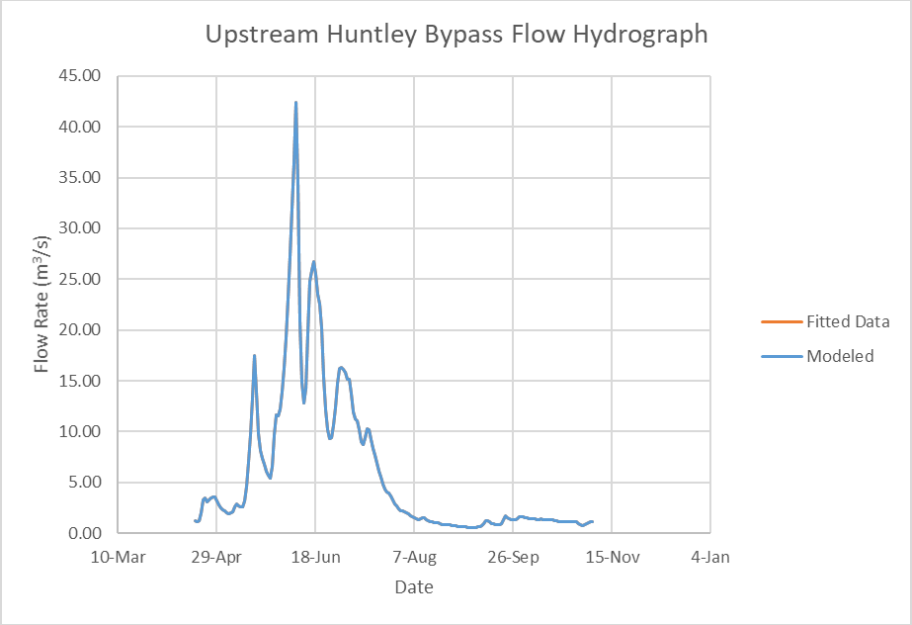


Figure 29. Fitted and modeled flow rates (identical) into the most upstream cross section of the Huntley nature-like bypass channel.

Model output indicated a peak flow rate of 42.43 $m^3/s$ into the most upstream cross section of the main nature-like bypass channel. This occurred on June 8$^{th}$, 2019 in accordance with readings from the Yellowstone River USGS Billings Gage 06124500. Of this 42.43 $m^3/s$, the model showed 26.89 $m^3/s$ flowed into the main bypass channel, while 15.54 $m^3/s$ flowed into the old bypass channel. Low flow of 0.52 $m^3/s$ occurred on September 6, 2019; all this flow remained in the main bypass channel, and the old bypass channel was dry.

Results from this two-dimensional model were next compared to metrics from literature detailing fishway hydraulic characteristics likely to promote fish passage success. Santos et al. (2005) analyzed passage of eight morphologically diverse species through a nature-like bypass on a Portuguese lowland river; the site exhibited similar

channel widths (~ 6 m) and substrate characteristics to the Huntley bypass. Researchers determined water depths of at least 0.40 meters were optimal to provide all species with adequate resting locations as they ascended the bypass. To determine if this metric was met, distance from water surface to thalweg, the deepest portion of the cross section, was computed at each cross section every day of the modeled hydrograph. Minimum water depths at each cross section were then determined.

All but one of the cross sections of the upper Huntley bypass met the 0.40-meter minimum depth metric, but seven of the cross sections in the main Huntley bypass did not. Cross sections not meeting the minimum depth metric were denoted with red circles in Figure 30. Minimum depths recorded at each of these cross sections and their respective dates are listed in Table 5.

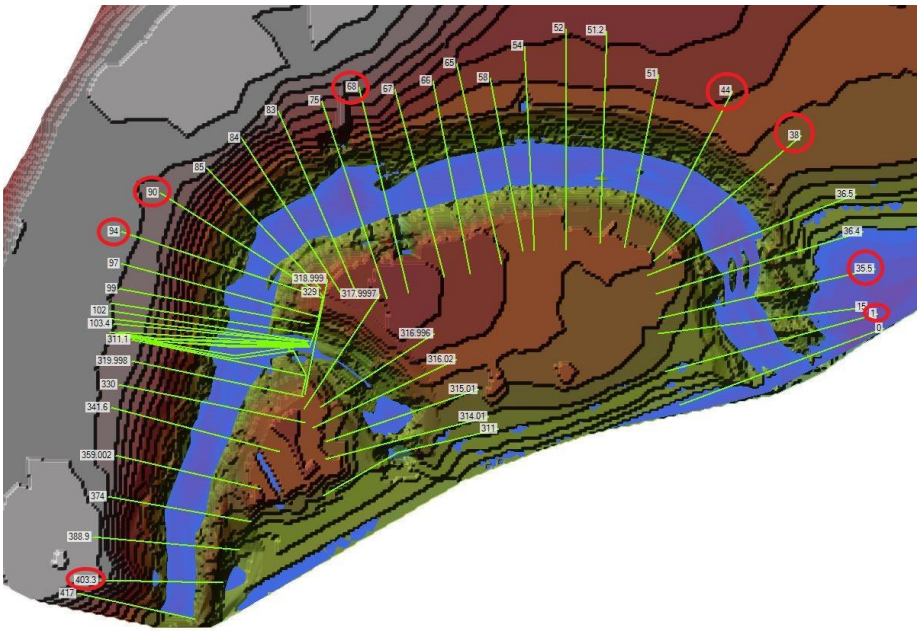


Figure 30. Cross sections not meeting the minimum depth metric (red circles) determined by Santos et al. (2005) at some point throughout the modeled hydrograph.

Table 5. Cross sections not meeting the minimum depth metric from Santos et al. (2005), minimum depths recorded, and date of occurrence.

| River Station Number | Minimum Depth Recorded (m) | Date Recorded |
|---|---|---|
| 403.3 | 0.332 | September 5, 2019 |
| 94.0 | 0.290 | August 27, 2019 |
| 90.0 | 0.226 | September 6, 2019 |
| 68.0 | 0.341 | August 27, 2019 |
| 44.0 | 0.354 | September 5, 2019 |
| 38.0 | 0.360 | September 6, 2019 |
| 35.5 | 0.296 | September 6, 2019 |
| 1.0 | 0.265 | September 6, 2019 |

Table 5 shows all cross sections that exhibited depths shallower than 0.40 m experienced these shallow depths during the period of August 27 – September 6, 2019. River Station 90, which is located just downstream of the junction between the main and old bypass channels, experienced the lowest recorded water depth at 0.226 meters. These cross sections may all create depth barriers to upstream fish passage during this low flow period; specifically, fish species may lack adequate resting locations as they ascend the bypass. However, the majority of the species in the Huntley bypass study primarily exhibit upstream movement during the months of May, June, and July, and the species-specific biological implications of these shallow water depths may necessitate further study.

Santos et al. (2005) also recommended optimal bypass discharges of 0.1 to 0.2 $m^3/s$ per meter of channel width to promote successful fish passage through a nature-like bypass. Hydraulics at two of the most upstream and downstream cross sections of the bypass channel were analyzed; for each day throughout the modeled hydrograph, flow rate at each cross section was divided by the top width of the inundated channel.

Discharge per meter of channel width at the upstream (RS 403.3) and downstream (RS 1) cross sections can be seen in Figures 31 and 33. Optimal bypass discharge ranges of 0.1 to 0.2 $m^3/s$ are bounded by the straight green lines in the figures.

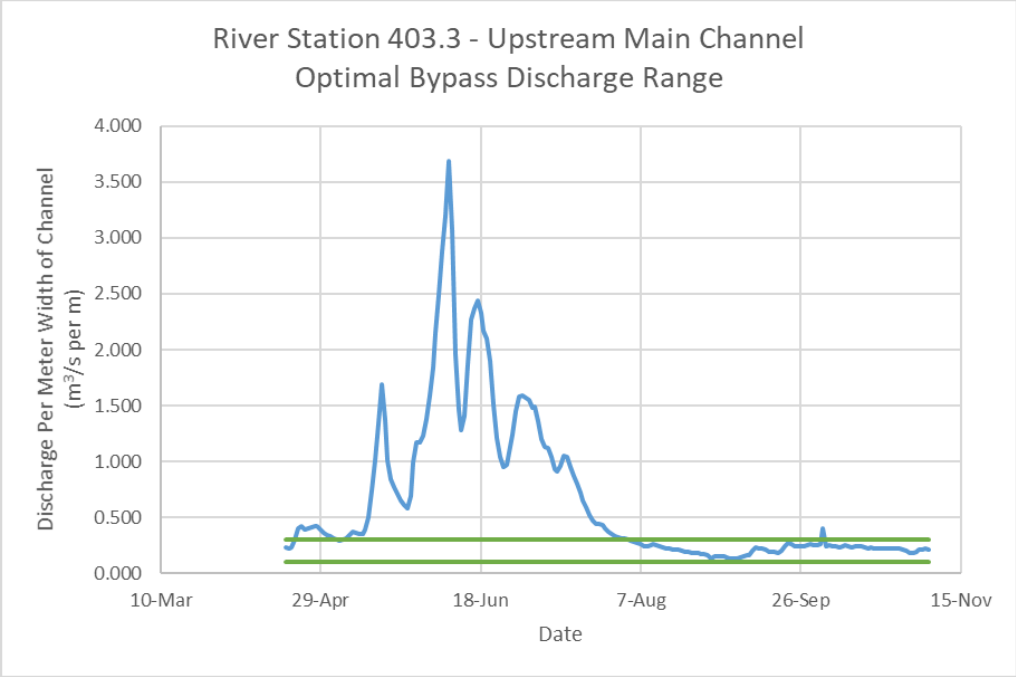


Figure 31. Discharge per meter of channel width at River Station 403.3 and optimal range bounded by green lines.

These elevated discharge ranges are likely due to the narrow shape of the channel at the most upstream portion of the bypass and the lack of large bed roughness elements present. A cross-sectional depiction of River Station 403.3 may be seen in Figure 32.

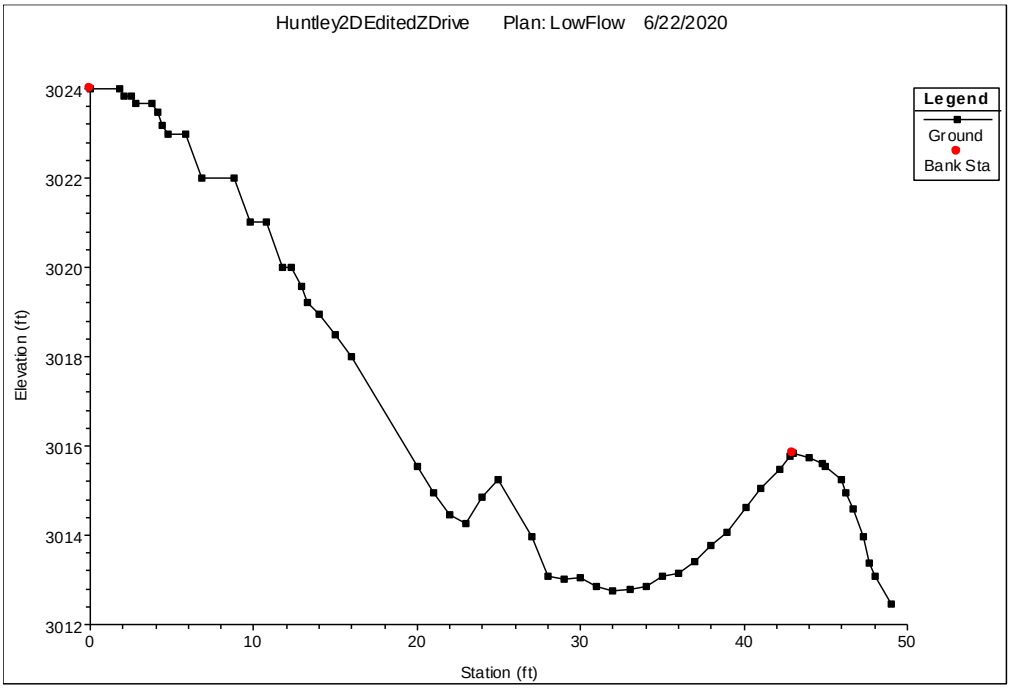


Figure 32. Cross-sectional depiction of River Station 403.3 located at upstream end of Huntley bypass channel.

Discharge per meter of channel width at River Station 403.3 regularly rises well above the suggested Santos et al. metric in early season but generally meets the guidelines from August 7 to November 5, 2019. Discharge per meter of channel width at River Station 1 is within the suggested guidelines near the beginning and midpoint of the modeled hydrograph but falls beneath the suggested range from August 7-November 5, 2019. Discharges above 0.1-0.2 $m^3/s$ per meter of channel width may cause velocities too high for fish to successfully ascend the bypass, while discharges below this metric may not provide adequate characteristics to attract fish to the bypass entrance.

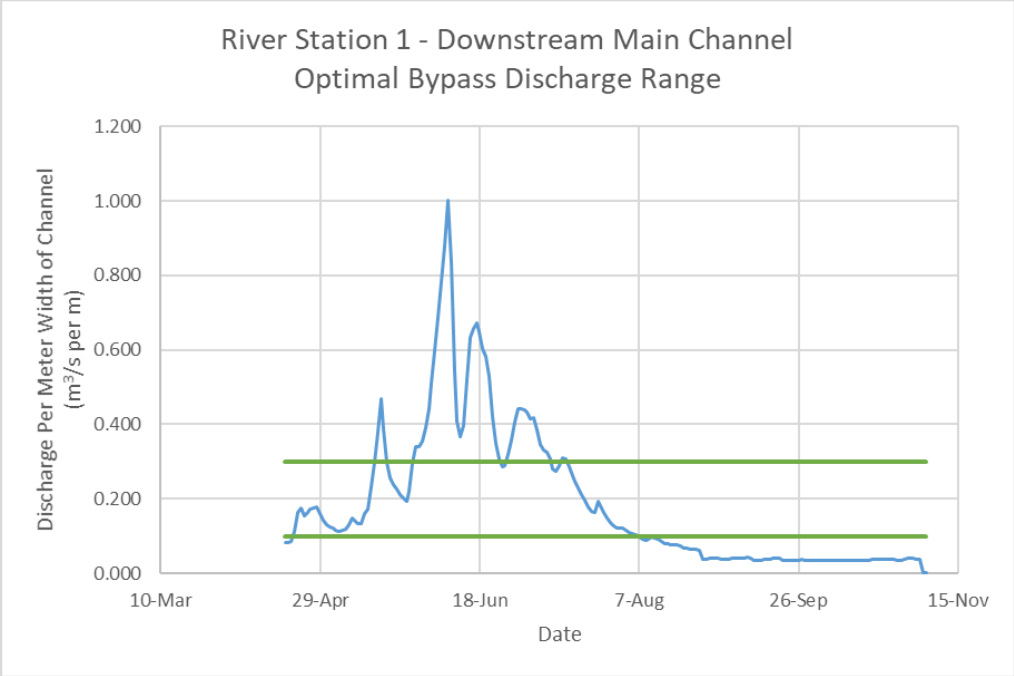


Figure 33. Discharge per meter of channel width at River Station 1 and optimal range bounded by green lines.

A cross-sectional depiction of River Station 1, located at the downstream portion of the Huntley bypass, may be seen in Figure 34. This cross section is significantly less U-shaped than River Station 403.3, and the large bed roughness elements present likely lead to discharges flowing more routinely in the recommended range.

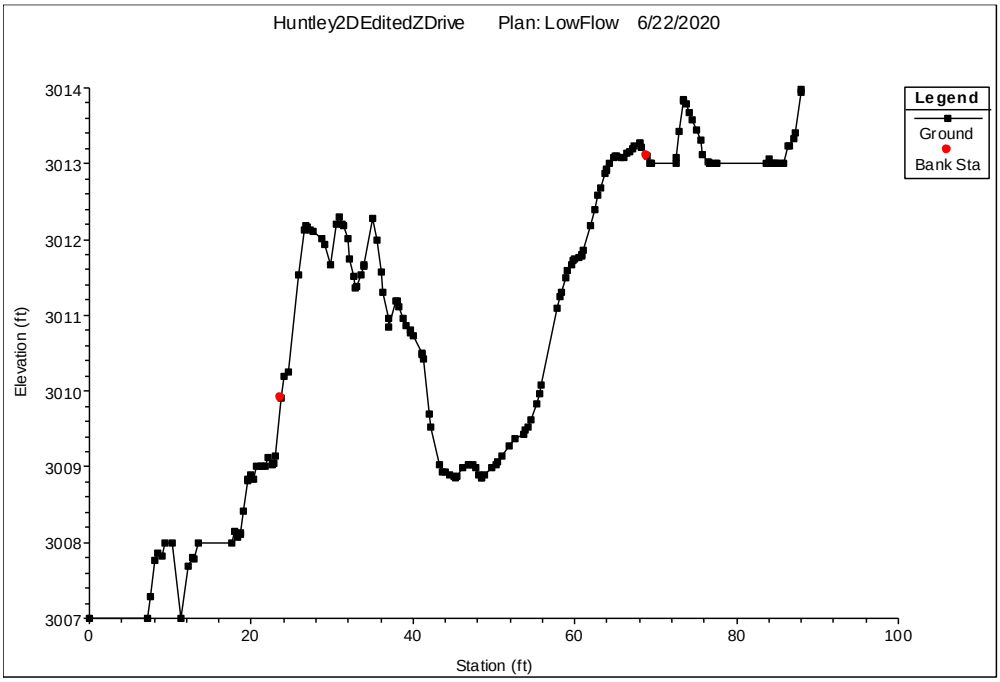


Figure 34. Cross-sectional depiction of River Station 1 located at downstream end of Huntley bypass channel.

Finally, Tran et al. (2016) used a two-dimensional depth-averaged TELEMAC-2D program to model experimental nature-like bypass designs. This 2016 study found this type of model was appropriate when the channel bed slope was less than 7% and channel hydraulics produced a Froude number of less than 0.7. The Huntley Diversion nature-like bypass channel has a bed slope of 1.25 % between the most upstream and downstream cross sections of the bypass and therefore meets the suggested slope metric. However, hydraulics at River Stations 94 and 68 cause the Froude number to rise to 1.01 and 1.00, respectively. These elevated Froude numbers are indicative of elevated velocities and shallow depths at these locations, which may present hydraulic barriers to upstream fish movement through the bypass.

Species-Specific Passage Results and Comparison to Literature Review

To determine species-specific fish passage through the Huntley Bypass, velocity maps predicted with the two-dimensional model were first analyzed in RAS Mapper. These channel-wide velocity maps, such as the one seen in Figure 35, used color profiles to indicate areas of low velocity (dark blue) and high velocity (brighter yellow and red). Areas with consistently elevated velocities were most likely to pose problems for fish passage; therefore, the most upstream portion of the channel was determined to be the greatest passage barrier and selected for further analysis.

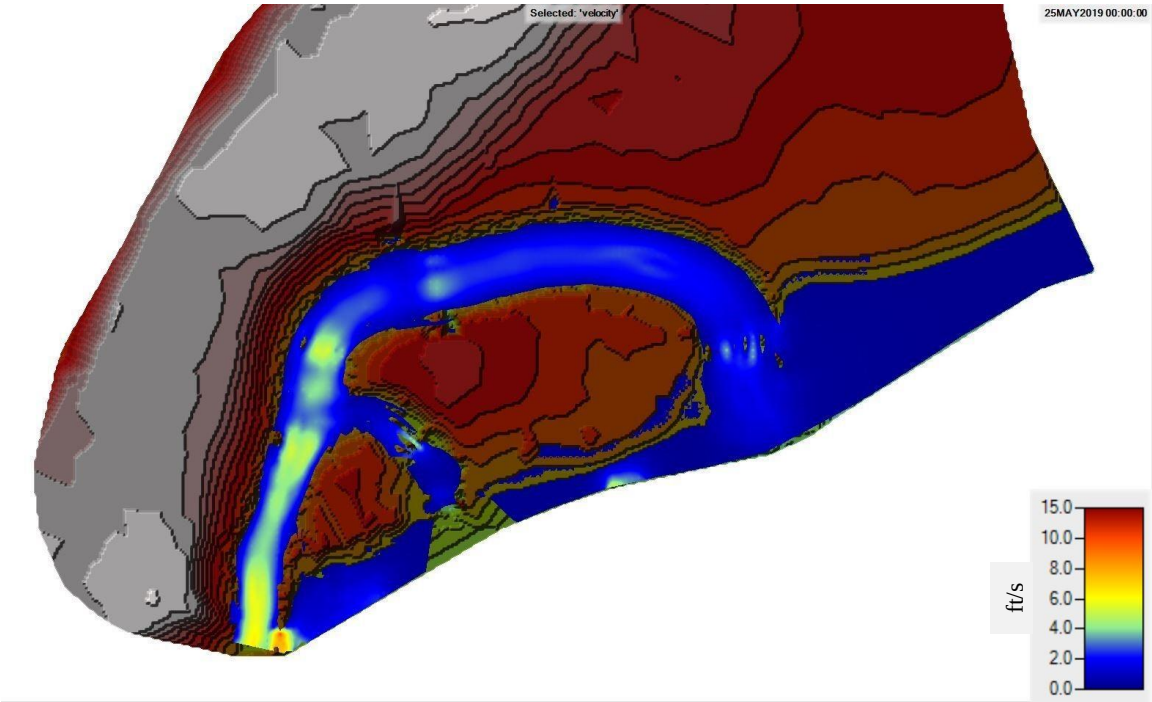


Figure 35. Sample velocity map output from two-dimensional channel model, as seen in RAS Mapper.

The two most upstream cross sections of the model, River Stations 417 and 403.3, were determined to have the highest average cross-sectional velocities. These cross

sections may be seen in the zoomed-in view of Figure 35. Mesh cell-specific velocity outputs were analyzed at cross sections 417 and 403.3, and a corridor of low velocity along the left side of the river at these two cross sections was identified. Widths of this low velocity corridor varied widely throughout the modeled hydrograph; generally, widths were observed ranging from 2.5 to 7.5 feet. Water depths in this corridor also varied temporally; for example, on May 14 at 12:00 PM, water depths in this corridor at cross sections 417 and 403.3 were recorded at 0.11 and 1 feet, respectively, while water depths on July 10 at 12:00 PM were recorded at 0.52 and 1.36 feet. It is important to note both width and depth of this corridor impact a species' ability to successfully ascend the most upstream portion of the nature-like bypass.

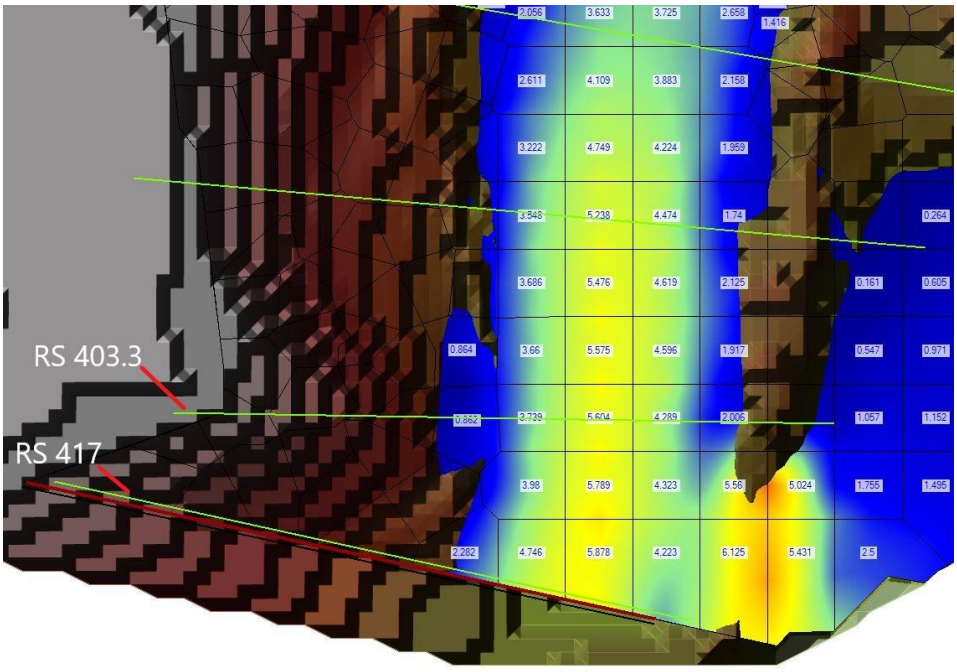


Figure 36. Zoomed-in plan view of two most upstream cross sections of main bypass channel and sample mesh cell-specific velocity outputs.

Daily velocities in this corridor at River Stations 417 and 403.3 were identified and recorded on a 24-hour basis using RAS Mapper. These velocities were then compared and graphed against species-specific swimming capabilities from literature, which have been summarized in Table 6. For example, on April 18th at 12:00 PM, the water velocity output value from the leftmost mesh cell (looking downstream) at River Station 417 was recorded at 0.635 m/s. The water velocity output value from the leftmost mesh cell of River Station 403.3 was also determined to be 1.051 m/s. Both these values were then graphed against recorded swim speeds for each species. These comparisons for Sauger, Channel Catfish, Burbot, and Smallmouth Bass can be seen in Figures 37, 38, 39, and 40.

Table 6. Summary of species-specific swimming capabilities from literature and the title of the associated study.

| **Species** | **Swimming Capability** | **Study** |
|---|---|---|
| Sauger (*Sander canadensis*) | 2.46 m/s (mean maximum swimming velocity) | Dockery et al., 2017 |
| Burbot (*Lota lota*) | 0 to 5 BL/s (prolonged)<br>1.25 m/s (complete failure) | Vokoun & Watrous, 2009 |
| Channel Catfish (*Ictalurus punctatus*) | 0.40 m/s (sustained, juvenile)<br>0.90 m/s (prolonged, juvenile)<br>1.20 m/s (burst, juvenile)<br>0.42 m/s (adult) | Beecham et al., 2007<br><br>Hocutt, 1973 |
| Smallmouth Bass (*Micropterus dolomieu*) | 1.20 m/s (failure velocity)<br>0.75 to 0.81 m/s (critical prolonged) | Peake & Farrell, 2005<br><br>Peake, 2004<br><br>Bunt et al., 1999 |

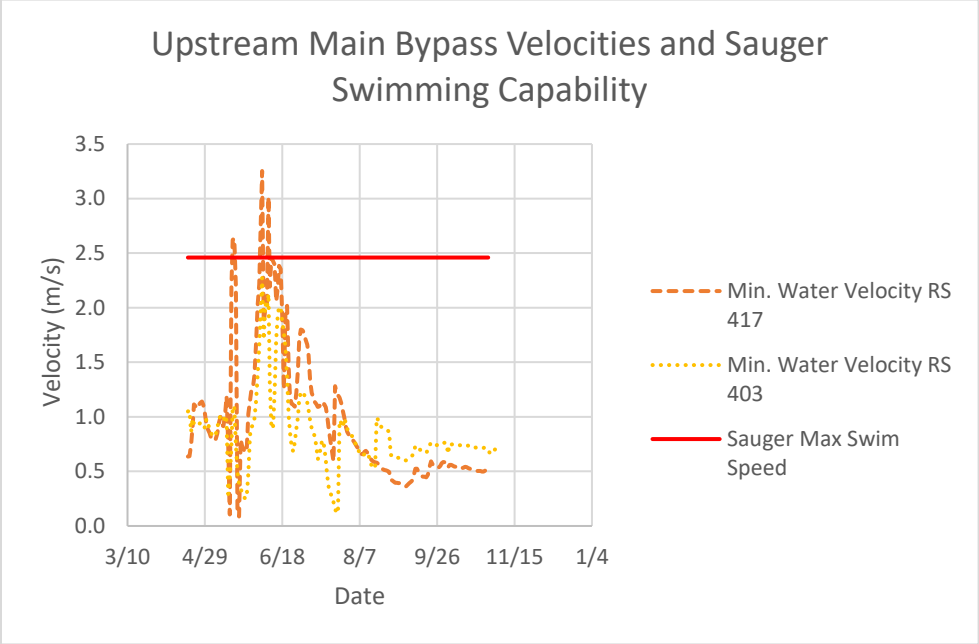


Figure 37. Minimum water velocities at River Stations 417 and 403.3 and maximum documented Sauger swimming capability in meters per second.

According to model results, water velocities in the low velocity corridor provided velocities suitable for Sauger passage every day except May 17, May 18, June 4, June 5, and June 9. On these days, water velocities at the two most upstream cross sections of the main bypass channel reached 2.62, 2.64, 2.70, 3.25, and 3.01 m/s, respectively. As water velocities were examined on a 24-hour basis, the analysis did not include timing of fish burst speeds necessary to navigate this most upstream portion of the bypass. Furthermore, if a velocity was observed above a species' recorded burst swim speed, that velocity was not considered to be within a burst speed "range" for that species. However, a few water velocities at River Station 417 were logged exactly at the recorded burst swim speed for Sauger. On June 11, water velocity at this cross section was recorded at 2.46 m/s. The edge of water measurements at these two cross sections on this day were roughly 3.63

meters apart; given this, Sauger would have to maintain burst speeds for only 1.48 seconds to successfully navigate these upstream cross sections.

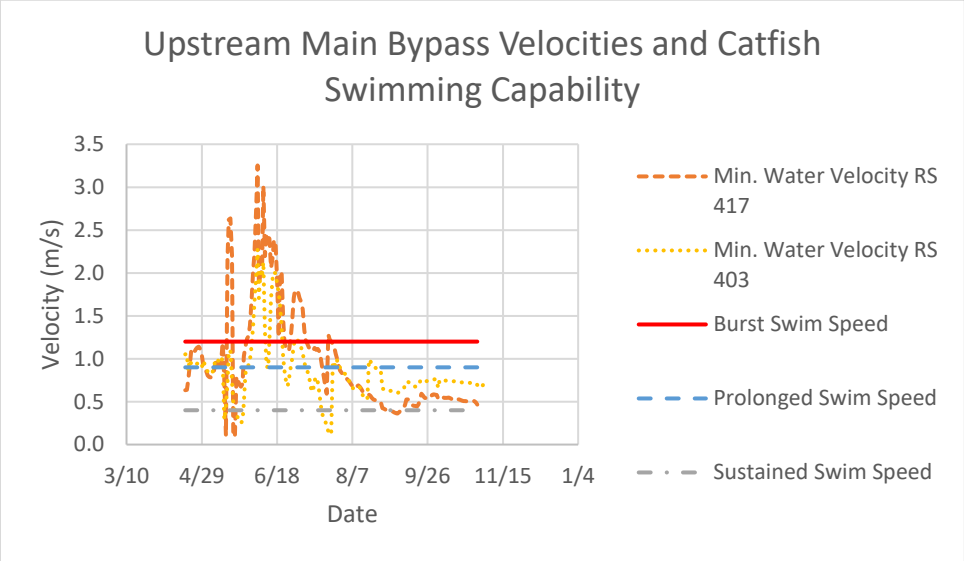


Figure 38. Minimum water velocities at River Stations 417 and 403.3 and maximum documented Channel Catfish swimming capability in meters per second.

Water velocities in the low velocity corridor may create difficulty for upstream passage of Channel Catfish. Model output velocities were above the recorded burst swimming speed for Channel Catfish on May 16-19, May 29-June 22, June 27-July 7, and July 22-24. Velocities in each of these periods rose to 2.64, 3.25, 1.80, and 1.28 m/s, respectively.

Again, model results were not produced on a basis of seconds, so exact timing of burst speeds necessary throughout the bypass were not analyzed. However, a few water velocities at River Station 417 were logged exactly at the recorded burst swim speed for Channel Catfish. On July 24, water velocity at this cross section was documented at 1.20 m/s. The edge of water measurements at these two cross sections on this day were

roughly 3.56 meters apart; given this, Channel Catfish would have to maintain burst speeds for 2.97 seconds to successfully navigate these upstream cross sections. Further research may be necessary to analyze velocities on a seconds-specific basis throughout the nature-like bypass and determine timing of burst speeds needed for successful ascension.

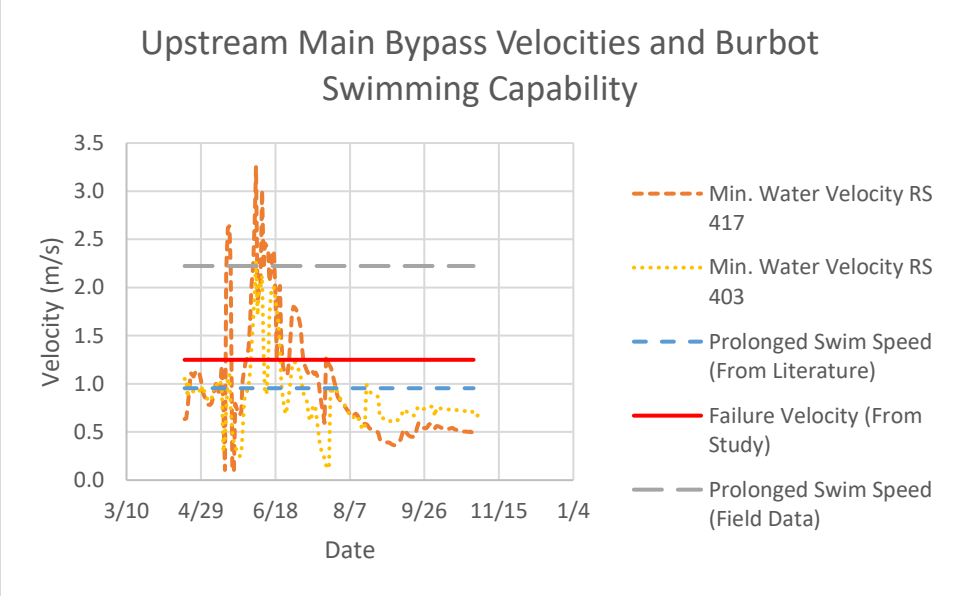


Figure 39. Minimum water velocities at River Stations 417 and 403.3 and maximum documented Burbot swimming capability in meters per second.

In Vokoun and Watrous (2009), Burbot were recorded completely failing to ascend a smooth flume when water velocities reached 1.25 m/s. If this metric is compared against model outputs, Burbot will fail to successfully pass through the nature-like bypass during the periods of May 16-19, May 30-June 22, June 28-July 6, and July 22. In this same study, Burbot prolonged swim speeds were recorded up to 5 BL/s with a mean fish length of 0.191 m. However, mean Burbot length at the Huntley bypass field site was recorded to be 0.445 m; if using the same 5 BL/s metric, Burbot prolonged swim speeds

would compute to 2.22 m/s. This potential prolonged speed would allow Burbot to comfortably pass the fishway on all days but May 17 and 18, June 4, 5, 9, 11-13, 16, and 17.

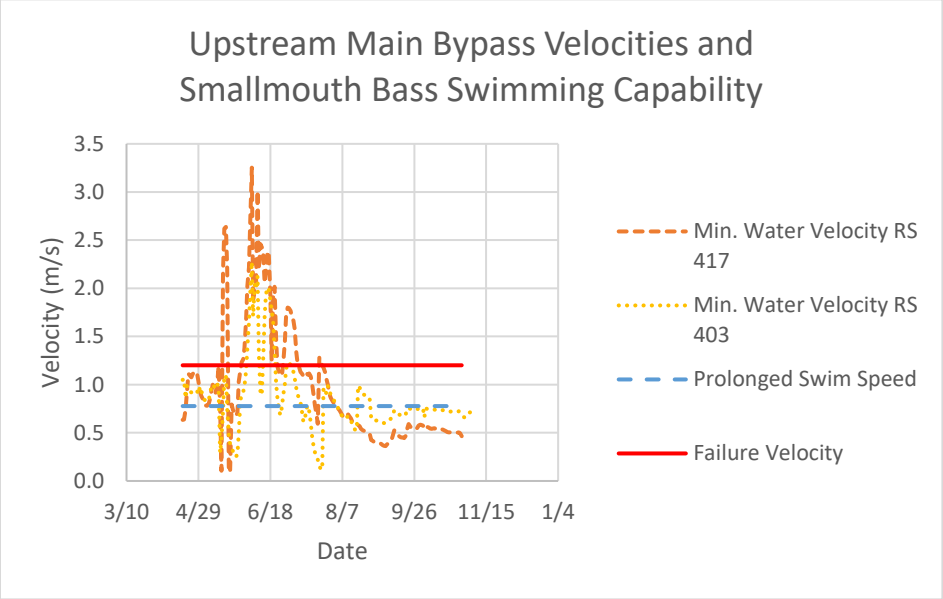


Figure 40. Minimum water velocities at River Stations 417 and 403.3 and maximum documented Smallmouth Bass swimming capability in meters per second.

Water velocities in the bypass provide similar upstream passage implications for Smallmouth Bass and Channel Catfish. Water velocities rose above the recorded failure velocity for Smallmouth Bass during the periods of May 16-19, May 29-June 22, June 27-July 7, and July 22-23.

Velocity outputs from River Stations 417 and 403.3 were next used to estimate successful or unsuccessful upstream movement through the bypass channel for Sauger, Burbot, Channel Catfish, and Smallmouth Bass. If velocities at both river stations were within a species' recorded swimming capability, that day was given a "PASS" designation. Conversely, if one or both the river stations exhibited velocities above a

species' maximum recorded swimming capability, that day was given a "FAIL" designation. Daily "PASS" and "FAIL" metrics were then plotted in green circles and red triangles throughout the modeled hydrograph and can be seen in Figures 41, 42, 43, and 44.

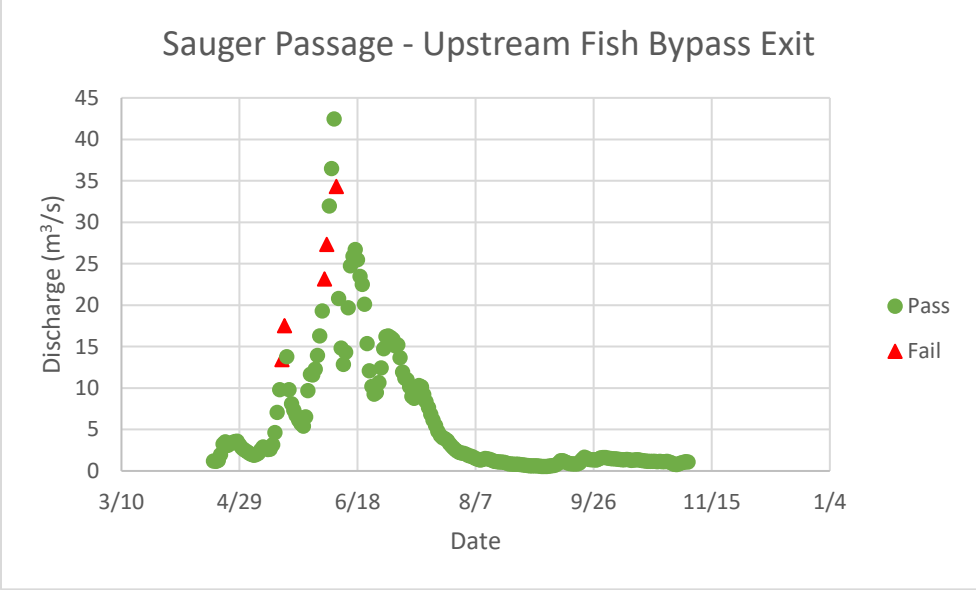


Figure 41. Sauger successful (green circles) and unsuccessful (red triangles) passage throughout modeled bypass hydrograph.

Model outputs indicated Sauger may be unsuccessful in ascending the nature-like bypass on May 17, May 18, June 4, June 5, and June 9. On these days, flow rates through the most upstream portion of the main bypass channel were measured at 13.4, 17.5, 23.2, 27.3, and 34.3 $m^3/s$, respectively. These flows are unique and only occurred at these specific times throughout the modeled hydrograph.

Past studies and literature have indicated Sauger move downstream rather than upstream to spawn in March and April and likely move upstream again in May and June (Brown, 1971). The days when Sauger are likely to be unsuccessful ascending the bypass

are all in the months of May or June, and these fish may therefore experience occasional difficulty returning to their pre-spawning habitat.

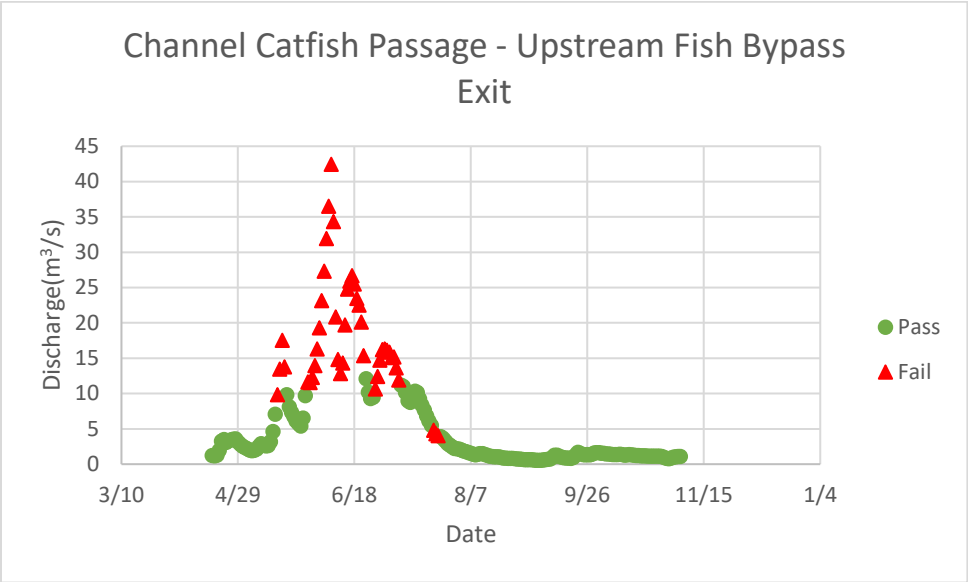


Figure 42. Channel Catfish successful (green circles) and unsuccessful (red triangles) passage throughout modeled bypass hydrograph.

Model outputs indicate Channel Catfish may fail to ascend the bypass at the following flow rates: 9.8-17.5 $m^3/s$ during May 16-19, 11.6-42.4 $m^3/s$ during May 29-June 22, 10.7-16.3 $m^3/s$ during June 27-July 7, and 4.0-4.8 $m^3/s$ during July 22-24. The "FAIL" output flow rates during the period of July 22-24 were an anomaly, but these specific flow values did not occur at any other point throughout the hydrograph. These "FAIL" values were likely due to a unique interaction between bypass flow and large roughness elements on these specific days. Due to the irregular shape and physical characteristics of a nature-like bypass channel, velocities are not likely to vary uniformly with changes in water depth. Large boulders in the channel may have created uniquely high water velocities on these days that did not occur at higher or lower flow rates.

Channel Catfish spawn in May and June; if these fish move upstream to spawn, this is likely to be significantly impacted by high water velocities throughout the nature-like bypass in these months.

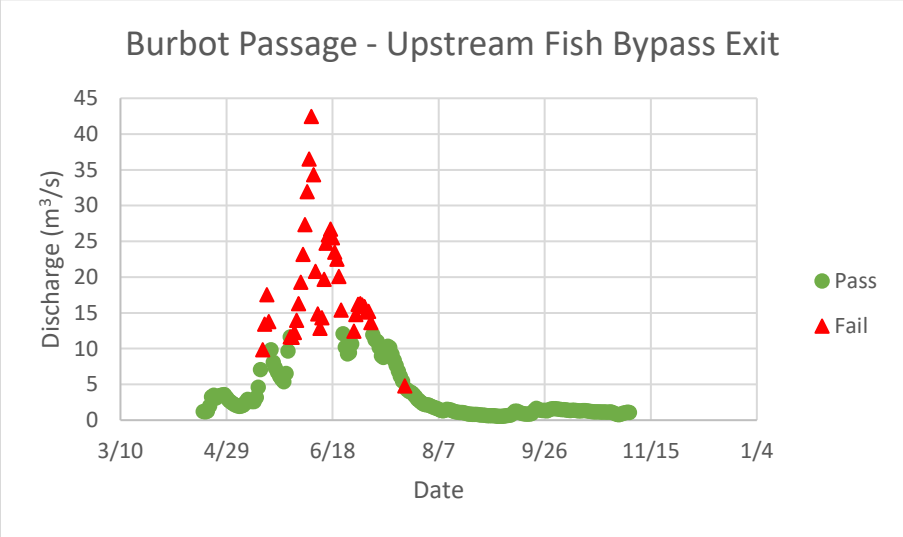


Figure 43. Burbot successful (green circles) and unsuccessful (red triangles) passage throughout modeled bypass hydrograph.

Given that the Burbot in the Vokoun and Watrous (2009) study were tested methodically in a laboratory setting, this conservative metric (failure velocity of 1.250 m/s) was used when determining Burbot passage through the nature-like bypass. Model outputs indicate Burbot may be unsuccessful when attempting to ascend the bypass during flow rates of 9.8-17.5 $m^3/s$ (May 16-19), 11.6-42.4 $m^3/s$ (May 30-June 22), 12.4-16.3 $m^3/s$ (June 28-July 6), and 4.8 $m^3/s$ (July 22). The flow rate exhibited on July 22, 4.8 $m^3/s$, again was an anomaly but did not occur at any other point during the hydrograph.

Burbot are most active in the winter, with spawning season occurring under ice in January and February (Brown, 1971). Winter months were not included in this study.

Though Burbot are likely unsuccessful in ascending the bypass for large periods of late spring and early summer, the biological implications of this may require further study.

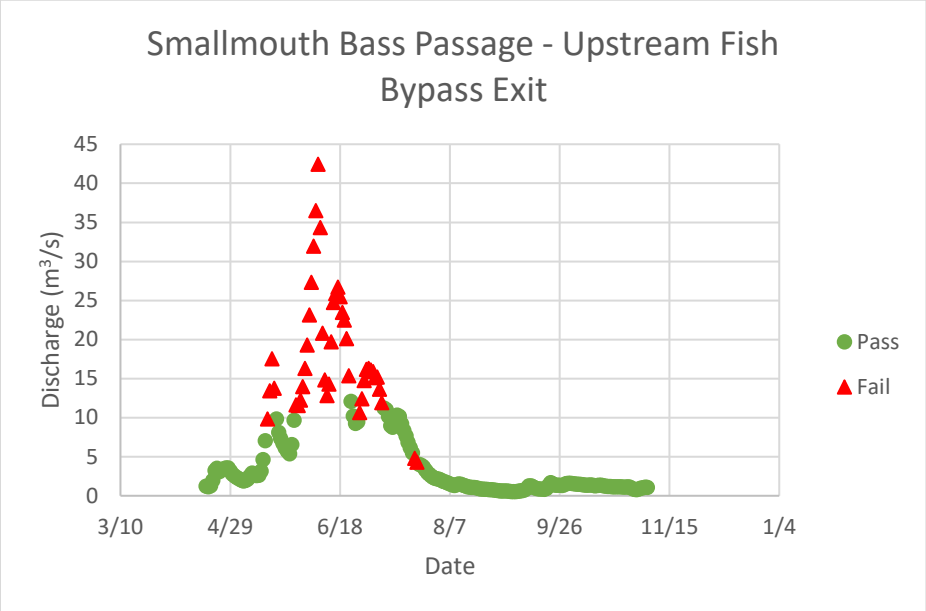


Figure 44. Smallmouth Bass successful (green) and unsuccessful (red) passage throughout modeled bypass hydrograph.

Model outputs indicate Smallmouth Bass may fail to ascend the bypass at the following flow rates: 9.8-17.5 $m^3/s$ during May 16-19, 11.6-42.4 $m^3/s$ during May 29-June 22, 10.7-16.3 $m^3/s$ during June 27-July 7, and 4.3-4.8 $m^3/s$ during July 22-23. Similar to the outputs seen in the Channel Catfish figure, output flow rates during the anomaly period of July 22-23 did not occur at any other point throughout the hydrograph.

Past studies have indicated Smallmouth Bass exhibit upstream movement during spawning season in May and June (Brown, 1971). These results indicate the nature-like bypass may present difficulties during Smallmouth Bass spawning season, as the latter

half of May and most of the month of June exhibit velocities above the maximum recorded swim speed for this species.

Passage has been specifically compared against species-specific spawning movement in this document. However, it is important to note that fish move upstream and downstream in these river systems for a wide variety of reasons not solely limited to spawning. Reasons for movement may also include migration for feeding purposes or to seek refuge from unfavorable environmental factors, like extreme flows (Schlosser & Angermeier, 1995). These movements are more difficult to quantify, and results from further ecology work on this project may aid in clarifying timing of these movements.

## Attraction Flow Model Results

Past studies have indicated the importance of providing adequate attraction flow to ensure fish can locate the downstream entrance to a bypass channel (Katopodis et al., 2001). Attraction flow remains difficult to quantify. Katopodis et al. (2001) recommended the use of multiple bypass entrances to provide adequate attraction flow, and Landsman et al. (2018) suggested the downstream entrance of a nature-like bypass should be as close as possible to the instream obstruction. The Huntley Diversion nature-like bypass does not meet either of these metrics; only one bypass entrance exists, and the downstream entrance to the nature-like bypass is over 73 meters from the Huntley Diversion dam. This large distance from the bypass entrance to the dam may cause fish to miss the entrance and continue following the largest amount of flow upstream to the dam. Should this happen, they can no longer enter the bypass channel and cannot continue their upstream movement.

Additionally, National Marine Fisheries Service guidance has recommended that "attraction flow from the fishway entrance should be between 5% and 10% of fish passage design high flow… for streams with mean annual streamflows exceeding 1000 cfs" (NMFS, 2011). To evaluate this, daily flow averages were obtained from the USGS Billings Yellowstone River Gage 06124500, as well as daily bypass channel outflow from the two-dimensional model results. Flow over the low-head, broad-crested dam was then estimated using the following equation:

$$q = \frac{2}{3} c_d b (2g)^{\frac{1}{2}} h^{\frac{3}{2}} \quad (30)$$

Where q is the flow rate in $m^3/s$, $c_d$ is the discharge coefficient, b is the width of the weir in meters, g is gravity, and h is the height of water over the dam. Here, a discharge coefficient of 0.56 was assumed, and daily h values were estimated using GPS data and stage outputs from the most upstream cross section of the bypass model. Attraction flow as a percentage of total flow was then determined by dividing daily bypass flow by estimated weir flow. Flow rates and attraction flow percentages may be seen in Figure 45.

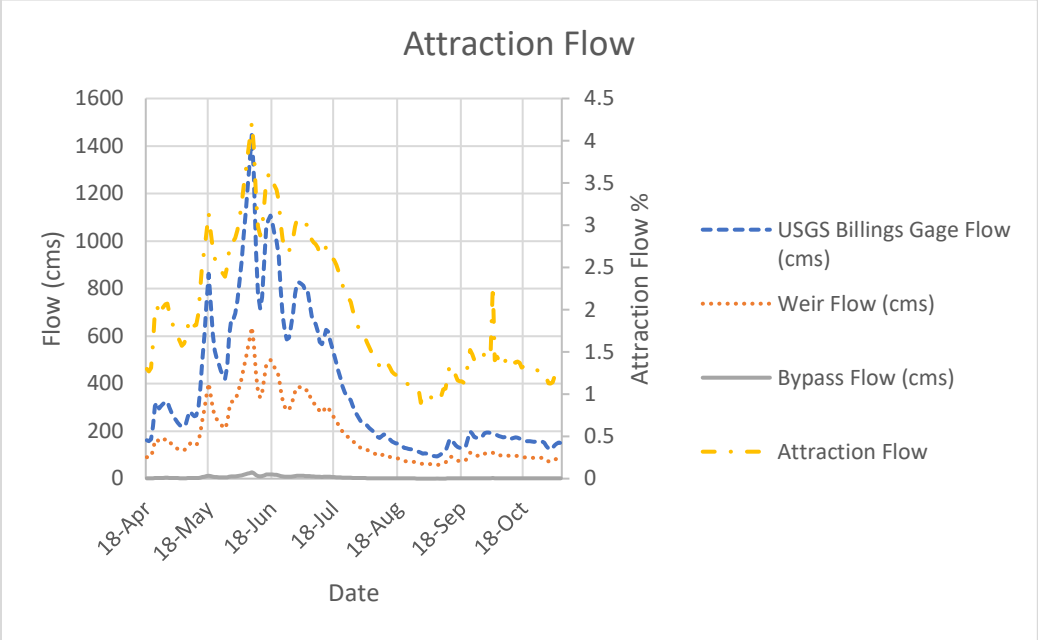


Figure 45. Pertinent flow rates and attraction flow percentages at the Huntley bypass site.

The maximum flow over the low-head, broad-crested Huntley Diversion Dam was estimated to be 637.6 $m^3/s$ on June 8, 2019. Model results showed that 26.89 $m^3/s$ exited the downstream end of the main bypass channel; this means that on this day, 4.22% of Yellowstone River flow exited the Huntley bypass channel. At this maximum modeled flow rate, attraction flow from the fishway entrance was not within the 5-10% recommended range from NMFS guidance (NMFS, 2011).

Katopodis et al. (2001) also recommended minimizing disorienting and exhausting turbulence and eddy formations near the downstream bypass entrance to ensure adequate fish attraction. To evaluate this, a two-dimensional model encompassing both the nature-like bypass channel and Yellowstone River was created to visualize and quantify their interaction. The model was run for three conditions: a “high” flow period using observed flow rates from May 21 and 22, an “average” flow period using observed

points from July 24 and 25, and a “low” flow period using data from August 20-23, 2019. Model visual outputs were analyzed for disorienting velocity patterns or eddy formations in RAS Mapper, and these outputs may be seen in Figures 46, 48, and 50. Photo point outputs at this location during these respective dates can also be seen in Figures 47, 49, and 51 for comparison.

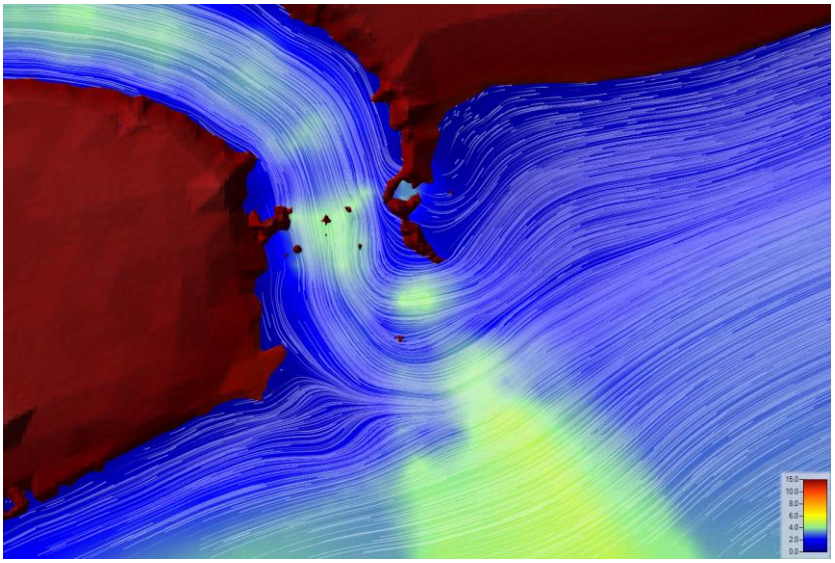

Figure 46. Velocity and particle tracking output in RAS Mapper for high flow period of May 21-22, 2019.

Figure 47. Photo point output at downstream end of main bypass channel and its interaction with the Yellowstone River on May 21, 2019.

On May 21, 2019, 6.9 $m^3/s$ of flow exited the downstream end of the bypass channel, while an estimated 264.6 $m^3/s$ flowed down the Yellowstone River. This amounts to an attraction flow value of 2.61%.

Velocity and particle tracking outputs from the high flow simulation in Figure 42 suggest minimal formation of disorienting hydraulic characteristics at the bypass entrance. This is likely due in part due to large inundation of the rock weir bordering the downstream bypass entrance. Water flows swiftly over this location, providing a large amount of attraction flow to fish swimming upstream on this side of the Yellowstone River.

This is confirmed by the photo taken on May 21, 2019 in Figure 47. The photo also suggests an increased backwater effect from Yellowstone River flow into the nature-like bypass channel, which may not be represented entirely in Figure 46.

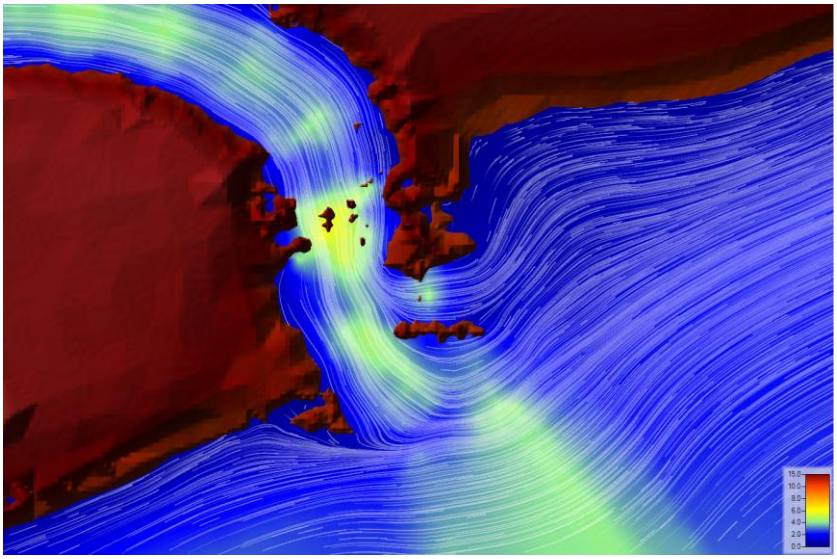

Figure 48. Velocity and particle tracking outputs in RAS Mapper for "average" flow period of July 24-25, 2019.

Figure 49. Photo point output at downstream end of main bypass channel and its interaction with the Yellowstone River on July 24, 2019.

On July 24, 2019, 3.86 $m^3/s$ of flow exited the downstream end of the bypass channel, while an estimated 178.5 $m^3/s$ flowed down the Yellowstone River. This amounts to an attraction flow value of 2.16%.

Velocity and particle tracking outputs from the "middle" flow simulation in Figure 48 suggest increased formation of disorienting hydraulic characteristics. As water stage drops, the downstream peninsula bordering the downstream bypass entrance is longer and less inundated. Because of this, an area of significantly lower velocity has begun to form in the inlet just downstream of the bypass. Fish may still experience adequate attraction flow if swimming up this side of the Yellowstone River, but likely would have to swim well offshore to avoid the disorienting or confusing area.

This is confirmed by the photo taken on July 24, 2019 in Figure 49. The photo does not suggest a backwater effect like the interaction observed at high flow and seems to generally support the model output.

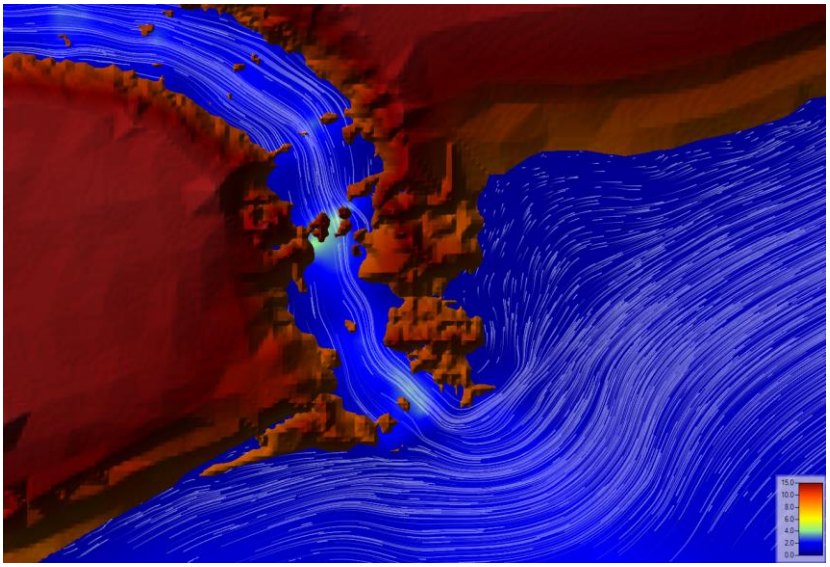

Figure 50. Velocity and particle tracking outputs in RAS Mapper for low flow period of August 20-23, 2019.

Figure 51. Photo point output at downstream end of main bypass channel and its interaction with the Yellowstone River on August 20, 2019.

On August 20, 2019, 0.93 $m^3/s$ of flow exited the downstream end of the bypass channel, while an estimated 78.8 $m^3/s$ flowed down the Yellowstone River. This amounts to an attraction flow value of 1.18%.

Velocity and particle tracking outputs from the low flow simulation seen in Figure 46 suggest large areas of disorienting hydraulic conditions just downstream of the bypass entrance. Particles can be seen exiting the bypass in a smooth fashion, denoting areas of faster velocity. Many of these particles exit the bypass, curl around the rock peninsula, and appear in more of a staccato fashion, indicating water velocities have significantly slowed down. This area of staccato-like particle tracking may indicate a large area of stagnant water.

It is important to note that an eddy is characterized by a circular movement of water (National Ocean Service, 2019); when examining the results of the particle tracking

simulation, no particles are specifically moving in a full circular fashion. However, the velocity behavior in this area may still present severely disorienting hydraulic characteristics to fish swimming upstream and attempting to locate the entrance to the bypass.

# SUMMARY

This project was performed to characterize the hydraulics, hydrology, and resulting fish passage at a novel nature-like bypass on the Yellowstone River in Montana. The bypass was constructed around the low-head Huntley Diversion Dam in 2015 and is meant to provide passage for a wide variety of morphologically different species, including Sauger (*Sander canadensis*), Burbot (*Lota lota*), Channel Catfish (*Ictalurus punctatus*), and Smallmouth Bass (*Micropterus dolomieu*).

Field methods were employed to measure and monitor water stage, flow rates, channel roughness, and channel bathymetry. To determine water stage, Onset HOBO U20-L data loggers, staff gages, and survey points were used and developed at multiple locations throughout the greater bypass channel area. Flow rates in the old and main nature-like bypass channels, both present at the site, were collected using three methods: the USGS Midsection Method, Float-Area Method, and Slope-Area Method. Channel roughness was characterized using the Wolman Pebble Count technique and later refined using a Monte Carlo analysis. Bathymetry data points were collected using a Trimble R8 GPS rover and base station; points were obtained in a grid-like fashion, and roughly 7600 points were obtained in total at the site.

A two-dimensional bypass channel hydraulic model was created using HEC-RAS, an Army Corps of Engineers program. Bathymetry points were used to develop a terrain model in Civil3D, which was then used a basis for development of a computational mesh. The mesh sizing balanced both time and output needs, allowing a relatively fine visualization of water velocity values across each channel cross section. Observed flow

and stage readings were used as the basis for model boundary conditions at all inlets and outlets to the bypass; any data gaps were filled using best-fit data obtained from linear regression analyses. Water surface elevation errors were minimized through a Monte Carlo analysis that varied Manning's n roughness values. The two-dimensional model was finally computed, and velocity and depth results were analyzed and compared to recommendations and species-specific swimming capabilities from literature.

Steps were also performed to analyze attraction flow, or the proportion of total Yellowstone River flow that exited the downstream bypass entrance. A model was created to visualize or quantify the flow interaction between bypass and Yellowstone River flow. This model used the same base terrain surface from the two-dimensional bypass channel model but interpolated additional points to form an "idealized" trapezoidal Yellowstone River channel. The model was run for three time periods encompassing the highest, lowest, and "average" flows observed on site. Flow interactions were monitored for disorienting or confusing hydraulic characteristics, and final fish attraction to the Huntley nature-like bypass was estimated.

Results from the two-dimensional bypass model indicated flow peaked in the nature-like bypass on June 8, 2019 at 42.43 $m^3/s$. Of this, 26.89 $m^3/s$ flowed into the main channel, while 15.54 $m^3/s$ flowed into the old bypass channel. Low flow occurred on September 6, 2019 at 0.52 $m^3/s$; of this, all flow remained in the main bypass channel. Water surface elevation error at the most upstream and downstream cross sections of the bypass channel was minimized to an average of 0.09 and 0.10 m, respectively, due to the Monte Carlo analysis.

Results from this model were compared to metrics from literature. One study recommended minimum water depths of 0.40 m throughout a nature-like bypass to provide adequate resting locations for morphologically diverse fish species as they ascend (Santos et al., 2005). Eight cross sections throughout the bypass experienced water depths shallower than this recommendation; these shallow depths occurred in the period of August 27-September 5, 2019. If species are heading upstream in this late summer/early fall period, these depths may create barriers to them as they attempt to ascend the Huntley bypass. This same 2005 study recommended optimal discharges of 0.1 to 0.2 $m^3/s$ per meter of channel width to promote successful passage in a nature-like bypass. Hydraulics at two of the most upstream and downstream cross sections of the bypass channel were analyzed, and discharges at the upstream end of the channel were routinely found to exceed this recommended range. This is likely due to the narrow U-shape and grouted characteristics of this upstream end of the bypass. These characteristics may play a part in elevated water velocities at the upstream end of the bypass that may present difficulties for fish passage.

Model output velocities at the most upstream portion of the bypass channel were compared to species-specific swimming capabilities for Sauger, Burbot, Channel Catfish, and Smallmouth Bass. Water velocities provide characteristics suitable for Sauger passage on all days throughout the modeled hydrograph except May 17, May 18, June 4, June 5, and June 9. Sauger are unique in that they move downstream rather than upstream to spawn in March and April and likely move upstream again in May and June (Brown,

1971); therefore, these fish may experience occasional difficulty returning to their pre-spawning habitat.

Burbot may fail to ascend the nature-like bypass for much of May, June, and early July. However, the Burbot in the 2009 study used for comparison had an average length of 0.191 meters (Vokoun & Watrous, 2009), while preliminary observations from the Huntley bypass site recorded Burbot average length at 0.443 meters. The discrepancy in this fish sizing may lead to a difference in swimming abilities and may necessitate further study. Regardless of sizing, Burbot are most active in the winter, with spawning season occurring under the ice of the Yellowstone River in January and February (Brown, 1971). Winter months were not included in the scope of this study.

Both Channel Catfish and Smallmouth Bass may fail to ascend the bypass for much of May, June, and early July. Channel Catfish spawn in May, June, and July, while Smallmouth Bass spawn in the months of May and June (Brown, 1971). If these species are exhibiting upstream movement to spawning grounds during these months, this movement is likely to be significantly impacted.

General movement in relation to spawning was well-documented throughout literature for these four species of interest. It is important to note that fish move upstream and downstream in river systems for a variety of reasons not limited to spawning, including movement for feeding purposes or to escape environmental hazards (Schlosser & Angermeier, 1995). Results from the ecology portion of this Huntley bypass study may shed light on fish movement in this system throughout the rest of the calendar year.

Attraction flow was analyzed at the downstream fish bypass entrance. Attraction flow was computed by dividing bypass outflow by flow over the Huntley Diversion Dam, which was estimated using known geometry, water surface observations, and a weir equation. Current guidelines recommend that between 5 and 10% of total channel flow exit the bypass to provide adequate attraction to the fishway entrance; here, the maximum attraction flow on June 8 was computed to be 4.22%. Average and median attraction flow percentages throughout the modeled hydrograph of April 18 to November 5 were computed to be 1.95% and 1.64%, respectively. All these values are beneath the recommended range established by the National Marine Fisheries Service (NMFS, 2011).

Finally, the model to visualize or quantify the interaction between bypass channel outflow and Yellowstone River flow was run at observed high, low, and "average" flow rates. No modeled flow produced velocities in specific circular eddy patterns. Of the flows modeled, low flow (August 20-23, 2019) produced the largest area of seemingly stagnant water near the downstream end of the bypass. This area of significantly slowed velocity may present confusing and disorienting hydraulic characteristics for fish, leading to low attraction to the bypass entrance at low flow rates. However, our four species of interest do not tend to exhibit upstream movement for spawning purposes in late August. The biological implications of low attraction flow in late summer may be clarified with further results from the ecology portion of this project.

Future opportunities exist at this site to measure rather than estimate the flow over the Huntley Diversion Dam, which would lead to a more accurate representation of attraction flow characteristics at the downstream bypass entrance. Additionally, observed

flow behavior onsite indicated the formation of a large eddy near the dam at high flow rates; at some flows, this eddy stretched from the dam to the downstream bypass entrance. This large eddy was not included in our study due to data and model constraints, but again may allow for more accurate representation of the flow barriers fish may face when locating the bypass entrance. Further research may also be needed to address the concept of introducing additional attraction flow to the bypass and whether this would simply create greater velocity barriers for upstream-moving fish to overcome.

# REFERENCES CITED

Beecham, R. V., Minchew, C. D., & Parsons, G. R. (2007). Comparative Swimming Performance of Juvenile Pond-Cultured and Wild-Caught Channel Catfish. *North American Journal of Fisheries Management*, 729-734.

Betsholtz, A., & Nordlöf, B. (2017). *Potentials and limitations of 1D, 2D, and coupled 1D-2D flood modelling in HEC-RAS: A case study on Höje river.* Lund University.

Bingham, D. M., Leary, R. F., Painter, S., & Allendorf, F. W. (2012). Near absence of hybridization between sauger and introduced walleye despite massive releases. *Conservation Genetics, 13*, 509-523.

Brown, C. (1971). *Fishes of Montana.* Bozeman, Montana: Big Sky Books.

Brunner, G. W. (2016). *HEC-RAS River Analysis System 2D Modeling User's Manual.* Davis, CA: U.S. Army Corps of Engineers.

Brunner, G. W. (2016). *HEC-RAS River Analysis System Hydraulic Reference Manual.* Davis, CA: US Army Corps of Engineers.

Brunner, G. W. (2016, February). *HEC-RAS River Analysis System User's Manual.* Davis, CA: US Army Corps of Engineers.

Bunt, C. M., Katopodis, C., & McKinley, R. S. (1999). Attraction and Passage Efficiency of White Suckers and Smallmouth Bass by Two Denil Fishways. *North American Journal of Fisheries Management*, 793-803.

Calles, E., & Greenberg, L. (2005). Evaluation of nature-like fishways for re-establishing connectivity in fragmented salmonid populations in River Emån. *River Research and Applications*.

Chapra, S. C. (2008). *Applied Numerical Methods with MATLAB.* New York: McGraw-Hill.

Chow, V. (1959). *Open-Channel Hydraulics.* Caldwell, New Jersey: The Blackburn Press.

Cooke, S. J., & Bunt, C. M. (2001). Assessment of Interal and External Antenna Configurations of Radio Transmitters Implanted in Smallmouth Bass. *North American Journal of Fisheries Management*, 236-241.

Dockery, D., McMahon, T., Kappenman, K., & Blank, M. (2017). Swimming performance of sauger (Sander canadensis) in relation to fish passage. *Canadian Journal of Fisheries and Aquatic Sciences*, 2035-2044.

Federal Emergency Management Agency. (2012). *Summary of Existing Guidelines for Hydrologic Safety of Dams: United States Dam Inventory Data.* Federal Emergency Management Agency.

Fuentes-Pérez, J., García-Vega, A., Sanz-Ronda, F., & de Azagra Paredes, A. (2017). Villemonte's approach: a general method for modeling uniform and non-uniform performance in stepped fishways. *Knowledge & Management of Aquatic Ecoystems*, 23.

Graf, W. L. (1999). Dam nation: A geographic census of American dams and their large-scale hydrologic impacts. *Water Resources Research*, *35*(4), 1305-1311.

Hocutt, C. H. (1973). Swimming Performance of Three Warmwater Fishes Exposed to a Rapid Temperature Change. *Chesapeake Science*, 11-16.

Johnson, S. L., & Swanson, F. J. (2014, January 14). *Wolman pebble count protocol.* Retrieved from GS002: Stream Cross-Section Profiles in the Andrews Experimental Forest and Hagan Block RNA 1978 to Present: https://andrewsforest.oregonstate.edu/sites/default/files/lter/data/studies/gs002/Wolman_Pebble_Count.pdf

Katopodis, C., Kells, J., & Acharya, M. (2001). Nature-Like and Conventional Fishways: Alternative Concepts? *Canadian Water Resources Journal*, 211-232.

Landsman, S., McLellan, N., Platts, J., & van den Huevel, M. (2018). Nonsalmonid versus Salmonid Passage at Nature-Like and Pool-and-Weir Fishways in Atlantic Canada, with Special Attention to Rainbow Smelt. *Transactions of the Ameriacan Fisheries Society*, 94-110.

Lewis, M. S. (2018). *Summary of Research: Statewide Estimates of Resident and Nonresident Hunter & Angler Trip Related Expenditures in Montana (2018).* Montana Fish, Wildlife & Parks.

McCammon, G., & LaFaunce, D. (1961). Mortality Rates and Movement in the Channel Catfish Population of the Sacramento Valley. *California Fish and Game*, 5-26.

McPhail, J., & Paragamian, V. (2000). *Burbot Biology and Life History.* American Fisheries Society.

Montana Fish, Wildlife and Parks. (n.d.). Species Distribution. *Fish MT*. MT, USA. Retrieved 2020, from https://myfwp.mt.gov/fishMT/distribution/speciesdistribution

Montgomery, J., Baker, C., & Carton, A. (1997). The lateral line can mediate rheotaxis in fish. *Nature*, 960-963.

National Ocean Service. (2019, 11 13). *What is an eddy?* Retrieved from Ocean Facts: https://oceanservice.noaa.gov/facts/eddy.html

NMFS (National Marine Fisheries Service). (2011). *Anadromous Salmonid Passage Facility Design.* Portland, OR: NMFS, Northwest Region.

Peake, S. (2004). An Evaluation of the Use of Critical Swimming Speed for Determination of Culvert Water Velocity Criteria for Smallmouth Bass. *Transactions of the American Fisheries Society*, 1472-1479.

Peake, S. J., & Farrell, A. P. (2005). Postexercise Physiology and Repeat Performance Behaviour of Free-Swimming Smallmouth Bass in an Experimental Raceway. *Physiological and Biochemical Zoology: Ecological and Evolutionary Approaches, 78*(5), 801-807.

Santos, J., Ferreira, M., Godinho, F., & Bochechas, J. (2005). Efficacy of a nature-like bypass channel in a Portuguese lowland river. *Journal of Applied Ichthyology*, 381-388.

Schlosser, I. J., & Angermeier, P. L. (1995). Spatial Variation in Demographic Processes of Lotic Fishes: Conceptual Models, Empirical Evidence, and Implications for Conservation. *American Fisheries Society Symposium*, 392-401.

Siddons, S. (2015). *Population Dynamics and Movement of Channel Catfish in the Red River of the North.* University of Nebraska.

Silva, A., Lucas, M., Castro-Santos, T., Katopodis, C., Baumgartner, L., Thiem, J., . . . Cooke, S. (2018). The future of fish passage science, engineering, and practice. *Fish and Fisheries*, 340-362.

Tamario, C., Degerman, E., Donadi, S., Spjut, D., & Sandin, L. (2018). Nature-like fishways as compensatory lotic habitats. *River Research and Applications*, 353-261.

Teppel, A., & Tymiński, T. (2013). Hydraulic Research for Successful Fish Migration Improvemnt - "Nature-Like" Fishways. Instytut Inżynierii Środowiska, Uniwersytet Przyrodniczy we Wrocławiu.

Tran, T., Chorda, J., Laurens, P., & Cassan, L. (2016). Modelling nature-like fishway flow around unsubmerged obstacles using a 2D shallow water model. *Environmental Fluid Mechanics*, 413-428.

Turek, J., Haro, A., & Towler, B. (2016). *Federal Interagency Nature-like Fishway Passage Design Guidelines for Atlantic Coast Diadromous Fishes.*

U.S. Department of the Interior - Bureau of Reclamation. (1997). Chapter 13 - Special Measurement Methods in Open Channels. In *Water Measurement Manual* (pp. 4-8). Denver: U.S. Government Printing Office.

U.S. Fish & Wildlife Service. (2008, July 15). *Huntley Project Irrigation District*. Retrieved from Yellowstone River Coordinator's Office: Mountain-Prairie Region: https://www.fws.gov/yellowstonerivercoordinator/Huntley.html

Vokoun, J., & Watrous, D. (2009). *Determining swim speed performance characteristics for fish passage of burbot using an experimental flume and nature-like fishway*. Storrs, CT: University of Connecticut.

Volpato, G., Barreto, R., Marcondes, A., Andrade Moreira, P., & de Barros Ferreira, M. (2009). Fish ladders select fish traits on migration–still a growing problem for natural fish populations. *Marine and Freshwater Behaviour and Physiology*.

Zale, A. V., Lance, M. J., Plymesser, K., Blank, M., Cahoon, J., Frazer, K. J., & Ruggles, M. P. (2018). Efficacy of the Nature-like Fish Bypass Channel at Huntley Diversion Dam, Yellowstone River, Montana.

# APPENDICES

# APPENDIX A

## WATER STAGE DATA FROM HOBO U20-L LOGGERS

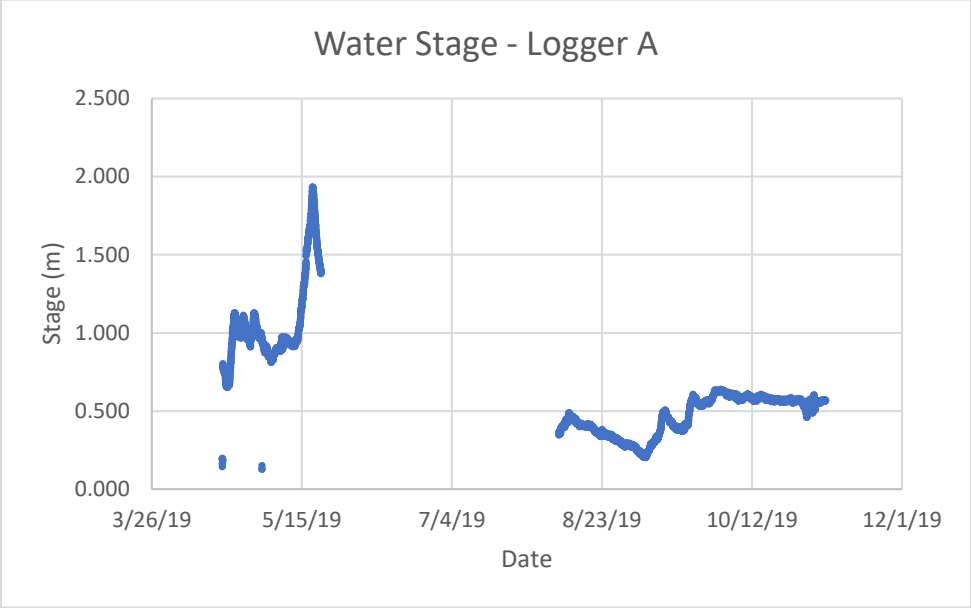


Figure 52. Total water stage data from HOBO logger placed at cross section A.

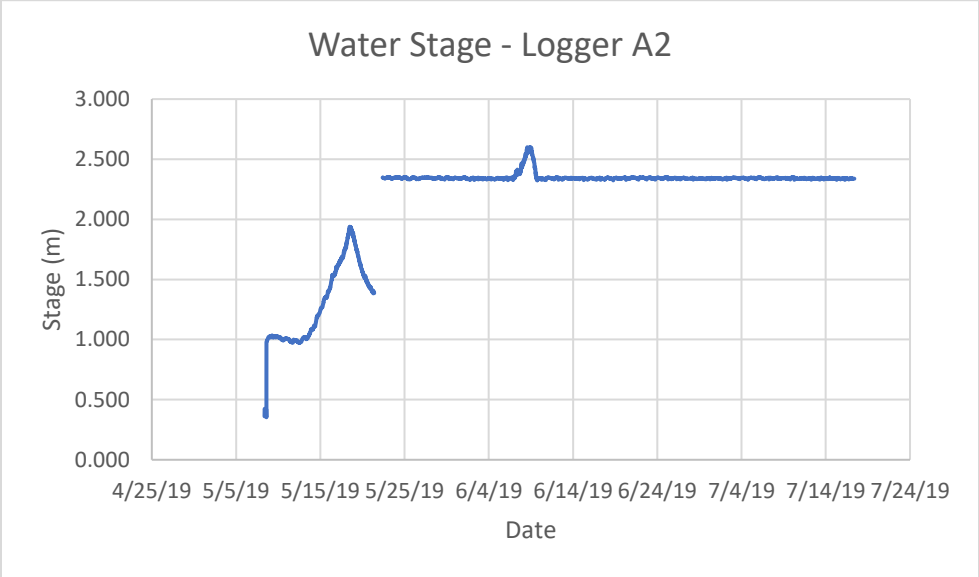


Figure 53. Total water stage data from logger A2, placed in close proximity to cross section A.

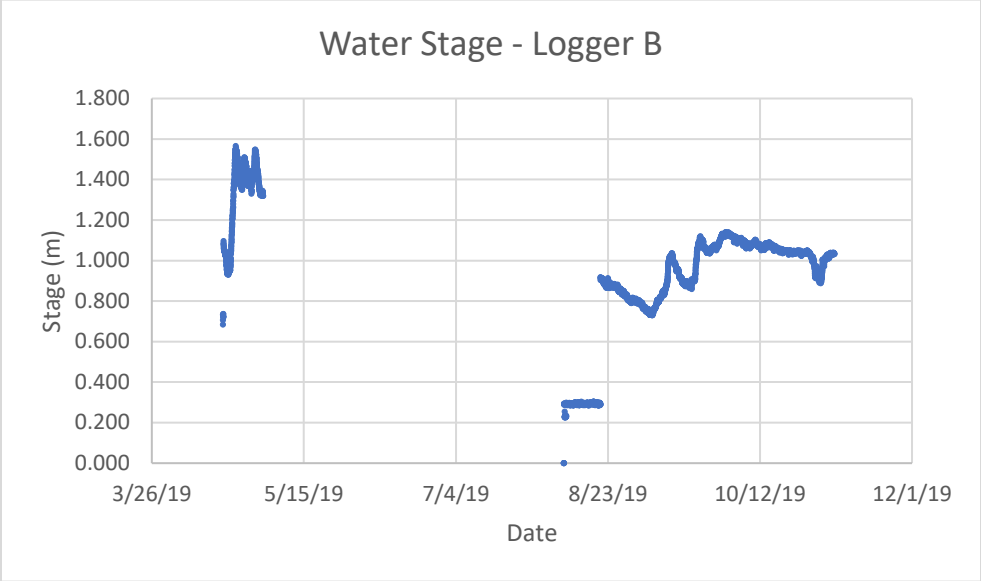


Figure 54. Total water stage data from logger B at downstream end of Huntley bypass.

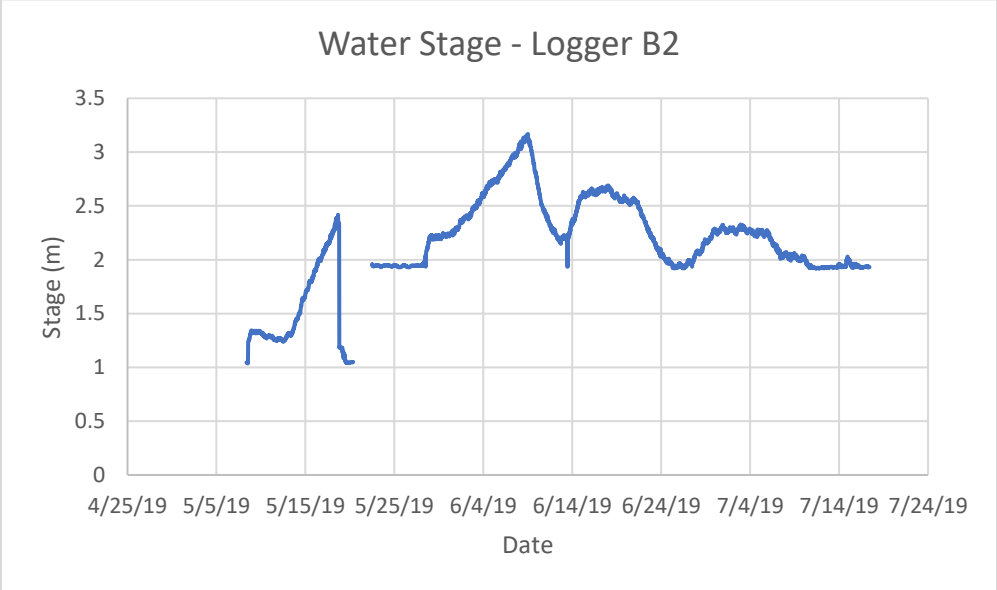


Figure 55. Total water stage data from logger B2, placed in close proximity to cross section B.

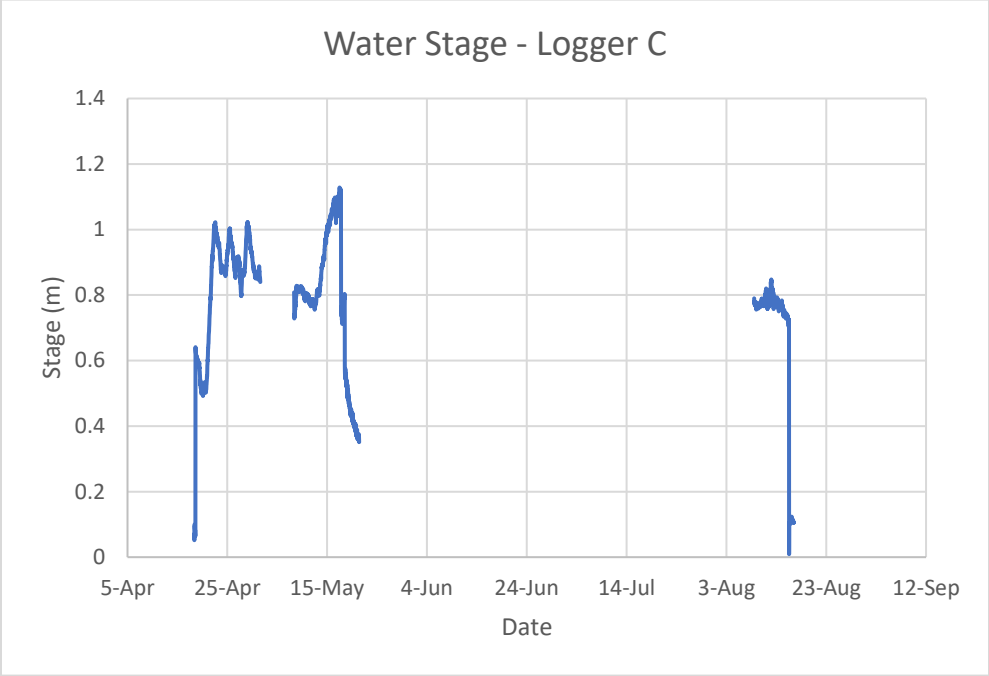


Figure 56. Total water stage data from Logger C at upstream end of Huntley bypass.

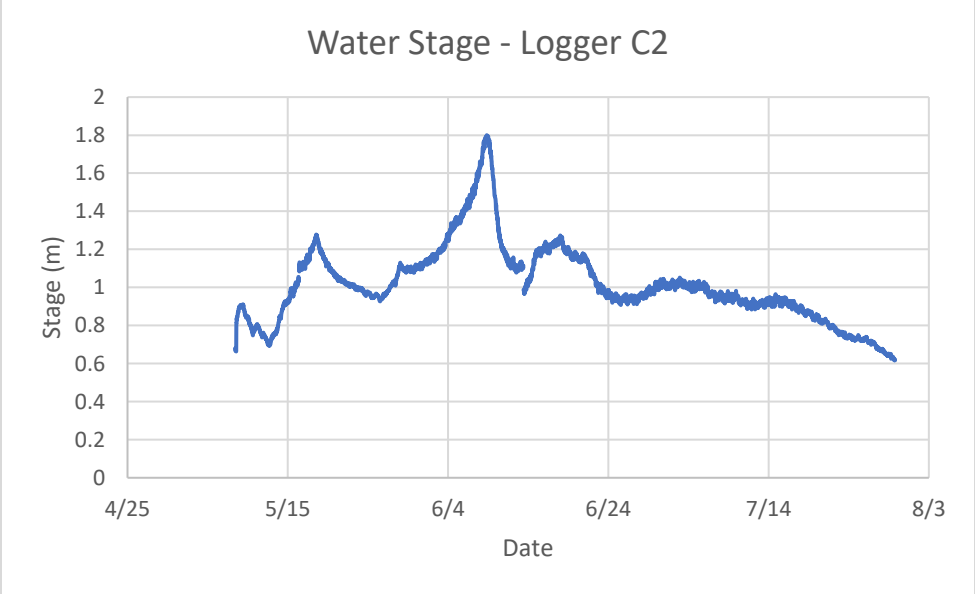


Figure 57. Total water stage data from logger C2, placed in close proximity to cross section C.

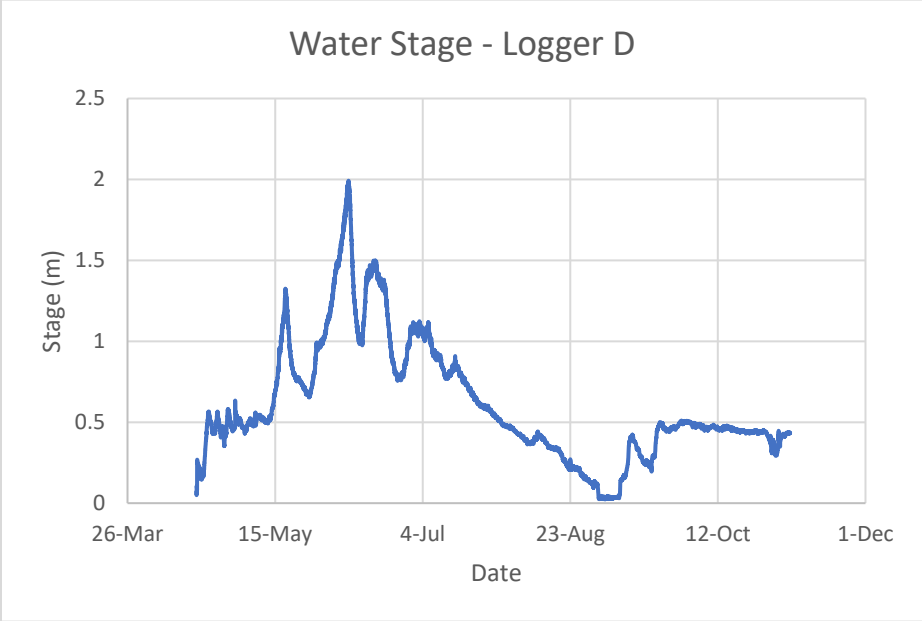


Figure 58. Total water stage data from logger D in old bypass channel.

# APPENDIX B

## WOLMAN PEBBLE COUNT SIZE CLASS TABLE

Table 7: Wolman Pebble Count size class and size ranges in millimeters.

| **Size Class** | **Size Range (mm)** |
|---|---|
| Sand | < 2 |
| Very Fine Gravel | 2-4 |
| Fine Gravel | 4-6 |
| Fine Gravel | 6-8 |
| Medium Gravel | 8-11 |
| Medium Gravel | 11-16 |
| Coarse Gravel | 16-22 |
| Coarse Gravel | 22-32 |
| Very Coarse Gravel | 32-45 |
| Very Coarse Gravel | 45-64 |
| Small Cobble | 64-90 |
| Medium Cobble | 90-128 |
| Large Cobble | 128-180 |
| Very Large Cobble | 180-256 |
| Small Boulder | 256-512 |
| Medium Boulder | 512-1024 |
| Large Boulder | 1024-2048 |
| Very Large Boulder | 2048-4096 |

# APPENDIX C

## SAMPLE PHOTO POINT OUTPUTS

Figure 59. Downstream fish entrance to Huntley Bypass on June 13th (L) and August 20th (R).

Figure 60. Looking upstream into Huntley Bypass on June 13th (L) and August 20th (R).

Figure 61. Water level in center of Huntley Bypass on June 13th (L) and August 20th (R).

Figure 62. Looking downstream into lower portion of bypass on June 13th (L) and August 20th (R).

Figure 63. Upstream fish exit of bypass on June 13th (L) and August 20th (R).

Figure 64. Looking upriver from site on June 13th (L) and August 20th (R).

Figure 65. Entrance to old bypass channel on June 13th (L) and August 20th (R).

# APPENDIX D

## ADDITIONAL FIELD MEASUREMENT DATA

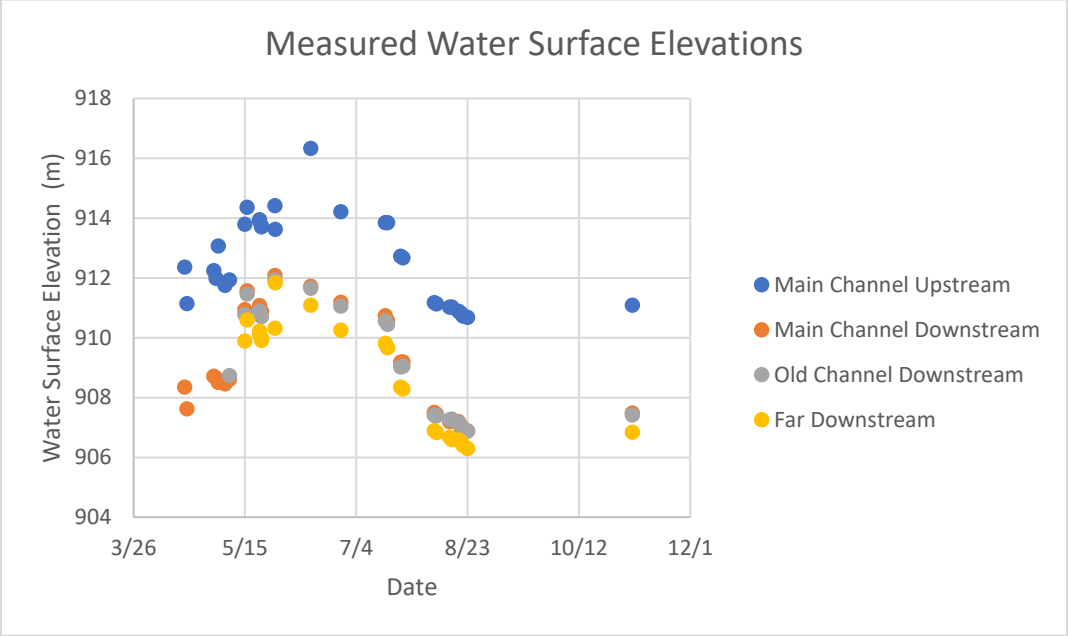


Figure 66. Water surface elevation readings at four specific survey points throughout the field season of April 18 to November 5, 2019.

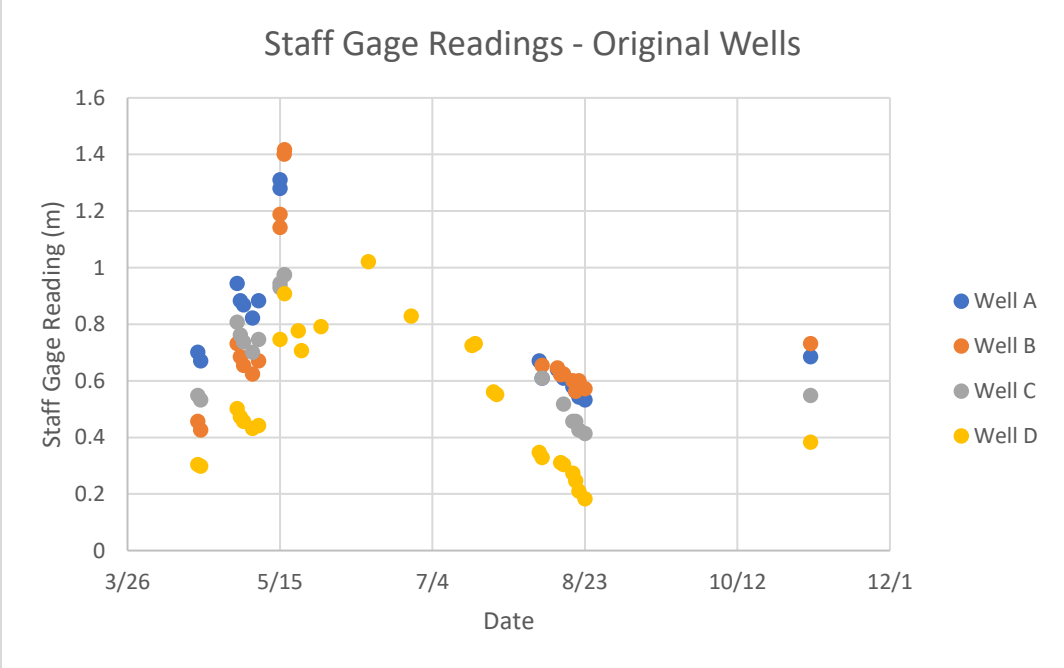


Figure 67. Staff gage readings at Wells A, B, C, and D throughout the field season of April 18 through November 5, 2019.

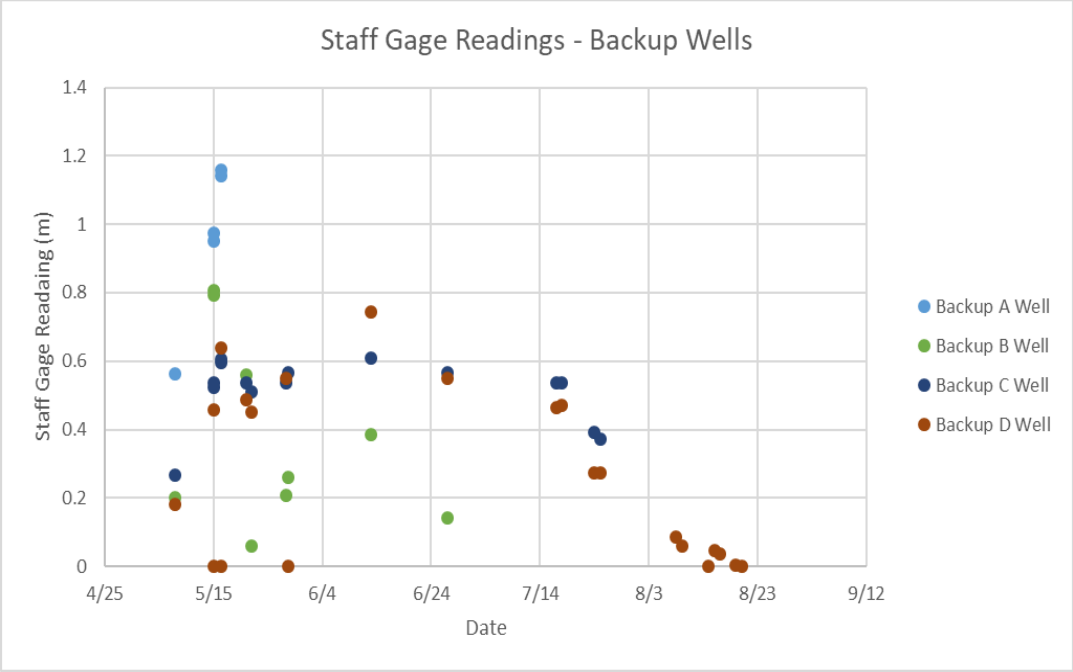


Figure 68. Staff gage readings at Wells A2, B2, C2, and D2 throughout the field season of April 18 through November 5, 2019.

# APPENDIX E

## ADDITIONAL RATING CURVE GRAPHS AND DATA

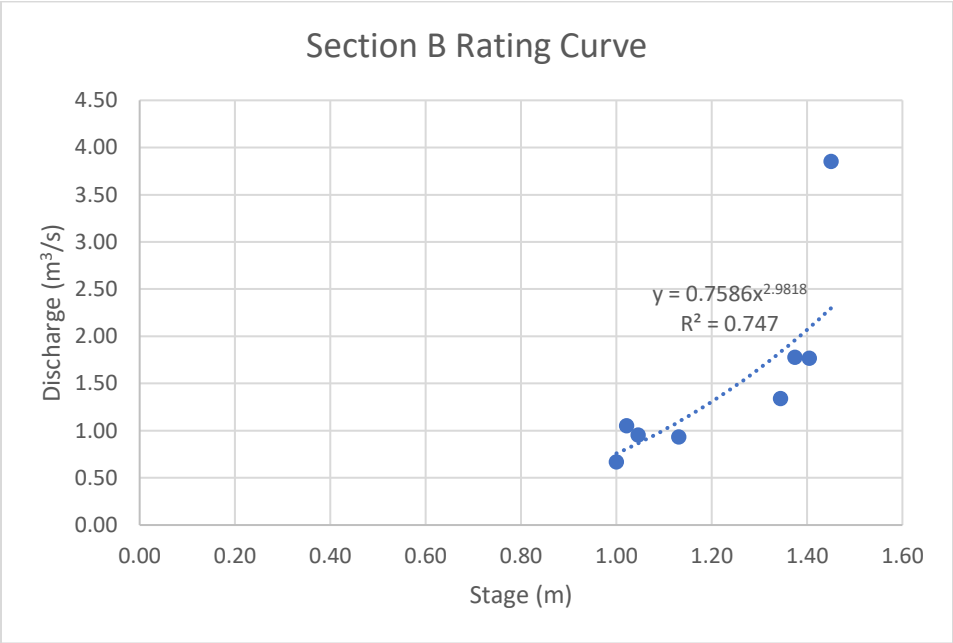


Figure 69. Power function rating curve developed from flow rate collection at Section B in main bypass channel.

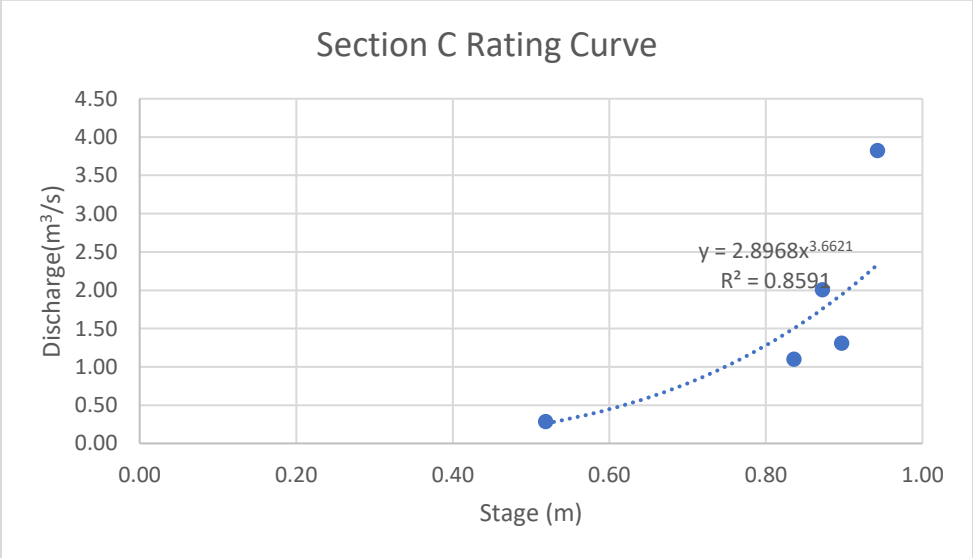


Figure 70. Power function rating curve developed from flow rate collection at Section C in main bypass channel.

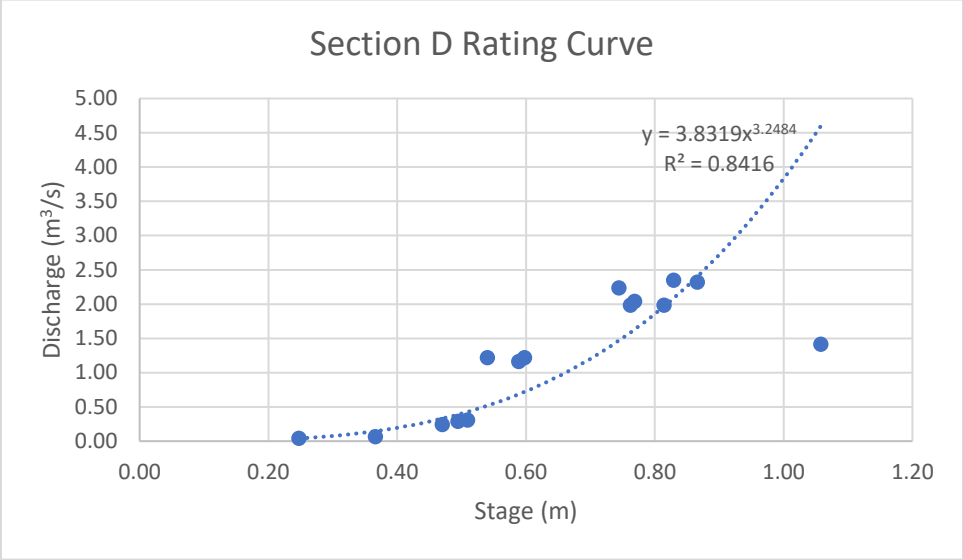


Figure 71. Power function rating curve developed from flow rate collection at Section D in old bypass channel.

# APPENDIX F

## OBSERVED, FITTED, AND MODELED FLOW RATE DATA

Table 8: Total daily modeled flow rates through the most downstream portion of the main nature-like bypass channel.

| Date | Lower Huntley Bypass Observed Flow ($m^3/s$) | Linear Regression Fitted Flow ($m^3/s$) | Modeled Flow ($m^3/s$) |
|---|---|---|---|
| 18-Apr | 0.98 | 1.08 | 42.06 |
| 19-Apr | 0.97 | 1.03 | 39.52 |
| 20-Apr | | 1.12 | 42.80 |
| 21-Apr | | 1.70 | 68.14 |
| 22-Apr | | 2.73 | 111.55 |
| 23-Apr | | 2.93 | 119.65 |
| 24-Apr | | 2.59 | 105.72 |
| 25-Apr | | 2.76 | 112.63 |
| 26-Apr | | 2.87 | 117.25 |
| 27-Apr | | 2.97 | 121.25 |
| 28-Apr | | 2.98 | 122.07 |
| 29-Apr | | 2.67 | 108.81 |
| 30-Apr | | 2.37 | 96.37 |
| 1-May | | 2.16 | 88.05 |
| 2-May | 2.10 | 2.01 | 81.52 |
| 3-May | 1.96 | 1.87 | 75.38 |
| 4-May | | 1.74 | 69.93 |
| 5-May | | 1.65 | 66.13 |
| 6-May | 1.74 | 1.71 | 68.54 |
| 7-May | | 1.83 | 73.68 |
| 8-May | 2.10 | 2.18 | 88.67 |
| 9-May | | 2.46 | 99.95 |
| 10-May | | 2.31 | 94.04 |
| 11-May | | 2.20 | 89.36 |
| 12-May | | 2.23 | 90.68 |
| 13-May | | 2.66 | 108.43 |
| 14-May | | 3.78 | 155.67 |
| 15-May | 6.82 | 5.56 | 225.88 |
| 16-May | 7.42 | 7.49 | 295.81 |
| 17-May | | 9.90 | 382.17 |
| 18-May | | 12.51 | 477.67 |
| 19-May | | 10.12 | 390.38 |
| 20-May | | 7.49 | 295.99 |

| | | | |
|---|---|---|---|
| 21-May | 6.33 | 6.29 | 253.18 |
| 22-May | 6.43 | 5.74 | 233.03 |
| 23-May | | 5.33 | 217.30 |
| 24-May | | 4.89 | 200.97 |
| 25-May | | 4.59 | 188.69 |
| 26-May | | 4.35 | 179.31 |
| 27-May | | 5.19 | 212.14 |
| 28-May | 3.68 | 7.38 | 291.92 |
| 29-May | | 8.72 | 340.22 |
| 30-May | | 8.67 | 338.37 |
| 31-May | | 9.12 | 354.92 |
| 1-Jun | | 10.23 | 394.08 |
| 2-Jun | | 11.74 | 448.33 |
| 3-Jun | | 13.61 | 520.67 |
| 4-Jun | | 15.96 | 617.00 |
| 5-Jun | | 18.42 | 722.92 |
| 6-Jun | | 21.06 | 840.71 |
| 7-Jun | | 23.59 | 960.45 |
| 8-Jun | | 26.83 | 1121.95 |
| 9-Jun | | 22.39 | 903.27 |
| 10-Jun | | 14.55 | 559.53 |
| 11-Jun | | 10.80 | 414.61 |
| 12-Jun | | 9.51 | 369.12 |
| 13-Jun | 11.27 | 10.46 | 402.36 |
| 14-Jun | | 13.86 | 530.65 |
| 15-Jun | | 16.91 | 658.01 |
| 16-Jun | | 17.57 | 686.42 |
| 17-Jun | | 18.05 | 706.78 |
| 18-Jun | | 17.34 | 676.45 |
| 19-Jun | | 16.15 | 625.95 |
| 20-Jun | | 15.57 | 600.92 |
| 21-Jun | | 14.11 | 540.90 |
| 22-Jun | | 11.15 | 426.97 |
| 23-Jun | | 9.02 | 351.13 |
| 24-Jun | | 7.74 | 305.36 |
| 25-Jun | | 7.11 | 281.70 |
| 26-Jun | | 7.23 | 286.32 |
| 27-Jun | 6.74 | 8.06 | 316.29 |
| 28-Jun | | 9.23 | 358.79 |

| | | | |
|---|---|---|---|
| 29-Jun | | 10.75 | 412.48 |
| 30-Jun | | 11.68 | 446.30 |
| 1-Jul | | 11.74 | 448.41 |
| 2-Jul | | 11.62 | 444.25 |
| 3-Jul | | 11.47 | 438.83 |
| 4-Jul | | 10.98 | 420.84 |
| 5-Jul | | 11.03 | 422.81 |
| 6-Jul | | 10.04 | 387.30 |
| 7-Jul | | 8.91 | 347.21 |
| 8-Jul | | 8.43 | 329.63 |
| 9-Jul | | 8.29 | 324.69 |
| 10-Jul | | 7.72 | 304.26 |
| 11-Jul | | 6.91 | 274.26 |
| 12-Jul | | 6.76 | 268.90 |
| 13-Jul | | 7.18 | 284.40 |
| 14-Jul | | 7.82 | 307.90 |
| 15-Jul | | 7.72 | 304.26 |
| 16-Jul | | 7.08 | 280.87 |
| 17-Jul | 6.34 | 6.49 | 259.60 |
| 18-Jul | 6.68 | 5.98 | 241.64 |
| 19-Jul | | 5.39 | 219.85 |
| 20-Jul | | 4.89 | 200.97 |
| 21-Jul | | 4.41 | 181.91 |
| 22-Jul | | 3.90 | 161.18 |
| 23-Jul | | 3.53 | 145.40 |
| 24-Jul | 4.76 | 3.31 | 136.02 |
| 25-Jul | 4.73 | 3.24 | 132.68 |
| 26-Jul | | 3.06 | 125.33 |
| 27-Jul | | 2.76 | 112.67 |
| 28-Jul | | 2.47 | 100.48 |
| 29-Jul | | 2.27 | 92.36 |
| 30-Jul | | 2.08 | 84.65 |
| 31-Jul | | 1.93 | 77.87 |
| 1-Aug | | 1.87 | 75.31 |
| 2-Aug | | 1.83 | 73.96 |
| 3-Aug | | 1.73 | 69.46 |
| 4-Aug | | 1.62 | 64.62 |
| 5-Aug | | 1.53 | 60.89 |
| 6-Aug | | 1.44 | 57.10 |

| | | | |
|---|---|---|---|
| 7-Aug | | 1.34 | 51.94 |
| 8-Aug | | 1.23 | 47.26 |
| 9-Aug | 0.94 | 1.17 | 44.74 |
| 10-Aug | | 1.24 | 47.91 |
| 11-Aug | | 1.33 | 51.39 |
| 12-Aug | | 1.30 | 50.48 |
| 13-Aug | | 1.21 | 46.60 |
| 14-Aug | | 1.11 | 42.70 |
| 15-Aug | | 1.02 | 39.10 |
| 16-Aug | | 0.98 | 37.59 |
| 17-Aug | | 0.95 | 36.40 |
| 18-Aug | | 0.95 | 36.40 |
| 19-Aug | | 0.93 | 35.38 |
| 20-Aug | 0.82 | 0.86 | 32.85 |
| 21-Aug | | 0.78 | 29.93 |
| 22-Aug | | 0.76 | 29.14 |
| 23-Aug | | 0.74 | 28.42 |
| 24-Aug | | 0.73 | 27.89 |
| 25-Aug | | 0.72 | 27.71 |
| 26-Aug | | 0.70 | 26.83 |
| 27-Aug | | 0.66 | 25.25 |
| 28-Aug | | 0.64 | 24.76 |
| 29-Aug | | 0.60 | 23.16 |
| 30-Aug | | 0.57 | 21.71 |
| 31-Aug | | 0.58 | 22.23 |
| 1-Sep | | 0.57 | 22.00 |
| 2-Sep | | 0.56 | 21.22 |
| 3-Sep | | 0.53 | 20.15 |
| 4-Sep | | 0.50 | 19.25 |
| 5-Sep | | 0.49 | 18.31 |
| 6-Sep | | 0.48 | 18.37 |
| 7-Sep | | 0.52 | 20.44 |
| 8-Sep | | 0.56 | 22.32 |
| 9-Sep | | 0.61 | 22.96 |
| 10-Sep | | 0.66 | 23.66 |
| 11-Sep | | 0.84 | 44.73 |
| 12-Sep | | 1.11 | 44.30 |
| 13-Sep | | 1.11 | 44.32 |
| 14-Sep | | 0.98 | 38.15 |

| | | | |
|---|---|---|---|
| 15-Sep | | 0.88 | 34.76 |
| 16-Sep | | 0.81 | 32.19 |
| 17-Sep | | 0.78 | 30.11 |
| 18-Sep | | 0.77 | 30.51 |
| 19-Sep | | 0.75 | 29.06 |
| 20-Sep | | 0.86 | 33.74 |
| 21-Sep | | 1.18 | 46.95 |
| 22-Sep | | 1.46 | 58.05 |
| 23-Sep | | 1.35 | 54.39 |
| 24-Sep | | 1.21 | 48.29 |
| 25-Sep | | 1.18 | 46.98 |
| 26-Sep | | 1.21 | 48.06 |
| 27-Sep | | 1.16 | 46.22 |
| 28-Sep | | 1.25 | 49.69 |
| 29-Sep | | 1.38 | 55.85 |
| 30-Sep | | 1.41 | 56.67 |
| 1-Oct | | 1.41 | 56.68 |
| 2-Oct | | 1.37 | 55.09 |
| 3-Oct | | 1.34 | 64.82 |
| 4-Oct | | 1.29 | 50.34 |
| 5-Oct | | 1.29 | 51.37 |
| 6-Oct | | 1.26 | 52.32 |
| 7-Oct | | 1.22 | 48.91 |
| 8-Oct | | 1.19 | 47.38 |
| 9-Oct | | 1.21 | 48.12 |
| 10-Oct | | 1.24 | 49.45 |
| 11-Oct | | 1.19 | 47.26 |
| 12-Oct | | 1.14 | 45.15 |
| 13-Oct | | 1.16 | 46.21 |
| 14-Oct | | 1.19 | 46.72 |
| 15-Oct | | 1.18 | 46.68 |
| 16-Oct | | 1.14 | 45.39 |
| 17-Oct | | 1.11 | 42.82 |
| 18-Oct | | 1.08 | 41.56 |
| 19-Oct | | 1.04 | 40.88 |
| 20-Oct | | 1.04 | 41.02 |
| 21-Oct | | 1.03 | 39.98 |
| 22-Oct | | 1.02 | 39.74 |
| 23-Oct | | 1.01 | 39.70 |

| | | | |
|---|---|---|---|
| 24-Oct | | 1.02 | 39.82 |
| 25-Oct | | 1.01 | 39.64 |
| 26-Oct | | 1.01 | 38.86 |
| 27-Oct | | 1.03 | 40.21 |
| 28-Oct | | 0.97 | 38.18 |
| 29-Oct | | 0.85 | 33.17 |
| 30-Oct | | 0.75 | 29.04 |
| 31-Oct | | 0.70 | 26.39 |
| 1-Nov | | 0.77 | 30.13 |
| 2-Nov | | 0.88 | 34.25 |
| 3-Nov | | 0.93 | 36.32 |
| 4-Nov | | 0.99 | 38.85 |
| 5-Nov | | 0.97 | 37.79 |

Table 9. Total daily modeled flow rates through the old nature-like bypass channel.

| **Date** | **Old Channel Observed Flow ($m^3/s$)** | **Linear Regression Fitted Flow ($m^3/s$)** | **Modeled Flow ($m^3/s$)** |
|---|---|---|---|
| 18-Apr | | 0.13 | 0.52 |
| 19-Apr | | 0.12 | 1.25 |
| 20-Apr | | 0.14 | 1.48 |
| 21-Apr | | 0.26 | 0.88 |
| 22-Apr | | 0.52 | 3.24 |
| 23-Apr | | 0.58 | 4.02 |
| 24-Apr | | 0.48 | 2.78 |
| 25-Apr | | 0.53 | 3.34 |
| 26-Apr | | 0.56 | 3.83 |
| 27-Apr | | 0.59 | 4.16 |
| 28-Apr | | 0.59 | 4.23 |
| 29-Apr | | 0.50 | 3.00 |
| 30-Apr | | 0.42 | 2.13 |
| 1-May | 1.22 | 0.37 | 1.25 |
| 2-May | 0.31 | 0.33 | 1.09 |
| 3-May | 0.29 | 0.29 | 0.97 |
| 4-May | | 0.27 | 0.89 |
| 5-May | | 0.25 | 0.90 |
| 6-May | 0.24 | 0.26 | 0.89 |
| 7-May | | 0.29 | 0.94 |

| | | | |
|---|---|---|---|
| 8-May | | 0.37 | 1.28 |
| 9-May | | 0.44 | 2.39 |
| 10-May | | 0.40 | 1.91 |
| 11-May | | 0.37 | 1.39 |
| 12-May | | 0.38 | 1.53 |
| 13-May | | 0.50 | 2.98 |
| 14-May | | 0.84 | 7.36 |
| 15-May | | 1.49 | 22.99 |
| 16-May | | 2.33 | 50.80 |
| 17-May | | 3.53 | 91.96 |
| 18-May | | 5.01 | 140.89 |
| 19-May | | 3.65 | 96.10 |
| 20-May | | 2.33 | 50.82 |
| 21-May | 1.98 | 1.80 | 32.61 |
| 22-May | 2.24 | 1.57 | 25.26 |
| 23-May | | 1.40 | 20.31 |
| 24-May | | 1.24 | 15.60 |
| 25-May | | 1.12 | 12.89 |
| 26-May | | 1.04 | 10.80 |
| 27-May | | 1.35 | 18.66 |
| 28-May | 2.35 | 2.28 | 49.38 |
| 29-May | | 2.92 | 70.88 |
| 30-May | | 2.90 | 69.96 |
| 31-May | | 3.13 | 77.79 |
| 1-Jun | | 3.71 | 98.39 |
| 2-Jun | | 4.55 | 126.81 |
| 3-Jun | | 5.68 | 160.31 |
| 4-Jun | | 7.20 | 200.50 |
| 5-Jun | | 8.91 | 242.19 |
| 6-Jun | | 10.88 | 287.35 |
| 7-Jun | | 12.89 | 327.87 |
| 8-Jun | | 15.61 | 376.48 |
| 9-Jun | | 11.92 | 308.50 |
| 10-Jun | | 6.27 | 175.81 |
| 11-Jun | | 4.02 | 109.17 |
| 12-Jun | | 3.33 | 84.23 |
| 13-Jun | 1.42 | 3.84 | 102.49 |
| 14-Jun | | 5.83 | 164.51 |
| 15-Jun | | 7.85 | 216.03 |

| | | | |
|---|---|---|---|
| 16-Jun | | 8.31 | 227.66 |
| 17-Jun | | 8.64 | 235.78 |
| 18-Jun | | 8.15 | 223.58 |
| 19-Jun | | 7.33 | 203.25 |
| 20-Jun | | 6.94 | 193.80 |
| 21-Jun | | 5.99 | 168.77 |
| 22-Jun | | 4.22 | 115.88 |
| 23-Jun | | 3.07 | 75.91 |
| 24-Jun | | 2.45 | 54.73 |
| 25-Jun | | 2.16 | 45.43 |
| 26-Jun | | 2.21 | 47.25 |
| 27-Jun | 2.32 | 2.60 | 59.95 |
| 28-Jun | | 3.19 | 79.70 |
| 29-Jun | | 3.99 | 107.95 |
| 30-Jun | | 4.52 | 125.61 |
| 1-Jul | | 4.55 | 126.80 |
| 2-Jul | | 4.49 | 124.41 |
| 3-Jul | | 4.40 | 121.69 |
| 4-Jul | | 4.12 | 112.33 |
| 5-Jul | | 4.15 | 113.55 |
| 6-Jul | | 3.61 | 94.55 |
| 7-Jul | | 3.02 | 74.03 |
| 8-Jul | | 2.78 | 66.03 |
| 9-Jul | | 2.71 | 64.02 |
| 10-Jul | | 2.44 | 54.43 |
| 11-Jul | | 2.07 | 42.66 |
| 12-Jul | | 2.00 | 40.36 |
| 13-Jul | | 2.19 | 46.57 |
| 14-Jul | | 2.49 | 56.14 |
| 15-Jul | | 2.44 | 54.42 |
| 16-Jul | | 2.14 | 44.96 |
| 17-Jul | 1.98 | 1.88 | 35.94 |
| 18-Jul | 2.04 | 1.67 | 28.44 |
| 19-Jul | | 1.43 | 21.15 |
| 20-Jul | | 1.24 | 15.60 |
| 21-Jul | | 1.06 | 11.34 |
| 22-Jul | | 0.88 | 7.86 |
| 23-Jul | | 0.76 | 6.30 |
| 24-Jul | 1.22 | 0.69 | 5.47 |

| | | | |
|---|---|---|---|
| 25-Jul | 1.16 | 0.67 | 5.17 |
| 26-Jul | | 0.61 | 4.48 |
| 27-Jul | | 0.53 | 3.34 |
| 28-Jul | | 0.45 | 2.41 |
| 29-Jul | | 0.39 | 1.72 |
| 30-Jul | | 0.35 | 1.17 |
| 31-Jul | | 0.31 | 1.01 |
| 1-Aug | | 0.29 | 0.96 |
| 2-Aug | | 0.29 | 0.95 |
| 3-Aug | | 0.26 | 0.89 |
| 4-Aug | | 0.24 | 0.91 |
| 5-Aug | | 0.22 | 0.96 |
| 6-Aug | | 0.20 | 1.02 |
| 7-Aug | | 0.18 | 1.66 |
| 8-Aug | | 0.16 | 1.67 |
| 9-Aug | 0.06 | 0.15 | 1.60 |
| 10-Aug | | 0.16 | 1.67 |
| 11-Aug | | 0.18 | 1.65 |
| 12-Aug | | 0.17 | 1.69 |
| 13-Aug | | 0.15 | 1.66 |
| 14-Aug | | 0.14 | 1.47 |
| 15-Aug | | 0.12 | 1.22 |
| 16-Aug | | 0.11 | 1.12 |
| 17-Aug | | 0.11 | 1.03 |
| 18-Aug | | 0.11 | 1.03 |
| 19-Aug | | 0.10 | 0.96 |
| 20-Aug | | 0.09 | 0.77 |
| 21-Aug | 0.04 | 0.08 | 0.52 |
| 22-Aug | | 0.08 | 0.45 |
| 23-Aug | | 0.07 | 0.37 |
| 24-Aug | | 0.07 | 0.31 |
| 25-Aug | | 0.07 | 0.29 |
| 26-Aug | | 0.07 | 0.19 |
| 27-Aug | | 0.06 | 0.09 |
| 28-Aug | | 0.06 | 0.02 |
| 29-Aug | | 0.05 | 0.01 |
| 30-Aug | | 0.05 | 0.27 |
| 31-Aug | | 0.05 | 0.09 |
| 1-Sep | | 0.05 | 0.00 |

| | | | |
|---|---|---|---|
| 2-Sep | | 0.05 | 0.33 |
| 3-Sep | | 0.05 | 0.33 |
| 4-Sep | | 0.04 | 0.01 |
| 5-Sep | | 0.04 | 0.22 |
| 6-Sep | | 0.04 | 0.00 |
| 7-Sep | | 0.04 | 0.00 |
| 8-Sep | | 0.05 | 0.00 |
| 9-Sep | | 0.06 | 0.54 |
| 10-Sep | | 0.06 | 1.72 |
| 11-Sep | | 0.09 | 0.00 |
| 12-Sep | | 0.14 | 0.00 |
| 13-Sep | | 0.14 | 0.00 |
| 14-Sep | | 0.11 | 0.33 |
| 15-Sep | | 0.10 | 0.00 |
| 16-Sep | | 0.08 | 0.00 |
| 17-Sep | | 0.08 | 0.19 |
| 18-Sep | | 0.08 | 0.00 |
| 19-Sep | | 0.08 | 0.08 |
| 20-Sep | | 0.09 | 0.01 |
| 21-Sep | | 0.15 | 0.00 |
| 22-Sep | | 0.20 | 0.75 |
| 23-Sep | | 0.18 | 0.00 |
| 24-Sep | | 0.15 | 0.04 |
| 25-Sep | | 0.15 | 0.01 |
| 26-Sep | | 0.15 | 0.01 |
| 27-Sep | | 0.15 | 0.06 |
| 28-Sep | | 0.16 | 0.01 |
| 29-Sep | | 0.19 | 0.00 |
| 30-Sep | | 0.19 | 0.04 |
| 1-Oct | | 0.19 | 0.03 |
| 2-Oct | | 0.19 | 0.00 |
| 3-Oct | | 0.18 | 0.00 |
| 4-Oct | | 0.17 | 1.18 |
| 5-Oct | | 0.17 | 0.30 |
| 6-Oct | | 0.16 | 0.00 |
| 7-Oct | | 0.16 | 0.00 |
| 8-Oct | | 0.15 | 0.10 |
| 9-Oct | | 0.15 | 0.01 |
| 10-Oct | | 0.16 | 0.00 |

| | | | |
|---|---|---|---|
| 11-Oct | | 0.15 | 0.04 |
| 12-Oct | | 0.14 | 0.00 |
| 13-Oct | | 0.15 | 0.00 |
| 14-Oct | | 0.15 | 0.69 |
| 15-Oct | | 0.15 | 0.37 |
| 16-Oct | | 0.14 | 0.00 |
| 17-Oct | | 0.13 | 1.00 |
| 18-Oct | | 0.13 | 0.99 |
| 19-Oct | | 0.12 | 0.34 |
| 20-Oct | | 0.12 | 0.00 |
| 21-Oct | | 0.12 | 0.79 |
| 22-Oct | | 0.12 | 0.53 |
| 23-Oct | | 0.12 | 0.18 |
| 24-Oct | | 0.12 | 0.44 |
| 25-Oct | | 0.12 | 0.00 |
| 26-Oct | | 0.12 | 0.78 |
| 27-Oct | | 0.12 | 0.28 |
| 28-Oct | | 0.11 | 0.07 |
| 29-Oct | | 0.09 | 0.09 |
| 30-Oct | | 0.08 | 0.01 |
| 31-Oct | | 0.07 | 0.88 |
| 1-Nov | | 0.08 | 0.01 |
| 2-Nov | | 0.10 | 0.08 |
| 3-Nov | | 0.10 | 0.34 |
| 4-Nov | | 0.11 | 0.01 |
| 5-Nov | | 0.11 | 0.19 |